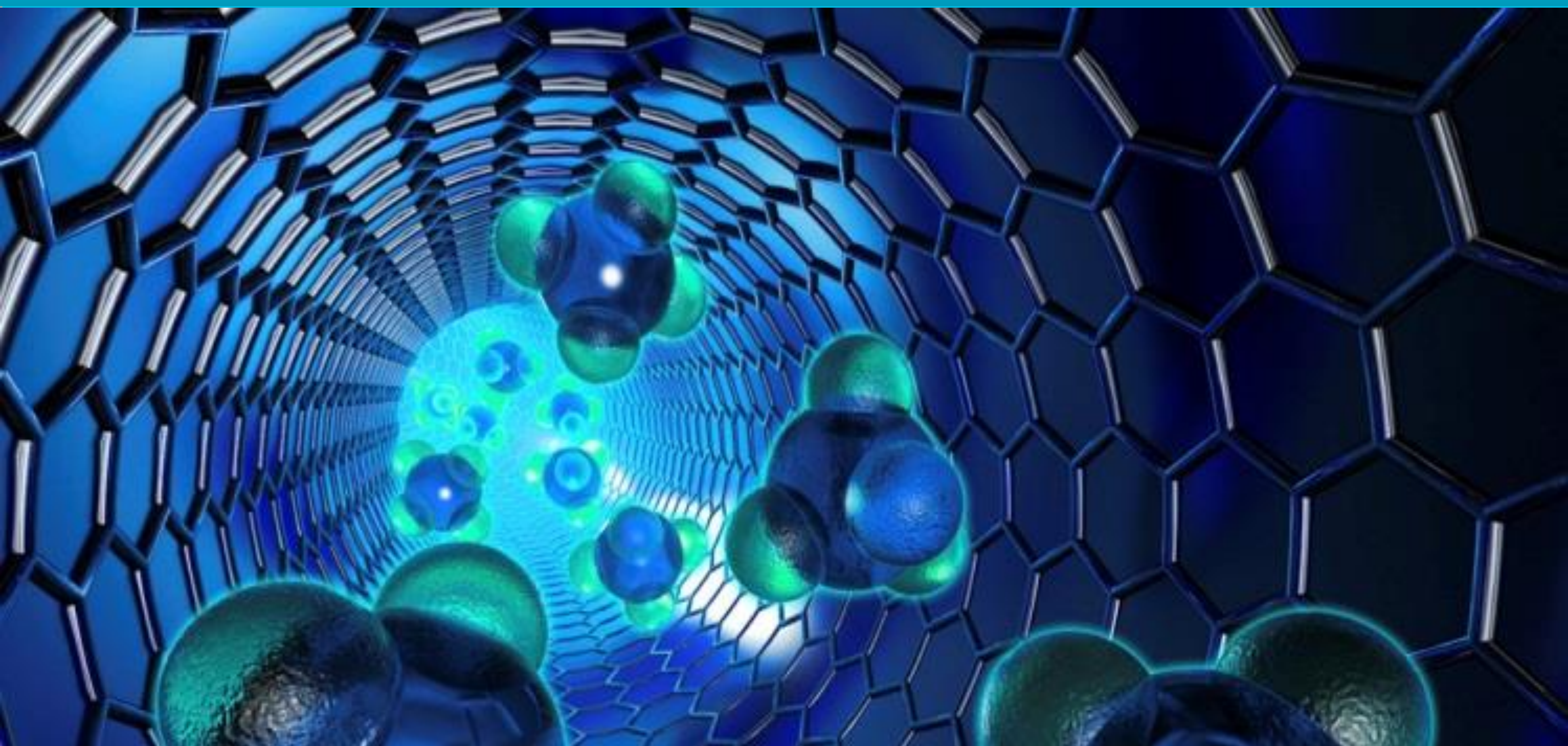


e-ISSN: 2602-277X

International Journal of Chemistry and Technology

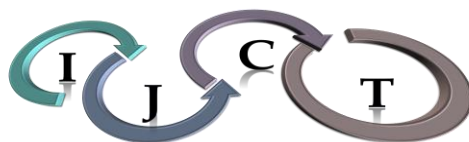


Volume:2, Issue:1

29 June 2018

E - Journal

<http://dergipark.gov.tr/ijct>

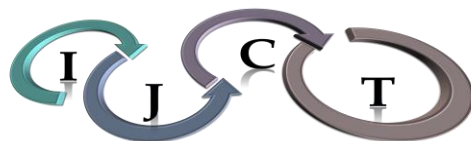


International Journal of Chemistry and Technology

JOURNAL INFO

Journal Name	International Journal of Chemistry and Technology
Journal Initial	IJCT
Journal Abbreviation	Int. J. Chem. Technol.
ISSN (Online)	2602-277X
Year of Launching	2017, August
Editor-in-Chief and Managing Editor	Prof. Dr. Bilal Acemioğlu
Manager of Publication	Assist. Prof. Mehmet Akyüz
Scope and Focus	Chemistry, Material Science, Technology
Review Type	Peer Review Double-Blinded
Ethical Rules	Plagiarism check, copyright agreement form, conflict of interest, ethics committee report
Access Type	Open Access
Publication Fee	Free
Article Language	English
Frequency of Publication	Biannually
Publication Issue	June, December
Publisher	Prof. Dr. Bilal Acemioğlu
Web Page	http://dergipark.gov.tr/ijct
Contact E-mail address	ijctsubmission@gmail.com, ijctsubmission@yahoo.com
Contact Address and Executive address	Kilis 7 Aralik University, Faculty of Science and Arts, Department of Chemistry, 79000, Kilis
Contact Telephone	90 5535983054 (Editor-in-Chief), 90 530 3645222 (Manager of Publication), 90 532233 17 38 (Secretary)
Publication Date	29/12/2017
Technical Editor	Assist. Prof. Dr. Evrim Baran
Spelling Editor	Assist. Prof. Dr. Evrim Baran, Dr. Oğuzhan Koçer, MSc. Rabia Acemioğlu
Language (Grammar) Editor	Doç. Dr. Gülcihan Güzeldağ, Assist. Prof. Dr. Muhammet Karaman, Dr. Oğuzhan Koçer, English Expert. Abdulkadir Doğan
Secretary	Dr. Oğuzhan Koçer, MSc. Rabia Acemioğlu

All detailed information including instructions for authors, aim and scopes, ethical rules, manuscript evaluation, indexing info, and manuscript template etc. can be found on the main web page of IJCT (<http://dergipark.gov.tr/ijct>).



International Journal of Chemistry and Technology

Volume: 2, Issue: 1, 29 June 2017

Founder of IJCT

Prof. Dr. Bilal Acemiođlu

EDITORIAL BOARD

Editor-in-Chief

Prof. Dr. Bilal Acemiođlu

(Kilis 7 Aralik University, Kilis, Turkey)

Associate Editors

Prof. Dr. İbrahim Demirtaş
(Organic Chemistry and Phytochemistry,
Çankırı Karatekin, University, Çankırı, Turkey)

Prof. Dr. M. Hakkı Alma
(Material Science and Technology,
K.Maraş Sütçü İmam/Iğdır University, Turkey)

Prof. Dr. Metin Bülbül
(Biochemistry, Dumlupınar University,
Kütahya, Turkey)

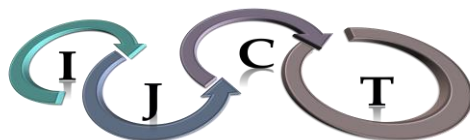
Prof. Dr. Fevzi Kılıçel
(Analytical Chemistry, Karamanođlu Mehmet
Bey University, Karaman, Turkey)

Prof. Dr. Yuh-Shan Ho
(Chemical and Environmental Engineering,
Asia University, Taichung City, Taiwan)

Prof. Dr. Yahya Güzel
(Theoretical Chemistry and Polymer Chemistry,
Erciyes University, Kayseri, Turkey)

Prof. Dr. Mustafa Arık
(Physical Chemistry, Atatürk University,
Erzurum, Turkey)

Prof. Dr. Mehmet Sönmez
(Inorganic Chemistry, Gaziantep University,
Gaziantep, Turkey)



International Journal of Chemistry and Technology

Advisory Editorial Board

Prof. Dr. Ahmet akır
(Kilis 7 Aralık University, Kilis, Turkey)

Prof. Dr. Shaobin Wang
(Curtin University, Perth, Australia)

Prof. Harun Parlar
(Technical University of Munich, München,
Germany)

Prof. Dr. Barbaros Nalbantođlu,
(Yıldız Technical University, İstanbul, Turkey)

Prof. Dr. Ö. İrfan Küfreviođlu
(Atatürk University, Erzurum, Turkey)

Prof. Dr. Anatoli Dimođlu
(Düzce University, Düzce, Turkey)

Prof. Dr. Mahfuz Elmastaş
(Health Sciences University, İstanbul, Turkey)

Prof. Dr. Ahmet Tutar
(Sakarya University, Sakarya, Turkey)

Prof. Dr. Birgöl Yazıcı
(Cukurova University, Adana, Turkey)

Prof. Dr. İsmet Kaya
(18 Mart University, anakklae, Turkey)

Prof. Dr. Nurullah Saraođlu
(Atatürk University, Erzurum, Turkey)

Prof. Dr. Giray Topal
(Dicle University, Diyarbakır, Turkey)

Prof. Dr. Salah Akkal,
(University of Mentouri Consatntine,
Consatntine, Algeria)

Prof. Dr. Gilbert Kapche Deccaux
(The University of Yaounde I, Yaounde,
Cameroon)

Prof. Dr. Mehmet ifti
(Bingöl University, Bingöl, Turkey)

Prof. Dr. M. Salih Ađırtaş
(Yüzünücü Yıl University, Van, Turkey)

Prof. Dr. Özer ınar
(Yıldız Technical University, İstanbul, Turkey)

Prof. Dr. Rahmi Kasımođulları
(Dumlupınar University, Kütahya, Turkey)

Prof. Dr. Ahmet Baysar
(Inonu University, Malatya, Turkey)

Prof. Dr. Hamdi Temel
(Dicle University, Diyarbakır, Turkey)

Prof. Dr. Papita Das
(Jadavpur University, Jadavpur, India)

Prof. Dr. Atiqur Rahman
(Islamic University, Kushita, Bangladesh)

Prof. Dr. İlhami Gülin
(Atatürk University, Erzurum, Turkey)

Prof. Dr. Mehmet Uđurlu
(Sıtkı Kocman university, Muđla, Turkey)

Prof. Dr. Şükrü Beydemir
(Anadolu University, Eskişehir, Turkey)

Prof. Dr. Ramazan Solmaz
(Bingol University, Bingöl, Turkey)

Prof. Dr. Ömer Şahin
(Siirt University, Siirt, Turkey)

Prof. Dr. Mehmet Dođan
(Balıkesir University, Balıkesir, Turkey)



International Journal of Chemistry and Technology

Advisory Editorial Board

Prof. Dr. Jaine H. Hortolan Luiz
(Federal University of Alfenas,
Unifal-MG, Brazil)

Prof. Dr. Mehmet Muhtar Kocakerim
(Çankırı University, Çankırı, Turkey)

Prof. Dr. İbrahim Işıldak
(Yıldız Technical University, İstanbul, Turkey)

Prof. Dr. Seyithan Taysi
(Gaziantep University, Gaziantep, Turkey)

Prof. Dr. Jon-Bae Kim
(College of Health Sciences, South Korea)

Prof. Dr. Duygu Ekinci
(Atatürk University, Erzurum, Turkey)

Assoc. Prof. Dr. Metin Açıkyıldız
(Kilis 7 Aralık University, Kilis, Turkey)

Assoc. Prof. Niyaz M. Mahmoodi,
(Institute for Color Science and Technology,
Tehran, Iran)

Assoc. Prof. Dr. Ali Kara
(Uludağ University, Bursa, Turkey)

Assoc. Prof. Dr. Şenay Şimşek
(North Dakota State University, Fargo, USA)

Assoc. Prof. Dr. Serhan Uruş
(Sütçü İmam University, K.Maraş, Turkey)

Assoc. Prof. Dr. Murat Ertaş
(Bursa Teknik University, Bursa, Turkey)

Assoc. Prof. Dr. Muhammet Köse
(Sütçü İmam University, K.Maraş, Turkey)

Assist. Prof. Dr. Mutasem Z. Bani-Fwaz
(King Khalid University, Asir-Abha, Saudi Arabia)

Prof. Dr. Vagif Abbasov
(Nef-Kimya Prosesleri Institutu, Baku,
Azerbaijan)

Prof. Dr. Murat Alanyalıoğlu
(Atatürk University, Erzurum, Turkey)

Prof. Dr. T. Abdulkadir Çoban
(Erzincan University, Erzincan, Turkey)

Prof. Dr. Ömer Işıldak
(Gaziosmanpaşa University, Tokat, Turkey)

Prof. Dr. Guang-Jie Zhao
(Beijing Forestry University, Beijing, China)

Prof. Dr. Hayrullah Yılmaz
(Dicle University, Diyarbakır, Turkey)

Assoc. Prof. Dr. Murat Sadıkoğlu
(Gaziosman Paşa University, Tokat, Turkey)

Assoc. Prof. Dr. Mustafa Özdemir
(Süleyman Demirel University, Isparta, Turkey)

Assoc. Prof. Dr. Mahjoub Jabli
(University of Monastir, Monastir, Tunisia)

Assoc. Prof. Dr. Mustafa Karataş
(Aksaray University, Aksaray, Turkey)

Assoc. Prof. Dr. Murat Saraçoğlu
(Erciyes University, Kayseri, Turkey)

Assoc. Prof. Dr. Halim Avcı
(Kilis 7 Aralık University, Kilis, Turkey)

Assoc. Prof. Dr. Ekrem Köksal
(Erzincan University, Erzincan, Turkey)

Assist. Prof. Dr. Bakhtiyor Rasulev
(North Dakota State University, Fargo, USA)



International Journal of Chemistry and Technology

Reviewers for June 2018, Vol: 2, Issue: 1

Prof. Dr. Mehmet Uğurlu
(Muğla Sıtkı Koçman University, Muğla,
Turkey)

Prof. Dr. Ayşe Gül Gürek
(Gebze Technical University, Kocaeli,
Turkey)

Prof. Dr. İbrahim Demirtaş
(Çankırı Karatekin University, Çankırı, Turkey)

Prof. Dr. Mustafa Tavasli
(Uludağ University, Bursa, Turkey)

Prof. Dr. Ramazan Erenler
(Gazi Osman Paşa University, Tokat, Turkey)

Prof. Dr. Erol Asiltürk
(Fırat University, Elazığ, Turkey)

Prof. Dr. Mehmet Salih Ağırtaş
(Yüzüncü Yıl University, Van, Turkey)

Prof. Dr. Rahmi Kasımoğulları
(Dumlupınar University, Kütahya, Turkey)

Prof. Dr. Gül Özyılmaz
(Mustafa Kemal University, Hatay, Turkey)

Prof. Dr. Ramazan Bilgin
(Çukurova University, Adana, Turkey)

Prof. Dr. Mehmet Tümer
(Sütçü İmam University, K.Maraş, Turkey)

Assoc. Prof. Dr. Ayşe Dinçer
(Celal Bayar University, Manisa, Turkey)

Assoc. Prof. Dr. Laçine Aksoy
(Afyon Kocatepe University, Afyon, Turkey)

Assoc. Prof. Dr. Ahmet Altun
(Cumhuriyet University, Sivas, Turkey)

Assoc. Prof. Dr. Muhammet Köse
(Sütçü İmam University, K.Maraş, Turkey)

Assoc. Prof. Dr. Metin Açıkyıldız
(Kilis 7 Aralık University, Kilis, Turkey)

Assist Prof. Dr. Mehmet Akyüz
(Kilis 7 Aralık University, Kilis, Turkey)

Assist. Prof. Dr. Lütfi Tutar
(Ahi Evran University, Kırşehir, Turkey)

Dr. Tuğba Özdemir
(Gazi Osman Paşa University, Tokat, Turkey)

Assist Prof. Dr. Evrim Baran
(Kilis 7 Aralık University, Kilis, Turkey)



International Journal of Chemistry and Technology

TABLE OF CONTENTS

Research Articles	Pages
1. Examining phase response curve of nerve cell by using three different methods Hasan Eskalen, Şükrü Özğan	1-9
2. Growth and norharmane production of Chroococcus minutus under various stress conditions Tunay Karan, Omer Kayir, Zekeriya Altuner, Ramazan Erenler	10-15
3. Evaluation of the wound healing potential of teucroside Seçil Erden Tayhan, Sema Bilgin, Mahfuz Elmastaş	16-19
4. Application of sepiolite-poly(vinylimidazole) composite for the removal of Cu(II) from aqueous solution: Isotherm and thermodynamics studies Ali Kara, Muhsin kılıç, Nalan Tekin, Nuray Dinibütün, Akif Şafaklı	20-33
5. Synthesis and characterization of alkyd resin based on soybean oil and glycerin using zirconium octoate as catalyst Mohamed E. Elba, Elsayed M. Abdel Rehim, Ramadan E. Ashery	34-43
6. The magnetic fructose imprinted polymer for determination of fructose from apple juice Burcu Okutucu	44-49
7. Practical synthesis, characterization and photo-physical properties of metallophthalocyanines bearing benzhydryloxy substituents Mehmet Salih Ağırtaş, Muhammed Yusuf Öndeş, Beyza Cabir	50-55
8. Biosorption of methylene blue and acid red 88 from wastewater by using peanut shell Onur Yel	56-62
9. Co-immobilization of pullulanase, glucoamylase and glucose isomerase together with cross-linked enzyme aggregates: fructose conversion from three enzymes and starch in one step Yakup Akkoç, S. Seyhan Tükel	63-67
10. Synthesis of complexes Co, Cu, Ni and Pd supported by “ONNO” type schiff base ligand and theirs DNA cleavage, antioxidant effects and antimicrobial studies Ahu Çelik, Hatice Gamze Sogukomerogullari, Sadin Ozdemir, M. Serkan Yalcin, Mehmet Sönmez	68-75



Examining phase response curve of nerve cell by using three different methods

Hasan ESKALEN¹, Şükrü ÖZĞAN^{2,*}

¹Bioengineering Program, Graduate School of Natural and Applied Science, Kahramanmaraş Sütçü İmam University, 46040, Kahramanmaraş, Turkey

²Department of Physics, Faculty of Arts and Sciences, Kahramanmaraş Sütçü İmam University, 46040, Kahramanmaraş, Turkey

Received: 13September 2017, Revised: 27 November 2017, Accepted: 05 December 2017

*Corresponding author's e-mail address: ozgans@gmail.com (Ş. Özğan)

ABSTRACT

Rhythmic motion is observed in a variety of different field including physical, chemical and biological systems. Neural system, that consists of billions of neurons are also exhibited periodic motion. Phase Response Curves (PRCs); act like a bridge between, a single neuron and neural network; briefly measure change in period of oscillation by giving perturbation at different points of oscillation. PRCs can determined from measurements of electrical activities of neurons by experimental methods or theoretically derived from three different methods. As far as we know from the literature, these three different methods have never been used at the same time before. The main purpose of this computational study is to the obtain Phase Response Curve by three different methods and compare them in terms of simulation times and peak to baseline ratio. First, the kinds of excitability of neurons, the types of Phase Response Curve and peak to baseline ratio are mentioned. After then, these three different methods to obtain PRC are explained deeply. At a final step, Phase Response Curves are obtained from three theoretical methods and compared regarding to peak to baseline ratio, simulation time and applicability.

Keywords: Phase response curve, direct method, linear adjoint method, adapted direct method.

Üç farklı metot kullanarak sinir hücrelerinin faz resetleme eğrilerinin incelenmesi

ÖZ

Ritmik hareket fiziksel, kimyasal ve biyolojik sistemleri ihtiva eden farklı alanların birçoğunda görülmektedir. Milyarlarca nöronlardan oluşan sinir sistemi periyodik hareket sergilemektedir. Faz Resetleme Eğrileri (PRCs), tek bir nöron ve nöron ağı arasında bir köprü gibi rol oynar ve kısaca farklı salınım noktalarında verilen uyarıcılar ile salınım periyodundaki değişimi ölçer. PRC'ler deneysel olarak nöronların elektriksel aktivitelerinin ölçümlerinden ya da teorik olarak türetilen üç farklı metottan hesaplanabilir. Literatürden bildiğimiz kadarıyla bu üç farklı teorik metot daha önce aynı anda hiç kullanılmamıştır. Bu hesaplamalı çalışmanın ana amacı üç farklı metot ile Faz Cevap Eğrilerini teorik olarak elde etmektir ve onları simülasyon süreleri ve tavan-taban oranları açısından kıyaslamaktır. İlk olarak nöronların uyarılabilirlik çeşitleri, PRC'lerin çeşitleri ve tavan-taban oranı bahsedilmiştir. Daha sonra PRC elde etmekte kullanılan üç farklı metot açıklanmıştır. Son aşamada üç teorik metotla Faz Resetleme Eğrileri türetilmiştir ve elde edilen şekiller tavan-taban oranı, simülasyon süresi ve uygulanabilirliği açısından karşılaştırılmıştır.

Anahtar Kelimeler: Faz tepki eğrisi, direkt metot, lineer adjoint metot, uyarlanmış direkt metot.

1. INTRODUCTION

Oscillating systems is in everywhere we encounter without realizing in everyday life. Some examples of oscillating systems from biology, chemistry, physics and engineering are single nerve cell that generates action potential¹⁻⁴, heart beat rhythm^{5,6}, human walking motion^{7,8}, circadian clock^{9,10}, oscillation in chemical reactions^{11,12} and earthquake dynamics.¹³ In short,

systems with dynamical elements that compose of spontaneous rhythms are used for Phase Response Curves (PRCs).¹⁴

Self-sustained oscillators have been proposed firstly by Andronov and Vitt in 1937 and are one of the areas that are of interest in the researchers working on dynamic systems. The most important feature of the self-sustained release is that it continues to oscillate with its own rhythm when abstracted from the environment.¹⁵ In a

clearer sense, they continue to oscillate without exerting a force on the system. Self-sustained oscillations can be represented geometrically by a stable limit cycle.¹⁶ The stable limit cycles are stable against small amplitude external forces. The oscillating systems do not occur if the limit cycle does not occur, and so PRC cannot be mentioned.¹⁷

Neurons are the basic operators and information-carrying units of the central nervous system. A single neuron cell emits periodically spikes when the externally applied current value rises above a certain threshold value, and the frequency of spikes increases with increasing amplitude of the applied current.^{18,19} Nerve cells at different points of the brain come together with complicated connections and emit spikes synchronously. This mechanism forms basis of fundamental physiological functions of the human such as attention and short-term memory.^{17,20} Although synchronous rhythm is a key specification of the human nerve system, the decreasing abnormal synchrony can cause Schizophrenia²¹⁻²³ and Alzheimer^{24,25}, and the increasing abnormal synchrony can also lead Parkinson²⁶⁻²⁸ and Epilepsy.^{29,30} These neurodegenerative diseases have also attracted the attention of the scientists that focus on biotechnological studies. Moreover, some institutes consider computational neuroscience as a subtopic of biotechnology. Phase response curve for 24-hour day rhythms is named as circadian clock. The scientists have won the Nobel Prize of 2017 year in physiology and medicine for their discovery of molecular mechanism controlling circadian rhythm.³¹ For these reasons, it is very important to examine the PRCs which is related to a single neuron cell, the behaviour of the neuron network, and circadian rhythm.

The PRC is one of the most important tools for investigating the dynamic structure of neurons. In the self-sustaining oscillation, the period of oscillating system dividing equally spaced phases according to a particular reference point and PRC measures how small perturbation given in different phases change the period of oscillations. The shape of PRC provides invaluable information about excitability of neurons, oscillation stability and synchrony in the neural network.³²⁻³⁸ Shape of PRCs can be obtained from two different fundamental methods. The first method (i.e. experimental method) is the measurement of electro-activity of nerve cells.³⁹⁻⁴⁶ The second method is to calculate PRC theoretically. To best of our knowledge, there are only three different theoretical ways to derive PRC and these three main ways have not been examined together.

In this study, firstly the types of excitability of neurons are examined and then peak to baseline ratio is investigated. Direct method, linear adjoint method and adapted direct method are examined in shortly. PRC of single neuron calculated by using these three different methods, their required time interval, and peak to base line ratios are compared.

2. MODEL AND METHODS

In our study, $I_{Na,p} + I_K$ model is used to simulate the neuron. This model is consist of sodium, potassium and leak current and it is similar to Morris Lecar model.² $I_{Na,p} + I_K$ model is represented by two nonlinear differential equations and it is considered as a simplified version of Hodgkin Huxley model. Nowadays, Hodgkin Huxley type models are known as conductance-based models. In all conductance-based models, the electrochemical processes at the current generation and signal transmission in a neuron are replaced by a facilitated electrical circuit.⁴⁷ Equations of the models are:

$$C \frac{dV}{dt} = I_{app} - g_L(V - E_L) - g_{Na}m_{\infty}(V)(V - E_{Na}) - g_Kn(V - E_K) \quad (1a)$$

$$dn/dt = (n_{\infty}(V) - n)/(tau(V)) \quad (1b)$$

In Eq. (1a), I_{app} implies external applied current and C represents membrane capacitance. The conductance values of sodium, potassium and leak currents, $g_{Na} = 20$, $g_K = 10$, $g_L = 8$ nS, respectively. The reversal potentials of sodium and potassium are 60 mV and -90 mV. In Eq. (1b), the numerical value of $tau(V)$ is equal to one. The values of $m_{\infty}(V)$ and $n_{\infty}(V)$ are calculated from Eq. (2),

$$x_{\infty}(V) = 1/1 + \exp\{(V_{1/2} - V)/k\}; \quad x = m, n \quad (2)$$

Parameters obtained for different types of excitabilities are given in Table 1.

Table 1. Some parameters of $I_{Na,p} + I_K$ model with different excitability

	Type-1 excitability		Type-2 excitability	
	k	$V_{1/2}$	k	$V_{1/2}$
$m_{\infty}(V)$	15	-20 (mV)	15	-20 (mV)
$n_{\infty}(V)$	5	-25 (mV)	5	-45 (mV)
E_L		-80		-78

The model equations and model parameters are obtained from Izhikevich's book.² In this paper, all simulations were performed using a personal laptop, with 10.0 GB RAM and 2.4 GHz Intel i5 processor. Moreover, solutions of differential equations were performed by using the ode45 function (implements fourth order Runge-Kutta numerical integration algorithms) in MATLAB software (R2012b) on a 64-bit mac osx operation systems.

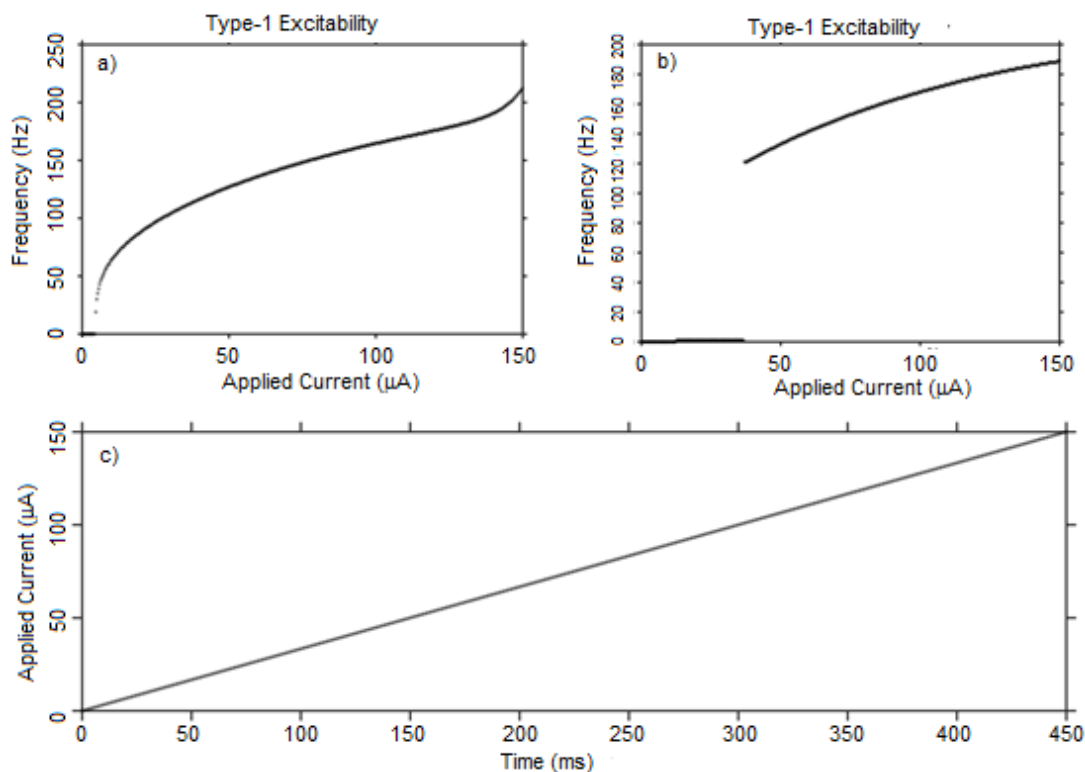


Figure 1. The types of excitation derived from the $I_{Na,p} + I_K$ model and the applied current: a) Excitability Type-1, b) Excitability Type-2, c) Change of applied current with time.

2.1. Types of excitability

Nerve cells were stimulated under different voltages applied by using, $I_{Na,p} + I_K$ model, and the obtained parameters are given in Table 1. The frequencies versus currents applied are plotted in Figure 1. The nerve cell first time emits spike before the applied current reaches 5 pA and as the applied current increases, the spike frequency also increases. This type of excitability is known as Type-1 Excitability^{48,49} and it is shown in Figure 1a. On the other hand, if the nerve cell does not emit spikes linearly with the applied currents and the frequency and applied current are relatively high when the nerve cell first time emits spike in Type-2 Excitability.⁵⁰ Figure 1b illustrates Type-2 Excitability.⁵⁰ Applied current is increased linearly with simulation time and it is given in Figure 1c. To sum up, as indicated in Table 1, the excitability of $I_{Na,p} + I_K$ model changes with only changing values of two parameters that are $V_{1/2}$ and E_L .

2.2. Types of PRCs

Excitability types of $I_{Na,p} + I_K$ model by using parameters in Table 1 and their corresponding PRC types are shown in Figure 2. Generally, Type-1 PRC has an

either positive or negative single curve, but Type-2 PRC is represented by both the combination of positive and negative parts. The Type-1 and Type-2 PRCs are illustrated in Figures 2a and 2b, respectively.

2.3. Peak-to-baseline ratio

Peak-to-baseline ratio is applicable for only Type-2 PRCs and it is given by Eq. (3)⁵¹,

$$r = \frac{|m_l - m_e|}{|m_l + m_e|} \quad (3)$$

At Eq. (3), r implies peak-to-baseline ratio, m_e and m_l represent early and late peak amplitude of PRC. Since Type-2 PRCs are composed of two different sign peaks, m_e and m_l are opposite signs. The magnitude of m_e and m_l could be easily found from PRC curve.⁵² The general shape of Type-2 PRC is given in Figure 3a. The corresponding PRC value of early peak is positive and the late peak is negative. The shape of Type-2 PRC in Figure 3a is derived from $I_{Na,p} + I_K$ model, and the early (first) peak is positive and it is represented by m_e .

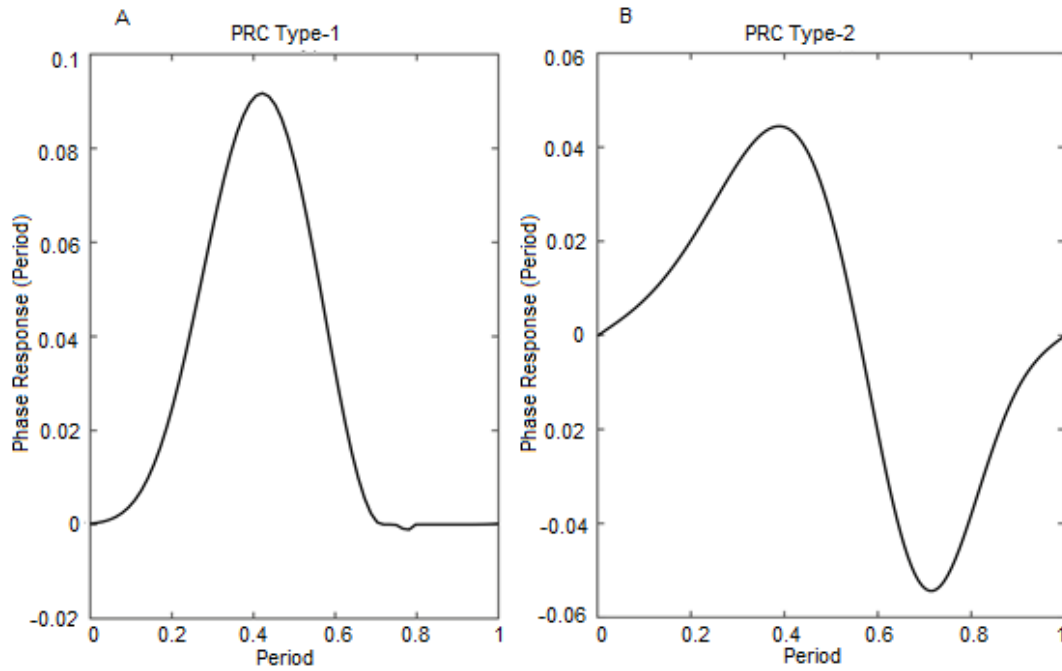


Figure 2. PRC types of $I_{Na,p} + I_K$ model: a) PRC Type-1, b) PRC Type-2.

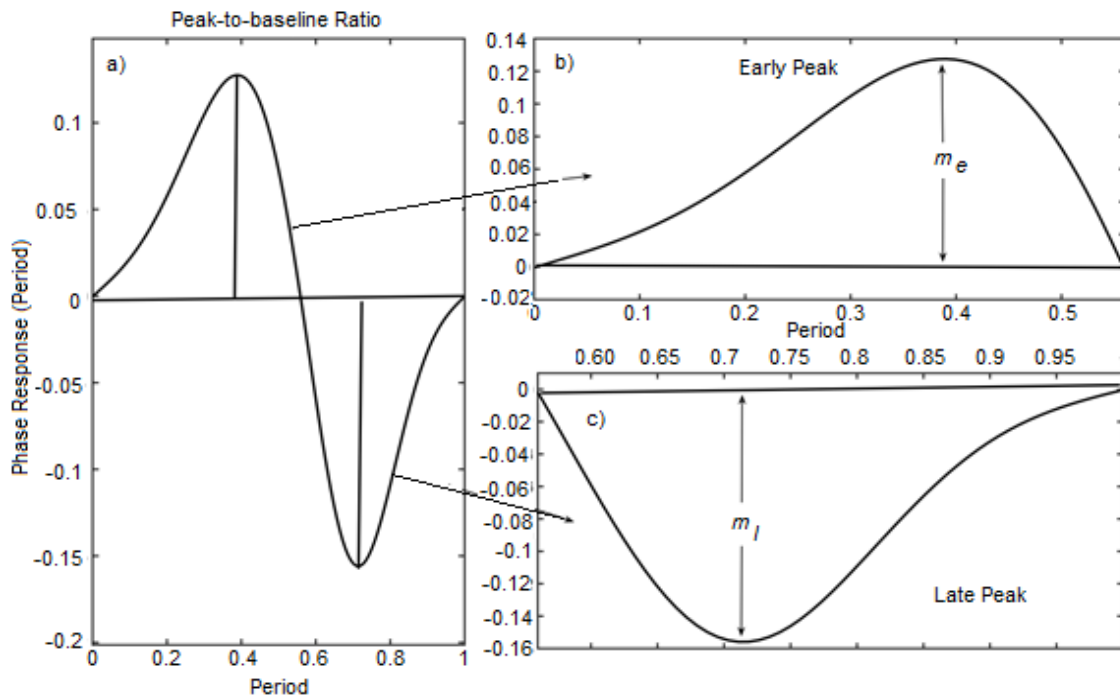


Figure 3. a) Peak-to-Baseline Ratio of PRC Tip-2, b) The first peak of PRC, c) The second peak of PRC.

The late peak is negative and it is represented by m_l . The early peak is illustrated in Figure 3b and the late peak is shown in Figure 3c.

In this study, phase response curves of $I_{Na,p} + I_K$ model are theoretically calculated by using three different methods and their simulation times and peak-to-

baseline ratios are calculated. Direct method, linear adjoint methods and adapted direct method are the used methods. To best of our knowledge, these three different methods have not been used and compared together, so far.

2.4. Direct method

Suppose the period of self-sustained oscillation is equal to T and the period of the oscillation after the short perturbation is equal to T' . The PRC can be calculated with direct method by using Eq. (4),

$$PRC = \frac{T-T'}{T} \quad (4)$$

The first step to find PRC by using direct method is to stimulate self-sustained oscillation for long enough to find initial condition independent solution, i.e. to find limit cycle solution. After then, the time interval for one period oscillation is found, and this period is divided into certain points. Voltage and gating variable values for these certain points are determined. The short perturbation is given to this oscillating system and their voltage and gating variables are found. By using these variable corresponding period points determined. By using time difference between oscillations before and after perturbation, phase response values of one point is obtained and also by giving perturbation at different point of oscillation, phase response curve is obtained.

Figure 4a illustrates voltage versus time graph of $I_{Na,p} + I_K$ model. The small amplitude, 6 pA, perturbation current is given at 28thms during 0.5 ms. The magnitude of perturbation is 0 pA other than 28th ms, this red colored current perturbation curve is given at the voltage axis to only more clearly show the time of the perturbation (Figure 4a). Although the model emits spike periodically before perturbation, the model emits spike early after this perturbation. Figure 4a also illustrates the behaviour of the model if no perturbation was given. The negative and different amplitude perturbation is given at the different time point as shown in Figure 4b. At the 45.5thms-14 pA square pulse current applied to oscillator during 0.8 ms. As shown in this figure, the period of oscillation changed very slightly with this perturbation. The voltage-time graph zooms in at the insert. Figure 4c shows limit cycle attractor, the initial condition of the oscillator and applied perturbation point of the negative amplitude current, -14 pA, in more detail.

Although direct method (see Eq. (4)) is a simple method, this method is not exactly correct.⁵³ Since the magnitude and duration of applied current could change or different for varied oscillators and these are important factors which directly change shape of PRCs.

2.5. Linear adjoint method

The used neural model is composed of two equations, Eq. (1a) and Eq. (1b), the detailed description mentioned above. These two equations imply 2-dimensional state

space $X = (X_v, X_n)$. The $I_{Na,p} + I_K$ model can be written as follow,

$$\frac{d}{dt}X = F(X) \quad (5)$$

Assume that this system moves on stable limit cycle attractor with a period of T . The angular velocity of this system is $w=2\pi/T$ and $X_0(t+T) = X_0(t)$. The phases of points in the limit cycle can be converted to the length of limit cycle, angle and time. If the phases of points are converted to time mode, the phase of any point on limit cycle is written as

$$\theta = wt \pmod{2\pi}, \text{ and } \theta(t) \in [0, 2\pi) \quad (6)$$

At Eq. (6), θ represents the phase of point, w implies angular velocity, and t represents time. It is also possible to find phases of the point which are not on limit cycle but attract it with time. The small perturbation given to limit cycle attractor which generates the basis of PRC is given by

$$\frac{d}{dt}X = F(X) + \varepsilon P(t) \quad (7)$$

At Eq. (7), $P(t)$ represents small perturbation. Eq. (8a) represents phase model of weakly connected oscillators. Phase deviation is given by φ and the period of oscillations is the same for all oscillators.² Eq. (8b) represents time derivative of phase model given in Eq. (8a).

$$\theta(t) = t + \varphi(t) \quad (8a)$$

$$\dot{\theta}(t) = 1 + \dot{\varphi}(t) \quad (8b)$$

Eq. (9) shows the parameters related to the derivative of phase deviation. In this equation, $P(t)$ implies small amplitude perturbation, $Q(\theta)$ represents phase response curve, in other words, $Q(\theta)$ implies the sensitivity of phase of $\theta(t)$ to perturbation $P(t)$.⁵⁴

$$\dot{\varphi}(t) = Q(\theta(t))P(t) \quad (9)$$

If the value of Eq. (9) is written in Eq. (8b), Eq. (10) is obtained.

$$\dot{\theta}(t) = 1 + Q(\theta(t))P(t) \quad (10)$$

At this equation, Q is a solution of linear adjoint equation with a function of T -period.

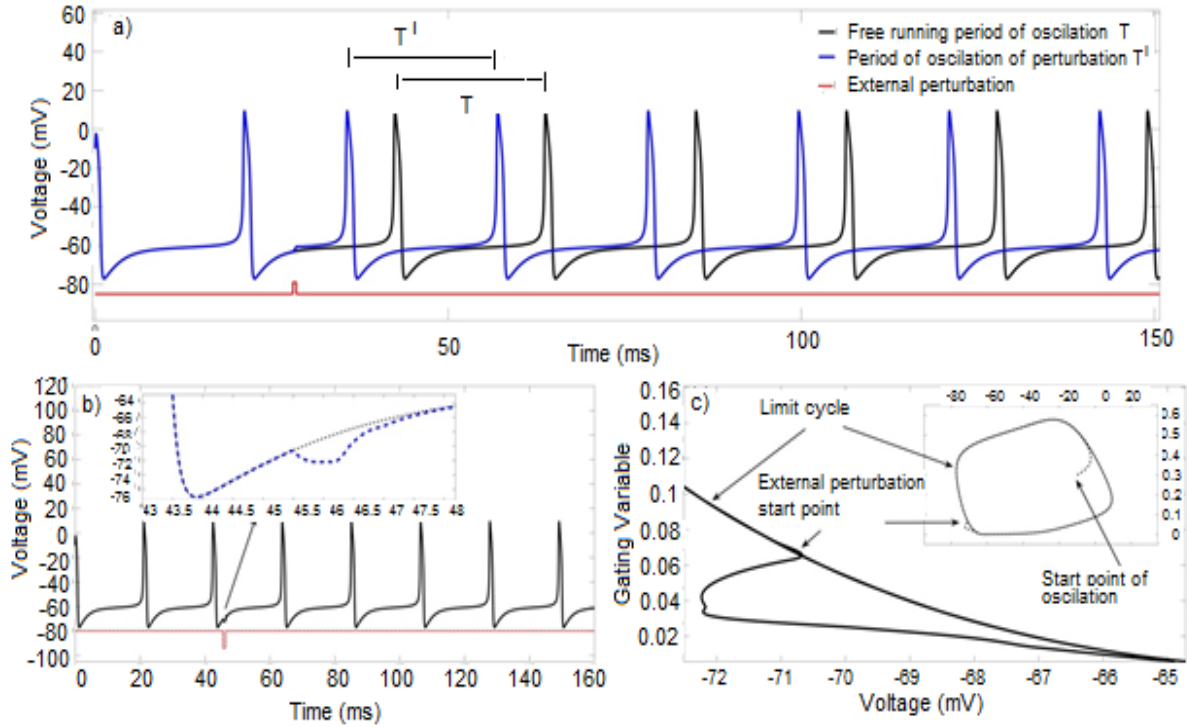


Figure 4. Voltage-time graph of the neuron model: a) Positive stimulus, b) Negative stimulus, c) Change of limit cycle.

At Eq. (11a), $\{DF(X(t))\}^T$ is the transposed Jacobian matrix of function F on the limit cycle attractor at the point $X(t)$. Eq. (11b) represents the initial condition of the system.

$$\dot{Q} = -\{DF(X(t))\}^T Q \quad (11a)$$

$$Q(0) \cdot F(X(0)) = 1 \quad (11b)$$

Adjoint method has centered on Malkin's approach.⁵⁵ Calculated PRC must be periodic, i.e. $Q(T)=Q(0)$, because of this reason, the direct integration of this equation is not suitable due to boundary value problem.⁵³ To find the periodic solution of Eq. (11a) is integrated backward in time.^{32,56} The proof of adjoint equation⁵⁵ and invaluable studies for obtaining PRC are available at the selected papers.^{2,14,57}

2.6. Adapted direct method

Adapted Direct Method proposed by Noviĉenko and Pyragas was tested for different neural models. The results of these tests show that adapted directed method

up to 10 to 100 times faster than linear adjoint method.⁵³ Although linear adjoint method getting very slow at the situation when the limit cycle is near to bifurcation point, the speed of adapted direct method does not depend on it. Adapted direct method described by

$$PRC(\theta) = \frac{L_1(\theta)}{L_1^T(\theta)V(\theta)} \quad (12)$$

At Eq. (12), L_1 is left eigenvector, and $V(\theta)$ is equal to the velocity vector. The detailed proof of this method can be found from Noviĉenko study.⁵³ PRC is calculated by using this method by means of the Viktor Noviĉenko software code. So, the computation of PRC is done numerically by the help of this software code.⁵⁸

3. RESULTS

The PRCs of $I_{Na,p} + I_K$ model were calculated by the help of three different methods and the results are given in Figure 5. The PRCs calculated by using direct method, linear adjoint method and adapted direct method are illustrated in Figure5a-c, respectively. Although the shapes of numerically calculated PRCs were similar to

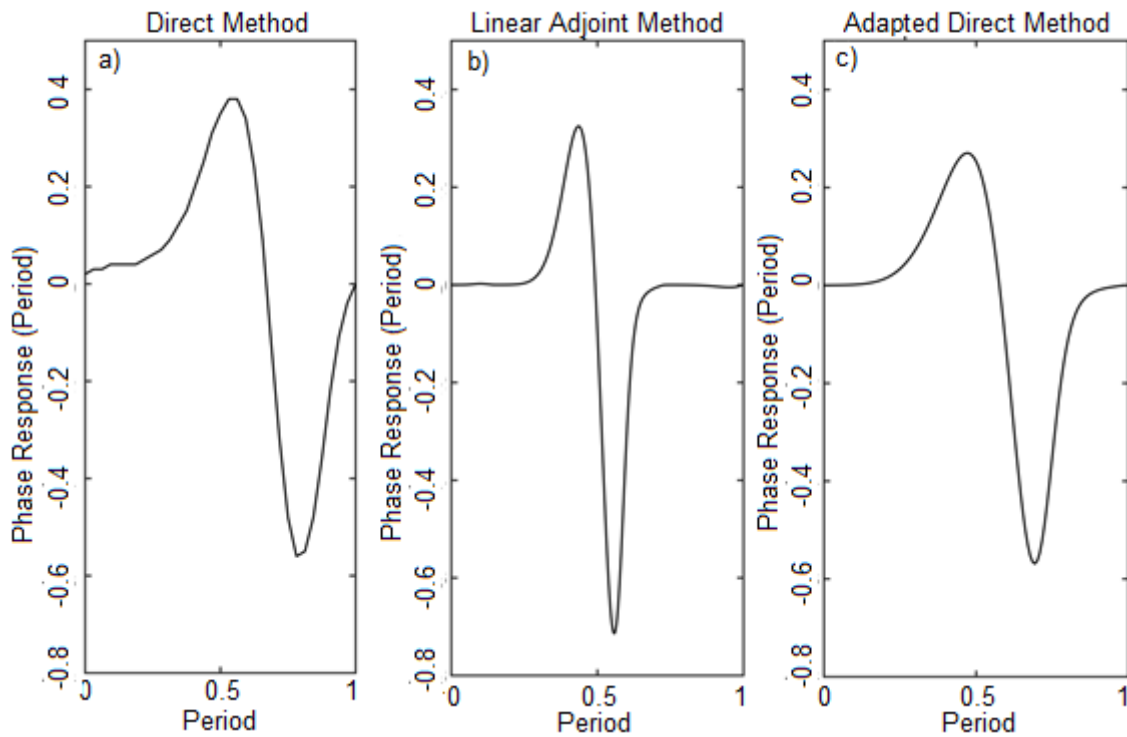


Figure 5. Phase response curves: a) Direct method, b) Linear adjoint method, c) Adapted direct method.

each other's, they were not exactly the same. The calculated phase response values of direct method are approximately ten times smaller than the other methods. The magnitude of the early and late peak of PRC was biggest at the linear adjoint method. These PRCs were calculated by using Type-2 excitability parameters (Table 1), and 35 pA external current applied.

The results of early and late peaks, peak-to-baseline ratios and required time intervals are given in Table 2 for these three methods. The required simulation time for direct method was approximately 190 times longer than adapted direct method and 40 times longer than linear adjoint methods. This means that the PRC computation speed is fastest at the adapted direct method and the slowest calculation speed is at the direct method. Linear adjoint method and adapted direct method gave similar results considering to the peak-to-baseline ratio. It is assumed that the reason of varied peak to baseline ratio at the direct method is due to the fact that the magnitude and duration of perturbations are not standard at this model. To conclude that, in this study, at first, excitability types and their corresponding phase response curves were derived for $I_{Na,p} + I_K$ model. The peak to baseline ratio is mentioned. After then, PRC of $I_{Na,p} + I_K$ model were calculated by using direct method, linear adjoint method and adapted direct method. The results of these three different methods were compared in terms of simulation speed and peak to baseline ratios.

Table 2. The peak-to-baseline ratios and simulation times for the PRCs derived for Type-2 excitability of $I_{Na,p} + I_K$ model

	Direct method	Linear adjoint method	Adapted direct method
m_e	0.038	0.325	0.270
m_l	-0.056	-0.708	-0.569
Peak-to-baseline ratio(r)	5.22	2.697	2.806
Required time interval (s)	107.85	2.75	0.56

This study can enlighten how to calculate PRC in terms of three different methods and gives the idea about advantage and disadvantage of these methods.

ACKNOWLEDGEMENT

Authors thank to Kahramanmaraş Sütçü İmam University for continuous motivation. Hasan ESKALEN thanks to Scientific and Technological Research Council of Turkey (TUBITAK) for Ph.D. scholarship (2211-C Program).

Conflict of interest


We declare that there is no a conflict of interest with any person, institute, and company, etc.


REFERENCES

1. Hodgkin, A.L.; Huxley, A. F. *J. Physiol.* **1952**, 117 (4), 500-544.
2. Izhikevich, E.M. *Dynamical systems in Neuroscience*, MIT press: 2007.
3. Rich, S.; Booth, V.; Zochowski, M. *Front. Neural Circuits* **2016**, 10, 82.
4. Park, Y.; Ermentrout, B. *J. Comput. Neurosci.* **2016**, 40 (3), 269-281.
5. Van Der Pol, B.; Van Der Mark, J. *The London, Edinburgh, and Dublin Phil. Mag. J. Sci.* **1928**, 6 (38), 763-775.
6. Kralemann, B.; Frühwirth, M.; Pikovsky, A.; Rosenblum, M.; Kenner, T.; Schaefer, J.; Moser, M. *Nat. Commun.* **2013**, 4, 3418.
7. Funato, T.; Yamamoto, Y.; Aoi, S.; Imai, T.; Aoyagi, T.; Tomita, N.; Tsuchiya, K. *PLoS Comput. Biol.* **2016**, 12 (5), e1004950.
8. Nessler, J.A.; Spargo, T.; Craig-Jones, A.; Milton, J.G. *Gait Posture* **2016**, 43, 187-191.
9. Minors, D. S.; Waterhouse, J. M.; Wirz-Justice, A. *Neurosci. Lett.* **1991**, 133 (1), 36-40.
10. Eck, S.; Helfrich-Förster, C.; Rieger, D. *J. Biol. Rhythm.* **2016**, 31 (5), 428-442.
11. Field, R. J.; Noyes, R. M. *J. Chem. Phys.* 1974, 60 (5), 1877-1884.
12. Proskurkin, I.S.; Vanag, V.K., *Phys. Chem. Chem. Phys.* **2015**, 17 (27), 17906-17913.
13. Franović, I.; Kostić, S.; Perc, M.; Klinshov, V.; Nekorkin, V.; Kurths, J. *Chaos* **2016**, 26 (6), 063105.
14. Nakao, H. *Contemp. Phys.* **2016**, 57 (2), 188-214.
15. Pikovsky, A.; Rosenblum, M.; Kurths, J. *Synchronization: a universal concept in nonlinear sciences*. Cambridge University Press: 2003; Vol. 12.
16. Strogatz, S.H. *Nonlinear dynamics and chaos: with applications to physics, biology, chemistry, and engineering*. Hachette UK: 2014.
17. Smeal, R.M.; Ermentrout, G.B.; White, J.A. *Philos. Trans. R. Soc. Lond. B: Biol. Sci.* **2010**, 365 (1551), 2407-2422.
18. Stein, R. Proceedings of the Royal Society of London B: *Biological Sciences* 167 (1006), 64-86, 1967.
19. Tateno, T.; Harsch, A.; Robinson, H. *J. Neurophysiol.* **2004**, 92 (4), 2283-2294.
20. Uhlhaas, P. J.; Singer, W. *Neuron* **2006**, 52 (1), 155-168.
21. Spencer, K.M.; Nestor, P.G.; Perlmutter, R.; Niznikiewicz, M.A.; Klump, M.C.; Frumin, M.; Shenton, M.E.; McCarley, R.W. Proceedings of the National Academy of Sciences of the United States of America 101 (49), 17288-17293, 2004.
22. Uhlhaas, P.J.; Linden, D.E.; Singer, W.; Haenschel, C.; Lindner, M.; Maurer, K.; Rodriguez, E. *J. Neurosci.* **2006**, 26 (31), 8168-8175.
23. Krishnan, G.P.; Vohs, J.L.; Hetrick, W.P.; Carroll, C. A.; Shekhar, A.; Bockbrader, M. A.; O'Donnell, B.F. *Clin. Neurophysiol.* **2005**, 116 (3), 614-624.
24. Stam, C.J.; Jones, B.; Nolte, G.; Breakspear, M.; Scheltens, P. *Cereb. Cortex* **2006**, 17 (1), 92-99.
25. König, T.; Prichep, L.; Dierks, T.; Hubl, D.; Wahlund, L.; John, E.; Jelic, V. *Neurobiol. Aging* **2005**, 26 (2), 165-171.
26. Hammond, C.; Bergman, H.; Brown, P. *Trends Neurosci.* **2007**, 30 (7), 357-364.
27. Schnitzler, A.; Gross, J., *Nat. Rev. Neurosci.* **2005**, 6 (4), 285-296.
28. Holt, A.B.; Wilson, D.; Shinn, M.; Moehlis, J.; Netoff, T.I. *PLoS Computat. Biol.* **2016**, 12 (7), e1005011.
29. Milton, J. G. *Epilepsy Behav.* **2010**, 18 (1), 33-44.
30. Bressloff, P. C.; Ermentrout, B.; Faueras, O.; Thomas, P. J. *J. Math. Neurosci.* **2016**, 6 (4), 1-9.
31. Delaunay, F. *B. Cancer* **2017**, 104 (10), 821-822.
32. Ermentrout, B. *Neural Comput.* **1996**, 8 (5), 979-1001.
33. Brown, E.; Moehlis, J.; Holmes, P. *Neural Comput.* **2004**, 16 (4), 673-715.
34. Marella, S.; Ermentrout, G.B. *Phys. Rev. E*, **2008**, 77 (4), 041918.

35. Ermentrout, G. B.; Galán, R. F.; Urban, N. N. *Trends Neurosci.* **2008**, 31 (8), 428-434.
36. Qiao, W.; Wen, J. T.; Julius, A. *IEEE T. Automat. Contr.* **2017**, 62 (1), 445-450.
37. Sato, Y. D.; Aihara, K. *Neural Comput.* **2014**, 26 (11), 2395-2418.
38. Canavier, C. C. *Curr. Opin. Neurobiol.* **2015**, 31, 206-213.
39. Buchin, A.; Rieubland, S.; Häusser, M.; Gutkin, B. S.; Roth, A. *PLoS Comput. Biol.* **2016**, 12(8), e1005000.
40. Cui, J.; Canavier, C.C.; Butera, R.J. *J. Neurophysiol.* **2009**, 102 (1), 387-398.
41. Tateno, T.; Robinson, H. *Biophys. J.* **2007**, 92 (2), 683-695.
42. Galán, R.F.; Ermentrout, G.B.; Urban, N.N. *Phys. Rev. Lett.* **2005**, 94 (15), 158101.
43. Saifee, T.A.; Edwards, M.J.; Kassavetis, P.; Gilbertson, T. *J. Neurophysiol.* **2015**, 115 (1), 310-323.
44. Jones, J. R.; Tackenberg, M. C.; McMahon, D.G. *Nat. Neurosci.* **2015**, 18 (3), 373-375.
45. Ostojic, S.; Szapiro, G.; Schwartz, E.; Barbour, B.; Brunel, N.; Hakim, V. *J. Neurosci.* **2015**, 35 (18), 7056-7068.
46. Miranda-Dominguez, O.; Netoff, T.I. *J. Neurophysiol.* **2013**, 109 (9), 2306-2316.
47. Kobelevskiy, I. Bifurcation analysis of a system of Morris-Lecar neurons with time delayed gap junctional coupling. Mater Thesis, University of Waterloo, 2008.
48. Izhikevich, E.M. *IEEE T. Neural Networ.* **1999**, 10 (3), 499-507.
49. Izhikevich, E.M. *Int. J. Bifurcat. Chaos* **2000**, 10 (06), 1171-1266.
50. Yu, T.; Sejnowski, T. J.; Cauwenberghs, G. *IEEE T. Biomed. Circ. S.* **2011**, 5 (5), 420-429.
51. Phoka, E.; Cuntz, H.; Roth, A.; Häusser, M. *PLoS Computat. Biol.* **2010**, 6 (4), e1000768.
52. Couto, J.; Linaro, D.; De Schutter, E.; Giugliano, M. *PLoS Comput. Biol.* **2015**, 11 (3), e1004112.
53. Novičenko, V.; Pyragas, K. *Nonlinear Dynam.* **2012**, 67 (1), 517-526.
54. Fang, Y.; Yashin, V. V.; Jennings, B. B.; Chiarulli, D. M.; Levitan, S. P. *ACM J. Emerg. Tech. Com.* **2016**, 13 (2), 14.
55. Hoppensteadt, F. C.; Izhikevich, E.M. *Weakly connected neural networks*. Springer Science & Business Media: 2012; Vol. 126.
56. Ermentrout, B. *Simulating, analyzing, and animating dynamical systems: a guide to XPPAUT for researchers and students*. Book Code: SE14, SIAM, 2002.
57. Nakao, H.; Yanagita, T.; Kawamura, Y. *Phys. Rev. X*, **2014**, 4, 021032 (1-23).
58. Novičenko V webpage. <http://www.itpa.lt/~novicenko/index.php?page=soft> (accessed June 14, 2017).

 ORCID

 0000-0002-4523-6573 (H. Eskalen)

 0000-0001-9334-327X (Ş. Özğan)



Growth and norharmane production of *Chroococcus minutus* under various stress conditions

Tunay KARAN¹, Omer KAYIR², Zekeriya ALTUNER¹, Ramazan ERENLER^{2,*}

¹Department of Biology, Faculty of Arts and Sciences, Gaziosmanpaşa University, 60240 Tokat, Turkey

²Department of Chemistry, Faculty of Art and Science, Gaziosmanpaşa University, 60240, Tokat, Turkey

Received: 01 November 2017, Revised: 09 January 2018; Accepted: 18 January 2018

*Corresponding author's e-mail address: renerler@gmail.com (R. Erenler)

ABSTRACT

Cyanobacterium samples were collected from fresh water of Tokat city in Turkey, and then isolation and cultivation of *Chroococcus minutus* were achieved successfully. TLC (Thin layer chromatography) and HPLC (High Performance Liquid Chromatography) analyses revealed that the *C. minutus* consisted of norharmane as a major product. So amount of norharmane was determined during the growth process. Growth and norharmane production of *C. minutus* were executed under salt stress and pH stress conditions. The most growth and the highest production of norharmane were detected at 16th day. Therefore inoculation process was performed at 16th day. Salt stress was evaluated at 0.5, 1.0, 3.0 and 5.0 M concentrations. The most norharmane was synthesized by *C. minutus* at 5 M concentration. The norharmane production and the growth were higher at pH 9 than that of the pH 5. Most norharmane was produced at pH 7.

Keywords: *Chroococcus minutus*, cyanobacteria, HPLC, norharmane.

Chroococcus minutus'un değişik stres koşullarında büyüme ve norharmane üretimi

ÖZ

Siyanobakteri örnekleri Türkiyede Tokat şehrinin tatlı sulardan toplandı ve *Chroococcus minutus*'un izolasyonu ve kültürü başarılı bir şekilde gerçekleştirildi. İTK (İnce tabaka kromatografisi) ve HPLC (Yüksek basınçlı sıvı kromatografisi) analizleri *Chroococcus minutus*'un ana ürün olarak norharman içerdiğini gösterdi. Böylece *C. minutus*'un gelişim döneminde norharman miktarı belirlendi. Tuz stresi ve pH stresi şartlarında *Chroococcus minutus*'un gelişimi ve norharman üretimi belirlendi. En fazla büyüme ve en çok norharman üretimi 16. günde gözlemlendi. Bu bakımdan inokulasyon işlemi 16. günde gerçekleştirildi. Tuz stresi 0.5, 1.0, 3.0 ve 5.0 M konsantrasyonlarında gerçekleştirildi. En fazla norharman 5 M konsantrasyonunda *C. minutus* tarafından sentezlendi. Norharman üretimi ve büyüme pH 5' teki şartlara göre pH 9' da daha yüksekti. En fazla norharman üretimi pH 7' de gerçekleşti.

Anahtar Kelimeler: *Chroococcus minutus*, siyanobakteri, HPLC, norharman.

1. INTRODUCTION

Cyanobacteria are able to adapt to wide environmental conditions. The abiotic effects including pH and salinity are helpful to create the suitable conditions for optimizing cyanobacteria growth. Cyanobacteria have to deal with altering environmental conditions by adapting to stress situations via syntheses of secondary metabolites. The optimum pH growth of cyanobacteria species are almost between 7.4-8.0¹ but some species prefer growing at alkaline and acidic medium.² Salt stress has a significant effect on cyanobac-

teria growth and development process. Salt stress is resulted in an increase in the intracellular lipid content of green alga, *Dunaliella tertiolecta*.³ Sodium chloride stress also causes an increase of antioxidative enzymes in the fresh water alga, *Chlamydomonas reinhardtii*.⁴ Cyanobacterial natural products reveal a wide range of biological and pharmaceutical properties that play a significant role in the drug discovery process.⁵

Cyanobacterial compounds mostly have fascinating chemical structures and strong biological effect due to the particularity of freshwater environment.⁶ Algae are simple organisms with chlorophyll including one cell or

living together in colonies, or as organisms with many cells and collaborating together as simple tissues. Algae are found in the sea, rivers, and lakes, on soil and walls in animal and plants as symbiotic; in fact almost everywhere in which there is a light to execute photosynthesis.⁷ Algae are classified as macroalgae and microalgae. The former inhabits in littoral area, contained green algae, brown algae and red algae. The later is found in both benthic and shore zone as well as in ocean as phytoplankton.⁸ Phytochemical investigations on algae have been resulted in the isolation of pharmaceutically and medicinally valuable secondary metabolites revealing a broad spectrum of biological activities such as antiinflammatory⁹, immunosuppressive¹⁰, antifungal¹¹, antineoplastic¹², antiviral¹³, hepatoprotective¹⁴, antioxidant¹⁵, antidiabetic¹⁶, anticancer¹⁷, anti-HIV¹⁸ activities. Norharmane, 9H-pyrindo (3, 4-b)indole is a derivative of β -carboline alkaloids which have several pharmacological effects including the inhibition of various enzymes such as monoamine oxidase¹⁹, indoleamine 2,3-dihydroxygenase, and nitric oxide synthesis.²⁰

Norharmane has significant properties in pharmacology as well as cyanobacterial life condition. Therefore, we determined the norharmane production under temperature and light conditions in previous work.²¹ Herein, we aimed to determine the norharmane production of *C. minutus* under salt and pH conditions. There is only a report revealing the existence of norharmane in *C. minutus*.²²

2. MATERIALS AND METHODS

2.1. General experimental procedure

Cyanobacteria genomic DNA isolation was executed with ZRFungal/Bacterial DNA kit according to the manufacturer's instructions. PCR amplification of specific primer 16S rRNA (27F-1492R) was carried out by Roche FastStart Taq DNA polymerase kit. All chemicals and solvents were supplied from Sigma-Aldrich (Darmstadt, Germany).

2.2. Collecting, isolation and cultivation of *Chroococcus minutus*

C. minutus was collected from Yesilirmak river, Tokat, Turkey (49° 19' 49.12" N, 36° 34' 2.06" E). It was filtered by filter paper (Whatmann, Germany) then was collected in petri dish. *C. minutus* was isolated by micropipette and micro injector under the inverted microscope and sample was streaked onto agarised Bristol medium (1.5% agar) (Table 1). During the cultivation process, incubation was kept for 2 weeks at

26 °C \pm 2 for 12/12 h (light/dark). The light intensity was 155 $\mu\text{mol s}^{-1} \text{m}^{-2}$.

Table 1. Composition of culture media

ml	Stock Solution	g/400 ml H ₂ O
10	NaNO ₃	10.0
10	CaCl ₂ × 2H ₂ O	1.0
10	MgSO ₄ × 7H ₂ O	3.0
10	K ₂ HPO ₄	3.0
10	KH ₂ PO ₄	7.0
10	NaCl	1.0

2.3. Morphological identification

C. minutus was identified under the light microscope by taking the photograph of sample as a micrometer. The cells existing as single or groups are in ovoid or spherical shape. The cells with big cover are 6–15 μm diameter and 4-10 μm diameter without cover.²³

2.4. Molecular identification

Thermal cyclic conditions were 4 min at 95°C for initial denaturation, 95°C for 1 min, 60°C for 45 s, 72°C for 1 min for 30 cycle and 72°C for 7 min for final extension step. PCR product was imaged by 1.5% agars jell electrophoresis and UV transilluminator (Figure 1). Sequence analysis of PCR product was carried out at REFGEN (METU Techno Center), Gene Research and Biotechnology Ltd. Co.

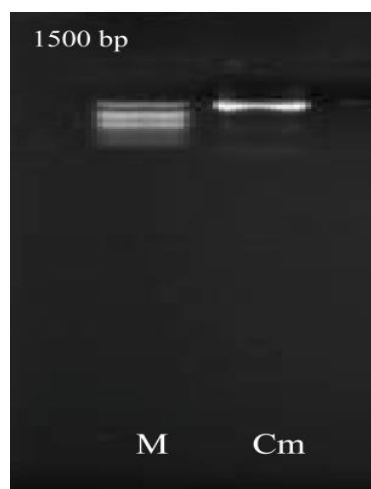


Figure 1. Digital photograph of an agarose gel with 27F-1492R primer PCR product from *C. minutus* (Cm), Marker (M).

2.5. Stress experiments

For salt stress experiments, nutrient media concentrations were 0.5, 1.0, 3.0 and 5.0 M. The control cultures were kept in the Bristol's Medium without sodium chloride (pH 7). For pH stress, pH values were adjusted to 5 and 9 in the culture medium.²⁴ To the nutrient media (235 ml) in each Erlenmeyer flask (250 ml), a stock culture (10%) was inoculated at 12-16th days of growth which had the most norharmane production. During the growth process, the cultures were shaken three times a day to homogenize the medium and accelerate the growth process. All stress trials were executed under the same temperature and light.

2.6. Cell number and biomass

Cell number was counted with a hemacytometer. Cell size was measured under an Olympus CX4 Boeco (Germany) light microscope. Culture samples (15 ml) were centrifuged at $5000 \times g$ for 10 min. After washing the pellets with distilled water (pH 4), they were dried at 50°C for 6-8 h, and then weighed.²⁵

2.7. Quantitative analysis of norharmane in *C. minutus* methanol extract

TLC (Thin layer chromatography) and HPLC analyses revealed the existence of norharmane in methanol extract by comparing the standard (norharmane). Then, quantitative analysis was executed on methanol extract to determine the amount of the norharmane variation under various stress conditions including pH and salt stresses. HPLC analyses were carried out by Shimadzu UV-260 spectrometer with diode array detector (Thermo Finnigan, Cambridge, England). Norharmane was purchased from Sigma-Aldrich (Steinheim, Germany, Product number: N6252). The samples with various concentrations were vortexed for 1 min then kept into the ultrasonic bath. After filtration by PTFE syringe (Chrom Tech, 0.45 0.45 μm 13 mm), 20 μl aliquot was injected to the HPLC column at 40 °C. C18 120A reverse phase column (4.6 \times 150 mm, 3 μm particle size) was used. The flow rate was adjusted to 1 ml/min using a gradient system of A, water with 0.1% formic acid and B, acetonitrile (Figure 2). The gradient program was fixed as follows: 0-14 min, 100% A; 15-29 min, 80% A, 30-32 min, 60% A, 33-34 min, 0% A. UV spectra were measured at 247 nm.²⁶ The amount of norharmane was calculated by the calibration curve using the Gauss method.

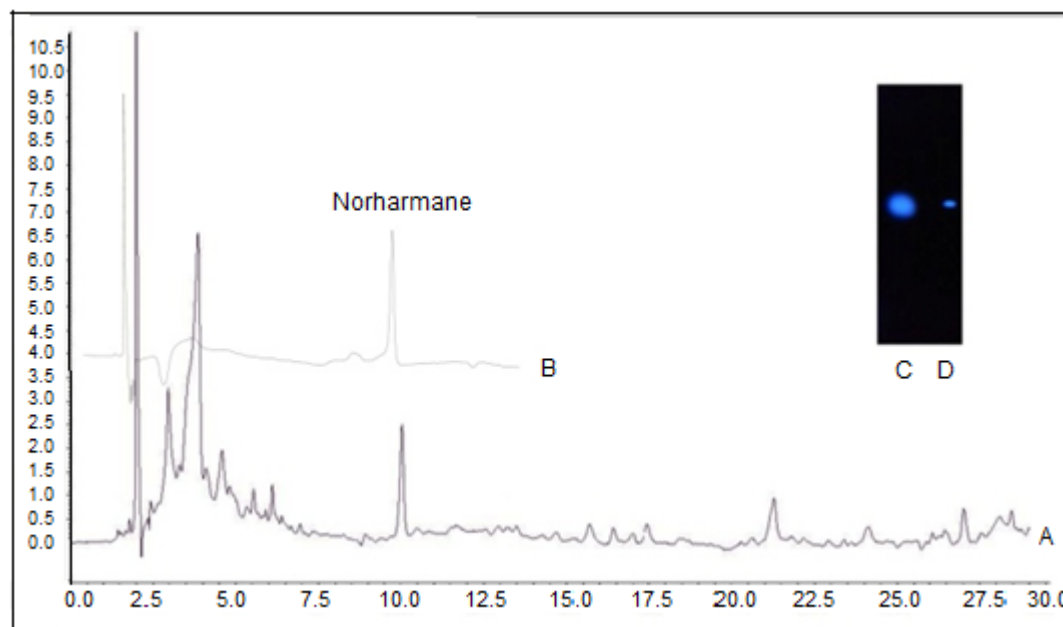


Figure 2. HPLC chromatograms of extract (A), standard, norharmane (B), TLC (UV 254 nm) of *C. minutus* extract (C), and norharmane (D), EtOAc as a mobile phase.

2.8. Statistical Analyses

All experiments were executed with three times. The statistical analysis were carried out by ANOVA and using the SPSS software (SPSS Inc., version 20).

3. RESULTS AND DISCUSSION

The identification of *C. minutus* was carried out by NCBI-BLAST analysis. According to 16 S rRNA analysis, a partial sequence of 1437/1437 base pairs (bp)

similarities were 100%. Nucleotide sequence accession number was GQ375047.1. The samples taken for every 4 days were calculated by thoma lame. The growth curve of *C. minutus* was presented (Table 2). To determine time and amount of norharmane production, HPLC analyses were executed. The most growth rate was observed at 12-16 days and the maximum production of norharmane was also detected at same time interval. Algae can live within a certain range of enhanced salt concentrations. The salt stress was evaluated at 0.50, 1, 3, and 5 M concentrations of nutrient media (Table 3).

Table 2. Cell number, biomass and norharmane production of *C. minutus* under stress conditions. Values are means \pm standard deviation (n= 3)

Stress conditions	Cell number ($\times 10^4$ ml $^{-1}$)	Biomass (g l $^{-1}$)	Total norharmane (μ g g $^{-1}$)
5 (pH)	63.333 \pm 4.163 ^a	0.028 \pm 0.005 ^a	0.146 \pm 0.002 ^a
9 (pH)	133.667 \pm 4.041 ^c	0.194 \pm 0.003 ^c	3.192 \pm 0.008 ^c
7 (pH) Control	124.000 \pm 3.000 ^b	0.160 \pm 0.011 ^b	8.816 \pm 0.323 ^b
0.5 M	124.667 \pm 4.163 ^c	0.178 \pm 0.004 ^d	9.823 \pm 0.421 ^b
1.0 M	133.667 \pm 3.512 ^d	0.210 \pm 0.004 ^e	10.803 \pm 0.055 ^c
3.0 M	88.667 \pm 8.327 ^b	0.085 \pm 0.004 ^b	12.720 \pm 0.087 ^d
5.0 M	67.667 \pm 3.215 ^a	0.074 \pm 0.004 ^a	16.066 \pm 0.208 ^e
Control	124.000 \pm 3.000 ^c	0.160 \pm 0.011 ^c	8.816 \pm 0.323 ^a

*Means followed by different letters (a, b, c, d, e) are significantly different at $p < 0.001$. M indicates the salt concentration.

At 0.5 M the growth was almost same as the control (133.6×10^4 cell ml $^{-1}$). The growth was better than control at 1.0 M (133.6×10^4 cell ml $^{-1}$). The growth decreased at 3 and 5 M concentrations since the *C. minutus* did not tolerate the salt at these concentrations. There was a direct proportion with the production of norharmane and salt concentrations. All norharmane

production values were higher than that of the control. The production of norharmane was 9.823μ g g $^{-1}$ at 0.5 M concentration. At the 1.0 and 3.0 M the norharmane productions were 10.80μ g g $^{-1}$ and 12.72μ g g $^{-1}$ respectively. The maximum norharmane production was observed as 16.07μ g g $^{-1}$ at the 5.0 M.

Table 3. Cell number, biomass and total norharmane of *C. minutus* for days. Values are means \pm standard deviation (n= 3)

Days	Cell number ($\times 10^4$ ml $^{-1}$)	Biomass (g l $^{-1}$)	Total norharmane (μ g g $^{-1}$)
0-4	48.00 \pm 0.00 ^a	0.033 \pm 0.012	0.410 \pm 0.265
4-8	56.67 \pm 1.16 ^b	0.053 \pm 0.025	1.086 \pm 0.212
8-12	82.00 \pm 2.00 ^d	0.050 \pm 0.020	0.910 \pm 0.132
12-16	126.00 \pm 2.00 ^f	0.163 \pm 0.042	8.816 \pm 2.665
16-20	105.33 \pm 1.16 ^e	0.157 \pm 0.047	3.063 \pm 0.625
20-24	84.67 \pm 3.06 ^d	0.043 \pm 0.006	1.273 \pm 0.186
24-28	64.00 \pm 2.00 ^c	0.026 \pm 0.006	0.035 \pm 0.007

*Means followed by different letters (a, b, c, d, e) are significantly different at $p < 0.001$.

The norharmane production and growth were investigated at pH 5 and 9. The growth was 133.66×10^4 cells ml^{-1} and 63.33×10^4 cells ml^{-1} at pH 9 and 5, respectively. *C. minutus* preferred a basic medium for growth. The best norharmane production was observed as $8.82 \mu\text{g g}^{-1}$ at pH 7. The norharmane production was $0.146 \mu\text{g g}^{-1}$ at pH 5 whereas; it was $3.19 \mu\text{g g}^{-1}$ at pH 9 (Figure 2).

4. CONCLUSION

Cyanobacteria have been considered to be a promising source of highly valuable compounds for the pharmaceutical industry. The optimum norharmane synthesis requirements by *C. minutus* were depicted under the stress conditions. Recently, the identification of cyanobacteria has been executed by combination of morphologic and molecular aspect.²⁷ Therefore, the morphological characterization of cyanobacteria was supported by molecularly, 16S rRNA gene sequence in our research. The sample matched with 1437/1437 bp region of *C. minutus* at 100%. Cyanobacteria need the water, light, carbon dioxide, and inorganic compounds for survival.²⁸ Cyanobacteria can flourish under particular environmental conditions. The specific nutrient media are available for cultivation of cyanobacteria such as Bristol and BG-11.²⁹ Bristol medium has been preferred for cultivation of *C. minutus* for a month period. Maximum growth of *C. minutus* was observed at 12th and 16th days interval. In addition, *C. minutus* excreted the most norharmane at the same time interval. It was reported that the amount of metabolites has been increased proportionally with the culture age.³⁰ The exposure of salt stress of *C. minutus* resulted in the high norharmane production. The most norharmane production was observed at 5.0 M caused by the synthesis of secondary metabolites of *C. minutus* for adaptation to the environment. Life condition of *C. minutus* was presented. The conditions of most norharmane production were depicted. The cultivation conditions of *C. minutus* were revealed to isolate the most norharmane. Due to the containing of pharmaceutically significant compounds of cyanobacteria, isolation of corresponding compounds should be carried out in the further work.

ACKNOWLEDGEMENTS

The authors acknowledge the financial assistance provided by Gaziosmanpasa University Research Council (No: 2013/128).

Conflict of interest


Authors declare that there is no a conflict of interest with any person, institute, company, etc.


REFERENCES


- Bano, A.; Siddiqui, P. J. A. *Pakistan J. Bot.* **2004**, 36 (1), 133-143.
- Burja, A.; Abou-Mansour, E.; Banaigs, B.; Payri, C.; Burgess, J.; Wright, P. *J. Microbiol. Meth.* **2002**, 48 (2), 207-219.
- Goyal, A. *Plant Physiol. Bioch.* **2007**, 45 (9), 705-710.
- Yoshida, K.; Igarashi, E.; Wakatsuki, E.; Miyamoto, K.; Hirata, K. *Plant Sci.* **2004**, 167 (6), 1335-1341.
- Hu, Y. W.; Chen, J. H.; Hu, G. P.; Yu, J. C.; Zhu, X.; Lin, Y. C.; Chen, S. P.; Yuan, J. *Mar. Drugs* **2015**, 13 (1), 202-221.
- Molinski, T. F.; Dalisay, D. S.; Lievens, S. L.; Saludes, J. P. *Nat. Rev. Drug Discov.* **2009**, 8 (1), 69-85.
- Erenler, R.; Pabuccu, K.; Yaglioglu, A. S.; Demirtas, I.; Gul, F. Z. *Naturforsch. C* **2016**, 71 (3-4), 87-92.
- Faulkner, D. J. *Nat. Prod. Rep.* **2002**, 19 (1), 1-48.
- Awad, N. E. *Phytother. Res.* **2000**, 14 (8), 641-643.
- Chen, J. L.; Gerwick, W. H.; Schatzman, R.; Laney, M. *J. Nat. Prod.* **1994**, 57 (7), 947-952.
- Mao, S. C.; Guo, Y. W.; Shen, X. *Bioorg. Med. Chem. Lett.* **2006**, 16 (11), 2947-2950.
- Kubanek, J.; Jensen, P. R.; Keifer, P. A.; Sullards, M. C.; Collins, D. O.; Fenical, W. *P Natl. Acad. Sci. USA* **2003**, 100 (12), 6916-6921.
- Pereira, H. S.; Leao-Ferreira, L. R.; Moussatche, N.; Teixeira, V. L.; Cavalcanti, D. N.; Costa, L. J.; Diaz, R.; Frugulhetti, I. C. P. *Antivir. Res.* **2004**, 64 (1), 69-76.
- Kim, Y. C.; An, R. B.; Yoon, N. Y.; Nam, T. J.; Choi, J. S. *Arch. Pharm. Res.* **2005**, 28 (12), 1376-1380.
- Fisch, K. M.; Bohm, V.; Wright, A. D.; Konig, G. M. *J. Nat. Prod.* **2003**, 66 (7), 968-975.
- Lee, Y. S.; Shin, K. H.; Kim, B. K.; Lee, S. *Arch. Pharm. Res.* **2004**, 27 (11), 1120-1122.
- Fuller, R. W.; Cardellina, J. H.; Jurek, J.; Scheuer, P. J.; Alvaradolindner, B.; Mcguire, M.; Gray, G. N.; Steiner, J. R.; Clardy, J.; Menez, E.; Shoemaker, R. H.; Newman, D. J.; Snader, K. M.; Boyd, M. R. *J. Med. Chem.* **1994**, 37 (25), 4407-4411.
- Schaeffer, D. J.; Krylov, V. S. *Ecotox. Environ. Safe.* **2000**, 45 (3), 208-227.


19. Robinson, E. S. J.; Anderson, N. J.; Crosby, J.; Nutt, D. J.; Hudson, A. L. *Ann. Ny. Acad. Sci.* **2003**, 1009, 157-166.
20. Chiarugi, A.; Dello Sbarba, P.; Paccagnini, A.; Donnini, S.; Filippi, S.; Moroni, F. *J. Leukocyte Biol.* **2000**, 68 (2), 260-266.
21. Karan, T.; Altuner, Z.; Erenler, R. *J. New Results Sci.* **2017**, 6 (1), 47-52.
22. Volk, R. B. *Microbiol. Res.* **2008**, 163 (3), 307-313.
23. John, D. M.; B.A., W.; Brook, A. J. *The Freshwater Algal Flora of the British Isles. An Identification Guide to Freshwater and Terrestrial Algae.* Cambridge University Press: England, 2002.
24. Mishra, A.; Jha, B. *Bioresource Technol.* **2009**, 100 (13), 3382-3386.
25. Pelah, D.; Sintov, A.; Cohen, E. *World J. Microb. Biot.* **2004**, 20 (5), 483-486.
26. Erenler, R.; Telci, I.; Ulutas, M.; Demirtas, I.; Gul, F.; Elmastas, M.; Kayir, O. *J. Food Biochem.* **2015**, 39 (5), 622-630.
27. Hoffmann, L.; Komarek, J.; Kastovsky, J. *Algol. Stud.* **2005**, 117 (1), 95-115.
28. Hagemann, M. *FEMS Microbiol. Rev.* **2011**, 35 (1), 87-123.
29. Gupta, N.; Bhaskar, A. S. B.; Rao, P. V. L. *World J. Microb. Biot.* **2002**, 18 (1), 29-35.
30. Dias, E.; Pereira, P.; Franca, S. *J. Phycol.* **2002**, 38 (4), 705-712.

ORCID

 0000-0002-9114-8400 (T. Karan)

 0000-0003-2335-2116 (Z. Altuner)

 0000-0002-4091-9033 (O. Kayir)

 0000-0002-0505-3190 (R. Erenler)

Evaluation of the wound healing potential of *Teucroside*Seçil ERDEN TAYHAN^{1,*}, Sema BİLGİN², Mahfuz ELMASTAŞ³¹Department of Genetic and Bioengineering, Faculty of Natural Science and Engineering, Gaziosmanpaşa University, 60240, Tokat, Turkey²Department of Chemistry, Faculty of Science and Arts, Gaziosmanpaşa University, 60240, Tokat, Turkey³Department of Basic Pharmacy Sciences, Faculty of Pharmacy, Sağlık Bilimleri University, 34668, İstanbul, Turkey

Received: 18 October 2017, Revised: 05 January 2018; Accepted: 07 February 2018

*Corresponding author's e-mail address: ysecilerden@gmail.com (S. Erden Tayhan)

ABSTRACT

Herbal medicines are being used for primary health care due to their efficacy, safety and less side effects. *Teucrium* genus is a member of the Lamiaceae family, which is a medicinal plant have been used in traditional medicine, especially for wound healing and inflammatory conditions. *Teucroside*, 9'-decarboxyrosmarinic acid-4'-O- α -rhamnosyl-(1'' \rightarrow 6''')-O- β -galactosyl-(1'' \rightarrow 4''')-O- α -rhamnoside is a natural phenolic compound which is isolated and identified from of *Teucrium* genus. In this study, because of bioactive properties of *Teucroside*, it was decided to examine its potential wound healing effect. Wound healing process was investigated by *in vitro* scratch assay which was an easy, inexpensive and well developed method to measure cell migration. In this context, firstly, cell viability was determined by MTT assay and the results were evaluated to find effective concentration for wound healing. Then the cells were incubated for 48 h with extract with defined concentration. Finally, after 48 hours of incubation with *teucroside*, the wound healing was calculated as 47%. When the data were compared with untreated control (49%), it was concluded that *teucroside* had not wound healing potential.

Keywords: *Teucroside*, *Lamiaceae*, wound healing, scratch assay.

Teukrosit'in yara iyileştirme potansiyelinin değerlendirilmesi

ÖZ

Bitkisel ilaçlar, etkinliği, güvenliği ve daha az yan etkileri nedeniyle primer sağlık hizmetinde kullanılmaktadır. *Teucrium* cinsi, özellikle yara iyileşmesi ve enflamatuvar durumlar için geleneksel tıpta kullanılan bir tıbbi bitki olan Lamiaceae familyasının bir üyesidir. *Teukrosit*, 9'-dekarboksiosmarinik asit-4'-O- α -ramnozil-(1'' \rightarrow 6''')-O- β -galaktozil-(1'' \rightarrow 4''')-O- α -ramnozid, *Teucrium* cinsinden izole edilen ve karakterize edilen doğal fenolik bir bileşiktir. Bu çalışmada, *Teukrosit*'in biyoaktif özelliklerinden dolayı onun potansiyel yara iyileştirme etkilerini incelemeye karar verilmiştir. Yara iyileşme süreci; kolay, ucuz ve hücre migrasyonunu ölçmek için iyi geliştirilmiş bir metot olan *in vitro* çizik testi ile araştırılmıştır. Bu bağlamda ilk olarak, hücre canlılığı MTT analizi ile gerçekleştirildi ve sonuçlar, yara iyileşmesinde etkin dozu bulmak için değerlendirildi. Ardından, hücreler, belli konsantrasyona sahip özütleme ile 48 saatliğine inkübe edildi. Son olarak, *Teukrosit* ile 48 saatlik inkübasyon sonunda, yara iyileşmesi % 47 olarak hesaplanmıştır. Bu veriler, negatif kontrolle (%49) karşılaştırıldığında *teukrosit*'in, yara iyileşme potansiyeline sahip olmadığı sonucuna varıldı.

Anahtar Kelimeler: *Teukrosit*, *Lamiaceae*, yara iyileşme, çizik testi.

1. INTRODUCTION

The genus *Teucrium*, belonging to the *Lamiaceae* family is represented by about 300 species widespread all over the world, 27 of which are grown in Turkey.¹ Due to its pharmacological effects, various species of this genus are used widely in traditional medicine for their antioxidant, diuretic, antiulcer, antitumor, anti-inflammatory antispasmodic and antibacterial

properties.² Therefore, the interest towards *Teucrium* species has increased recent years. One of the most common and highly investigated species in the genus is *Teucrium chamaedrys* (germander). Phytochemical constituents of this species comprise flavonoids, diterpenoids and glycosides.^{1,3} Phenylethanoid glycosides are the main phenolic compounds in *Teucrium* species. Recently reports have shown the wide range of biological and pharmacological properties of these

components. *Teucroside* (9'-decarboxyrosmarinic acid-4'-O- α -rhamnosyl-(1" \rightarrow 6")-O- β -galactosyl-(1" \rightarrow 4"))-O- α -rhamnoside) is L-lyxose containing phenylethanoid glycoside found in *Teucrium* genus.⁴

Wound healing is the general repair response of the body immediately after the disruption of skin integrity. Following injury, an inflammatory response occurs and the fibroblast cells in dermis produce collagen to regenerate connective tissue. Following this process, the epithelial cells of outer skin are repaired. Wound healing is a systematic and dynamic process which can be divided into four phases: hemostasis, inflammation, proliferation, and maturation. Although there has been an enormous development in pharmaceutical industry, the treatment of wounds is sometimes problematic by known wound healing drugs. Because they have low viability and various detrimental side effects.^{5,6} Therefore, plant derived drugs is under great demand due to common belief that they are safe, reliable and effective. Agents with wound healing potential, which are obtained from natural and synthetic bioactive materials have the antioxidant, chelation and antimicrobial activities; and may act by one or more of these mechanisms. Because of these bioactive properties of *teucroside*, it is decided to examine the potential wound healing effect of this phenolic compound.

Within the scope of this work, wound healing process was investigated by *in vitro* scratch assay which was an easy, inexpensive and well developed method for analysis of cell migration and proliferation *in vitro*. Two-dimensional *in vitro* cell migration assays are used to investigate the re-colonizing ability of cell populations.⁷ During this experiment, cells are placed on a culture dish and growth cell monolayer. Then, artificial wound is created with a p200 pipette tip and the images of spreading of the resulting collective cell, driven by combined cell migration and proliferation, are captured over 24-48 h.⁸

2. MATERIALS AND METHODS

2.1. Materials

Commercial reagents were purchased from chemical suppliers. L929 cell lines were kindly provided by Ege University Animal Cell Culture and Tissue Engineering Laboratory. All cell culture reagents and products were obtained commercially.

2.2. Methods

2.2.1. Extraction, isolation and identification of *Teucroside*

Teucroside was extracted, isolated and identified with methods which were explained in previous study by Dr. Elmastaş and his team.¹

2.2.2. Fibroblast cell culture

L929 mouse fibroblast cells were cultured with DMEM-high glucose supplemented with 10% FBS at 37°C in a humidified atmosphere of 95% air and 5% CO₂. Cultivating media was changed every 2 days.

2.2.3. MTT assay

In the present study, firstly MTT (3-(4,5-dimethylthiazol-2-yl)-2,5-diphenyltetrazolium bromide) assay was performed with L929 mouse fibroblast cells to determine effective concentration for *teucroside*. The L929 cell suspension was prepared at a concentration of 4x10⁴ cell/ml and dispensed onto 96-well cell culture plates. The multiwell plates were incubated for 24 h. This test was performed at ten concentrations (from 200 μ g ml⁻¹ to 0.4 μ g ml⁻¹) and cells left in contact with compound for 48 h. Stock solution (200 μ g ml⁻¹) of the compound was prepared in DMSO (< 0.1% in culture medium) and filter sterilized prior to addition to the culture plate. After incubation, 100 μ l of MTT solvent (5 mg ml⁻¹) was added into each well and then incubated at 37°C for 3 h. For the viability assay, MTT was removed and the formazan product was dissolved in 100 μ l of DMSO and the absorbance was measured at 570 nm with a multimode microplate reader.

2.2.4. *In vitro* wound healing assay

In the present study, preliminary investigation was performed for wound healing effect of *teucroside* by *in vitro* scratch assay. This assay is widely used when quantifying migration rate, as it provides a simple and economical set up in the hands of experienced users. The first step was creating an artificial wound in a cell monolayer. Then, capturing images at the beginning and at regular intervals during cell migration was performed. Finally the migration rate of the cells was quantified by comparing cell micrographs.⁹⁻¹¹

For *in vitro* scratch assay, The L929 cell suspension was prepared at a concentration of 5x10⁴ cell/ml and dispensed onto 6-well cell culture plate. When the cells reached to 90% confluency at this plate, the cell monolayer was scraped with sterile p200 pipette tip in a straight line to create a scratch. The debris was removed and smoothed the edge of the scratch by washing the cells with culture medium.¹¹ Then cells were incubated with *teucroside* containing media at 50 μ g ml⁻¹ concentration which was defined by MTT assay. After 24 and 48 h incubation, cell images were captured by phase contrast inverted microscope and analyzed quantitatively by image analysis software which was supplied by Olympus. Finally, percent wound healing was calculated and the results were plotted.

3. RESULTS AND DISCUSSION

To determine wound healing effect of *teucroside in vitro*, L929 cells were incubated with this fenolic compound. Firstly, MTT assay was performed and cell viabilities were calculated to determine effective concentration for scratch assay. As a result, L929 cells which were incubated with *teucroside* solution at 50 $\mu\text{g ml}^{-1}$ concentration for 48 hours, demonstrated the highest cell viability against negative control (Figure 1).

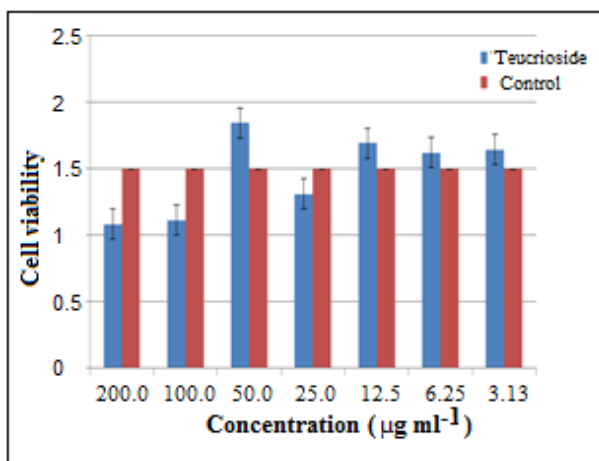


Figure 1. Effects of teucroside on the proliferation of L929 cell lines.

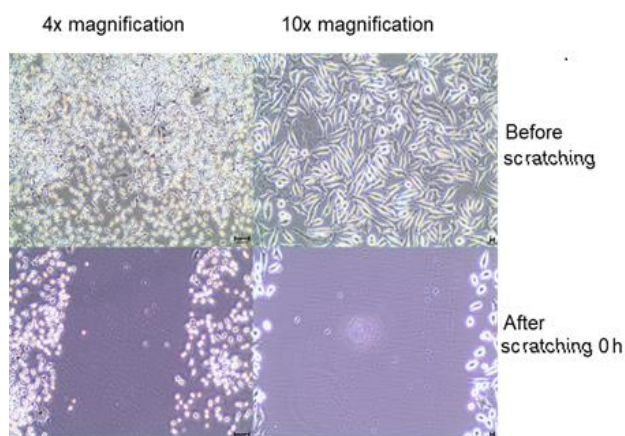


Figure 2. Inverted light microscope images of L929 cell lines before scratching and after scratching (0h). The scale bars indicated 10 μm .

According to MTT assay results, *in vitro* scratch assay was carried out with L929 cells and *teucroside* solution at 50 $\mu\text{g ml}^{-1}$ concentration. It was clearly observed that following 48 hours of incubation of the *teucroside* with L929 cells, the percent wound healing was calculated as 47% (Figure 2 and 3).

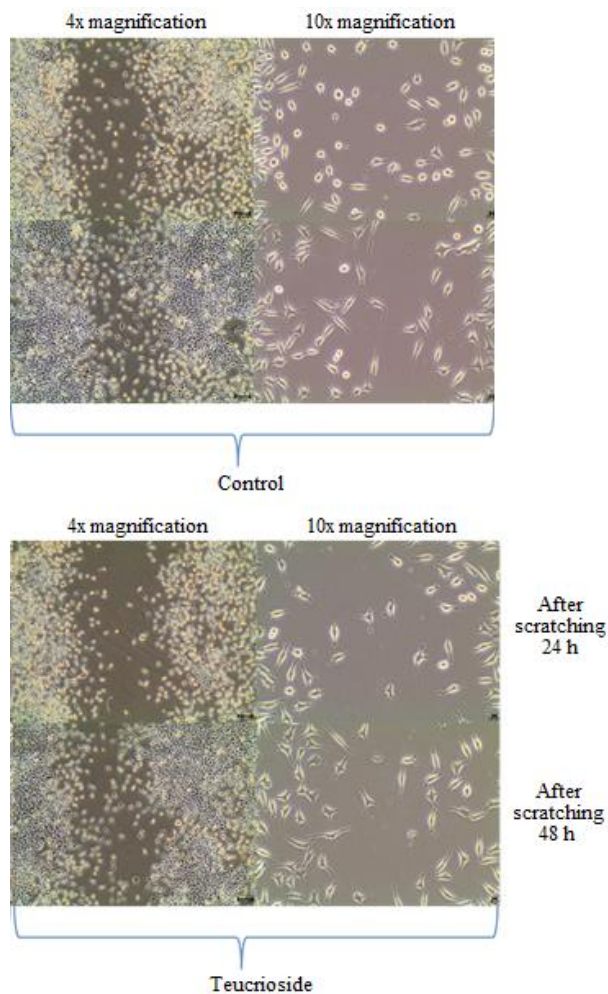


Figure 3. Inverted light microscope images of L929 cell lines after scratching (24 and 48 hours). The scale bars indicated 10 μm .

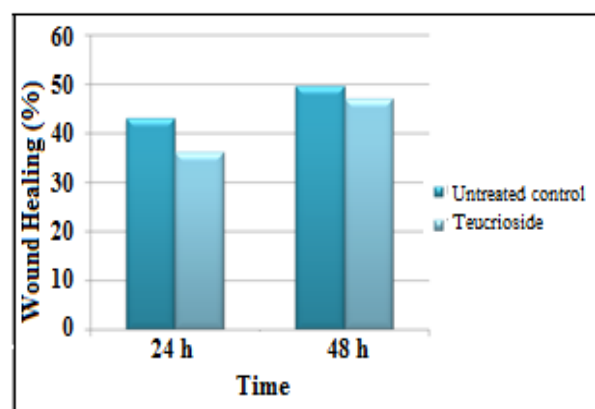


Figure 4. Wound healing effects of teucroside against untreated control.

When this data was compared with untreated control (49%), it was concluded that *teucroside* had not wound healing potential due to fibroblast stimulation (Figure 4).

4. CONCLUSIONS

Wounds can be defined as the disruption of tissue integrity because of several intrinsic and extrinsic factors. Complex reconstruction of the wound tissue requires cell activation to arrange proper transportation of nutrients and oxygen. In the current study, *teucroside* which was isolated from *Teucrium chamaedrys* was shown had not wound healing potential due to fibroblast stimulation, considered as important factor in dermis regeneration.

Conflict of Interest

Authors declare that there is no a conflict of interest with any person, institute, company, etc.

REFERENCES

1. Elmastas, M; Erenler, R; Isnac, B; Aksit, H; Sen, O; Genc, N; Demirtas, I. *Nat. Prod. Res.* **2016**, 30 (3), 299-304.
2. Antognoni, F; Iannello, C; Mandrone, M.; Scognamiglio, M; Fiorentino, A; Giovannini, P. P; Poli, F. *Phytochemistry.* **2012**, 81, 50-59.
3. Bedir, E.; Manyam, R; Khan, IA. *Phytochemistry.* **2003**, 63, 977-983.
4. El-Mousallamy, M.D; Hawas, U. W; Hussein, S. A.M. *Phytochemistry.* **2000**, 55, 927-931.
5. Demirci, S; Doğan, A; Demirci, Y; Şahin, F. *IJARNP.* **2008**, , 7(3), 37-44.

6. Lodhi, S; Jain, A.P; Rai, G; Yadaw, A. K. *J. Ayurveda Integr. Med.* **2016**, 7(1), 14-22.

7. Jin, W; Shah, E. T; Penington, C. J; McCue, S. W; Chopin, L. K; Simpson, M. J; *J. Theo. Biol.* **2016**, 390, 136-145.

8. Johnston, S. T; Ross, J. V; Binder, B.J; McElwain, D.L.S; Haridas, P; Simpson, M. J. *J. Theo. Biol.* **2016**, 400, 19-31.


9. Oh, J; Hlatky, L; Jeong, Y.S; Kim, D. T. *Toxins.* **2016**, 8, 199.


10. Alizadeh, AM; Sohanaki, H; Khaniki, M; Mohaghheghi, M.A; Ghmami, G; Mosavi, M. *Iran J. Basic Med. Sci.* **2011**, 14(6), 499-505.

11. Liang, C.C; Park, A.Y; Guan, J.L. *Nat. Protoc.* **2007**, 2(2), 329-333.

ORCID

 0000-0001-8473-5896 (S. Erden Tayhan)

 0000-0001-5921-5434 (S. Bilgin)

 0000-0002-7149-7427 (M. Elmastaş)



Application of Sepiolite-Poly(vinylimidazole) composite for the removal of Cu(II): Thermodynamics and isotherm studies

Ali KARA^{1,*}, Muhsin KILIÇ², Nalan TEKİN³, Nuray DINIBÜTÜN¹, Akif ŞAFAKLI³

¹Uludağ University, Faculty of Arts and Science, Department of Chemistry, 16059 Bursa, Turkey

²Uludağ University, Faculty of Engineering, Department of Machine, 16059 Bursa, Turkey

³Kocaeli University, Faculty of Arts and Science, Department of Chemistry, 41380 Kocaeli, Turkey

Received: 03 October 2017, Revised: 01 February 2018; Accepted: 13 February 2018

*Corresponding author's e-mail address: akara@uludag.edu.tr (A. Kara)

ABSTRACT

For removal of Cu(II) ions from aqueous solutions, a novel composite was prepared from 1-vinyl imidazole and sepiolite by the technique of in-situ polymerization. Adsorption of Cu(II) ions onto Sepiolite-Poly(vinylimidazole) composite prepared has been studied at 277–338 K and the experimental data were analyzed using various isotherm models. The Langmuir and the Toth models procured the best fit to the experimental data of the adsorption among the two-parameter and three-parameter models, respectively. The adsorption equilibrium was reached in 3 h and the optimum pH for the adsorption was found to be 5. Adsorption isotherm modeling showed that the interaction between adsorbate and adsorbent is localized to monolayer adsorption. Maximum adsorption capacity (q_m) calculated from Langmuir isotherm was found to be 261.91 mg g⁻¹ at 25°C. The calculated thermodynamic parameters indicated an endothermic adsorption process. The composite is thought to be a promising adsorbent for the removal of Cu(II) ions.

Keywords: Sepiolite, composite, heavy metal, nonlinear isotherms.

Cu(II)'nin giderimi için Sepiolite Poly (vinylimidazol) kompozitinin uygulanması: Termodinamik ve izoterm çalışmaları

ÖZ

Sulu çözeltilerden Cu(II) iyonlarının giderimi için 1-vinyl imidazole ve sepiyolit kullanılarak in-situ polimerizasyon yöntemi ile yeni bir kompozit hazırlandı. Hazırlanan Sepiolite-Poly(vinylimidazole) kompoziti üzerine Cu(II) iyonlarının adsorpsiyonu 277–338 K sıcaklık aralığında çalışıldı ve deneysel veriler çeşitli izoterm modelleri kullanılarak analiz edildi. Langmuir ve Toth modelleri, sırasıyla iki parametrelili ve üç parametrelili modeller arasındaki adsorpsiyonun deneysel verilerine en iyi uyumu sağlamıştır. Adsorpsiyon dengesine 3 saatte ulaşıldı ve adsorpsiyon için optimum pH'nın 5 olduğu bulundu. Adsorpsiyon izoterm modellemesi adsorbat ve adsorban arasındaki etkileşimin tek tabakalı adsorpsiyonla sınırlandırılmış olduğunu gösterdi. Langmuir izoterminden hesaplanan maksimum adsorpsiyon kapasitesinin (q_m) 25°C'de 261.91 mg g⁻¹ olduğu bulundu. Hesaplanan termodinamik parametreler endotermik bir adsorpsiyon prosesine işaret etti. Hazırlanan kompozitin Cu(II) iyonlarının giderimi için umut verici bir adsorban olduğu düşünülmektedir.

Anahtar Kelimeler: Sepiolite, kompozit, ağır metal, nonlinear izotermiler.

1. INTRODUCTION

Heavy metal contamination is dangerous for ecological systems and living species due to their high toxicity and non-biodegradability.¹ Copper is a heavy metal, and is used for different applications such as stabilizers, pigments, paints, mining, pesticides, fertilizers, electro-plating and catalysts.² Copper can cause health problems such as gastrointestinal disturbance, Wilson's disease and lesions in the central nervous system at higher level.³ Therefore, the removal

of copper from wastewater and water resources is important to protect the environment and human health.

For the removal of copper in wastewaters, there are various common methods used such as chemical precipitation, oxidation–reduction, ion exchange, membrane filtration, flocculation, electrocoagulation, liquid–liquid extraction, electrodialysis and adsorption.^{4,5} Among the conventional techniques, the adsorption process is mainly preferred due to its highly selective, easy handling, high efficiency, flexibility in design, avoidance of chemical sludge and wide availability of

different adsorbents.^{6,7} Thus, effective and low-cost adsorbents for removing heavy metal ions from waste waters need to be developed. In recent years, various adsorbents have been widely used for the removal of Cu(II) from wastewaters.⁸⁻¹⁵

Clay-polymer composites have been considered as highly promising materials for many applications due to their unique properties such as thermal and mechanical stability, high particle dispersion, fire retardant, gas permeability and structural flexibility.¹⁶ Clays are chosen as fillers for clay/polymer composites due to excellent chemical stability and large specific surface areas.¹⁷ Although a few studies are reported on the removal of heavy metal ions by using clay-polymer composites, to the best of our knowledge, there is no report on the use of Sepiolite-Poly(vinylimidazole) (Sep-PVI) composite for removal of Cu(II).

Imidazole is a base and proton accepting monomer. Among imidazole-containing polymers, poly(vinylimidazole) (PVI) is used in prevalent studies because its imidazole groups have complexing properties with catalytic divalent metallic ions^{18,19} besides antimicrobial activity and biodegradability^{20,21} and low cost.¹⁹ Sepiolite involves a continuous two-dimensional tetrahedral sheet and is a phyllosilicate, so the structure of sepiolite differs from other layer silicates.²² The discontinuity of the silica sheets arises to the presence of silanol groups (Si-OH) at the tunnels edges. Hence sepiolite has a high specific surface area ($> 300 \text{ m}^2 \text{ g}^{-1}$) because of the tunnels in this structure. Therefore the interaction of interfacial between polymer and sepiolite enhances because of existence of silanol groups (Si-OH). Therefore, for the composite synthesized, the good dispersion of sepiolite within the polymer and improving of the mechanical and thermal properties are expected.¹⁷⁻²³

The equations of adsorption equilibrium isotherm elucidate the adsorption process at the equilibrium conditions for an adsorption process or solid-liquid adsorption system.²⁴ From these adsorption isotherms, Freundlich and Langmuir isotherm models are the mostly used isotherms. The linear regression has been substantially used to estimate the parameters of the isotherm model in the literature. But, a transformation to linear form from nonlinear isotherm equations causes usually to culminate in the difference between experimental and theoretical data. Hence this result leads to deflect the fit in linear plots.²⁵ A nonlinear isotherm method is more suitable to obtain the parameters of the adsorption equilibrium isotherm.²⁶

In the present work, Sep-PVI composite samples were synthesized by in situ polymerization. For the preparation of the composite, sepiolite was used without any chemical treatment as reinforcement filler. The characteristics of Sep-PVI composite were examined with various instrumental analyses such as differential scanning calorimetry (DSC), X-ray diffraction (XRD), scanning electron microscope (SEM), and Fourier

transform infrared spectroscopy (FTIR). The Sep-PVI composite was also used to removal of Cu(II) ions from aqueous solution. The adsorption of Cu(II) onto the Sep-PVI composite has been investigated under various conditions such as temperature, type of adsorbent and initial solution concentration. Additionally, non-linear isotherm methods were used to evaluate the parameters of the adsorption isotherm model of Cu(II) onto Sep-PVI composite.

2. MATERIALS AND METHODS

2.1. Materials

Sepiolite was obtained from Aktaş Lületaş Co., Eskişehir-Turkey. The chemical composition of the sepiolite consists of 53.47 % SiO₂, 23.55 % MgO, 0.71 % CaO, 0.43 % NiO, 0.19 % Al₂O₃, 0.16 % Fe₂O₃, and it exhibits a 21.49 % loss on ignition from XRF measurement. From the BET analysis, the specific surface area was $342 \text{ m}^2 \text{ g}^{-1}$ for sepiolite.²⁷ Azobisisobutyronitrile (AIBN) and 1-vinyl imidazole (VIM) were purchased from Fluka and Aldrich, respectively. Copper (II) nitrate trihydrate was supplied from Fluka (Hannover, Germany). All other chemicals used this study were procured from Merck (Darmstadt, Germany) and were of reagent grade.

2.2. Synthesis of Sep-PVI composite

The clay sample was sieved to size fraction of 75 μm , dried at 105°C in an oven for 24 h and then used for the preparation of composite, and for the adsorption experiments. In this work, Sep-PVI composite was synthesized through in situ polymerization. Firstly, 0.16 g AIBN, 10 mL 1-vinylimidazole, calculated sepiolite (sepiolite content in polymer matrix is 2.5 % wt.), and 10 mL deionized water were mixed in the flask. For good dispersion of sepiolite, the suspension prepared was agitated vigorously for 3 hours by using the ultrasonic bath. After the preparation of the suspension, N,N'-methylenebisacrylamide (0.2 g) was added the mixture. The mixture was then heated to 65°C in a water bath for 200 min at under nitrogen atmosphere. The synthesized composite was washed with excessive deionized water. After the cleaning, the Sep-PVI composite was dried and ground to powder form.

2.3. Characterization of the composite

XRD patterns of the samples were recorded on a Rigaku Ultima IV X-ray Diffractometer. The experimental conditions were copper K alpha (CuK α) radiation generated at 40 kV voltages, 30 mA current and a scan speed of 1°/min. For FTIR experiments, IR spectra of the samples were recorded by a Bruker Tensor 27

spectrophotometer. The spectra were obtained by using Diamond ATR in the range of 4000–400 cm^{-1} , with a 2 cm^{-1} resolution over 30 scans. The thermal properties of the composite were studied by using a DSC (Perkin Elmer DSC 4000) at a heat rate of 10 $^{\circ}\text{C min}^{-1}$ between room temperature and 1000 $^{\circ}\text{C}$. The surface morphology of the samples was investigated by SEM-EDX (JOEL 50 A) microscope including operations at 10 kV accelerating voltage. The surfaces of the samples were sputter-coated with gold before analysis.

2.4. Batch adsorption experiments

The adsorption experiments were carried out stirring in a beaker at 200 rpm by using a magnetic stirrer. The contact time to reach equilibrium was determined as 3 h. 50 mL of 100 mg l^{-1} stock Cu(II) ions solution and 0.1 g of dried sample of Sep-PVI composite were used for the all adsorption experiments. The pH effect on the Cu(II) ion adsorption capacity of Sep-PVI composite was investigated in the pH range between 2.0 and 6.5. The further adsorption experiments were performed at 277, 298, 318, and 338 K at an optimum pH value of 5.0. After the adsorption equilibrium, the supernatants were separated from the suspension by centrifugation for 5 min at 4500 rpm, and Cu(II) ions were analyzed by using an UV-vis spectrophotometer (Shimadzu-2100 UV-Vis, Japan). The adsorption capacity was calculated according to the following equation:

$$q_e = (C_0 - C_e) \frac{V}{m} \quad (1)$$

where, m (g) is the mass of the dried adsorbent, C_0 and C_e are the initial and equilibrium concentrations (mg l^{-1}) of Cu(II), V (l) is the volume of the Cu(II) solution and q_e (mg g^{-1}) is the adsorption capacity.

The non-linear isotherm models were evaluated by using the Cu(II) solutions ranging from 100 to 1000 mg l^{-1} at temperatures of 277, 298, 318, and 338 K for the adsorption.

3. Theory

3.1. Single- and two-parameter isotherms

According to Henry's law, the number of active sites is much higher than the number of solute molecules.²⁸ The adsorption isotherm equation is expressed by Eq. (2) (Table 1), where K_{HE} (l g^{-1}) is Henry's constant and C_e is Cu(II) equilibrium concentration (mg l^{-1}).

The Freundlich isotherm equation²⁹ is used for the definition of multilayer adsorption. This equation is given as by Eq. (3) Table 1, where, K_F is the constant of Freundlich isotherm representing adsorption capacity. n is the adsorption intensity, C_e is the equilibrium concentration (mg l^{-1}) of Cu(II) ions, and q_e (mg g^{-1}) is

the amount Cu(II) ions adsorbed per unit of the composite (namely, adsorption capacity of the composite). If the value of n is between 1 and 10, the adsorption is suitable.³⁰

The Langmuir isotherm model describes monolayer adsorption.³¹ The Langmuir isotherm is given by Eq. (4) (Table 1), where, K_L (l g^{-1}) is the equilibrium constant related to the adsorption enthalpy by means of the van't Hoff equation, C_e (mg l^{-1}) is the equilibrium Cu(II) concentration in the solution, q_e (mg g^{-1}) is adsorption capacity of the composite and q_m (mg g^{-1}) is the monolayer adsorption capacity of the composite.

The Dubinin–Radushkevich isotherm supposes that the energy of adsorption is homogeneous on the surface of the adsorbent and the adsorption curve is related to the porous structure of the adsorbent.³² In Eq. (5) (Table 1), where T is absolute temperature (K), R is the gas constant ($8.314 \text{ J mol}^{-1} \text{ K}^{-1}$), ε is Polanyi potential and it was calculated by using $RT \ln(1 + 1/C_e)$ equation, q_m is the D–R isotherm constant and C_e is the equilibrium Cu(II) concentration in the solution (mg l^{-1}). B is a constant which related to the adsorption energy. The value of E is calculated from $E = 1/\sqrt{2B}$ and the equation can be used to determine of the adsorption type.³³

The Temkin isotherm model assumes that the heat of the adsorption of the adsorbate molecules would decrease linearly with coverage due to the adsorbent and adsorbate interactions.³⁰⁻³³ It is presented by Eq. (6) (Table 1), in this equation, b is the variation of adsorption energy (J mol^{-1}), T is the temperature (K), $B_T = RT/b$ is related to the adsorption heat, R is the universal gas constant ($\text{J mol}^{-1} \text{ K}^{-1}$) and K_T is the equilibrium binding constant (l mg^{-1}) related to the maximum binding energy.

The Halsey isotherm model is used to confirm the heteroporous nature of the adsorbent and suitable for multilayer adsorption.³⁴ It can be given by Eq. (7) (Table 1), where q_e (mg g^{-1}) is adsorption capacity of the composite, K_H is the Halsey isotherm constant, n_H is the Halsey isotherm exponent and C_e (mg l^{-1}) is equilibrium concentration of Cu(II) ions in the solution.

3.2. Three-, four- and five-parameter isotherms

The Redlich-Peterson isotherm³⁵ model can be applied to both of homogenous and a heterogeneous system for a wide concentration range and it combines the properties of the Freundlich and Langmuir isotherms in a single equation. The isotherm equation is displayed by Eq. (8) (Table 1), in this equation, β is an exponent and the value of the exponent lies between 0 and 1, and K_R and a_{RP} are the constants of isotherm model (l mg^{-1}). If $\beta = 0$, it becomes the Henry's law and if $\beta = 1$, the isotherm equation turns out to the Langmuir isotherm equation.

The Sips isotherm³⁶ is a unification of the Langmuir and Freundlich isotherms. For low adsorbate concentrations, this isotherm equation reduces to the

Freundlich isotherm. The Sips isotherm equation foresees a monolayer adsorption capacity characteristic of the Langmuir isotherm at high adsorbate concentrations.³⁷ The isotherm equation given by Eq. (9) (Table 1), where K_s is the constant of Sips isotherm ($l\ g^{-1}$), q_m ($mg\ g^{-1}$) is the monolayer adsorption capacity of the composite, and γ is the model exponent of Sips isotherm.

The Khan isotherm model³⁸ is suggested to the pure solutions.³⁷ The isotherm model can be expressed by Eq. (10) (Table 1), in this equation, a_K and b_K are the exponent of the isotherm model and the constant of Khan model, respectively. Maximum adsorption capacity, q_m is predicted by the model with the correlation coefficients. If a_K equals to 1, Eq. (10) turns into the Langmuir isotherm. When $b_K C_e$ value is much bigger than unity, Eq. (10) can be turns into the Freundlich isotherm.³⁹

The Radke-Prausnitz isotherm⁴⁰ can be given by Eq. (11) (Table 1), where r_R and a_R are the constants of Radke-Prausnitz model, and β_R is the exponent of Radke-Prausnitz isotherm.

The Toth model⁴¹ is a special type of the Langmuir isotherm and convenient in defining heterogeneous adsorption.³⁷ It is given by Eq. (12) (Table 1), where b_T is the constant of Toth model and n_T is the exponent of Toth model and is associated with surface heterogeneity. If n_T is unity, the isotherm reduces to the Langmuir equation.

The Koble-Corrigan isotherm⁴² incorporates the Freundlich and Langmuir isotherm models to point out the adsorption equilibrium data. It can be given by Eq. (13) (Table 1), where B_{KC} , A_{KC} and n_{KC} are the constants of Koble-Corrigan isotherm model. When the adsorption experiments carried out at high adsorbate concentrations, the isotherm model approaches the Freundlich isotherm.⁴³

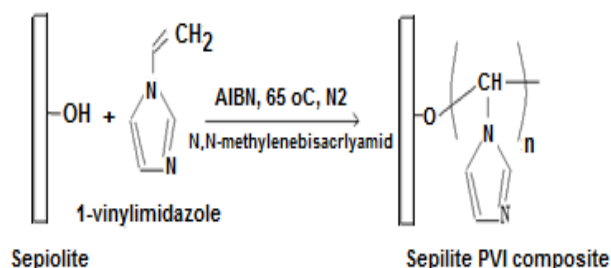
The Fritz and Schlunder model (four-parameter) developed to empirically four-parameter equation which is another form of Langmuir-Freundlich type isotherm model. The equation of this model expressed by Eq. (14) (Table 1), where B and A are the parameters of Fritz-Schlunder model, and α_{FS} and β_{FS} (α_{FS} and $\beta_{FS} \leq 1$) are the exponents of Fritz-Schlunder equation. For $\alpha_{FS} = \beta_{FS} = 1$, Eq. (15) reduces to the Langmuir equation and $K_L = B_{FS}$ is also the Langmuir isotherm constant ($l\ mg^{-1}$) related to the adsorption energy and $A = K_L q_m$.⁴⁵

The Fritz-Schlunder model (five-parameter) represents a wide field of equilibrium data through the five-parameter empirical expression.⁴⁴ It can be given by Eq. (15) (Table 1), where α_1 , α_2 , α , β_1 and β_2 (β_1 and $\beta_2 \leq 1$) are the Fritz-Schlunder parameters. When the exponent's β_1 and β_2 are equal to unity, the isotherm model reduces to Langmuir model and approaches the Freundlich model for higher liquid phase concentrations.⁴³

4. RESULTS AND DISCUSSION

4.1. Characterization of the Sep-PVI composite

The Sep-PVI composite was synthesized by in situ polymerization of sepiolite which was used without any chemical treatment and vinyl imidazole (VIM). The synthesis process was given in Scheme 1.



Scheme 1. The formation process proposed for Sep-PVI composite.

4.1.1. FTIR analysis

The FTIR spectra of Sep-PVI composite, PVI and sepiolite are given in Figure 1.

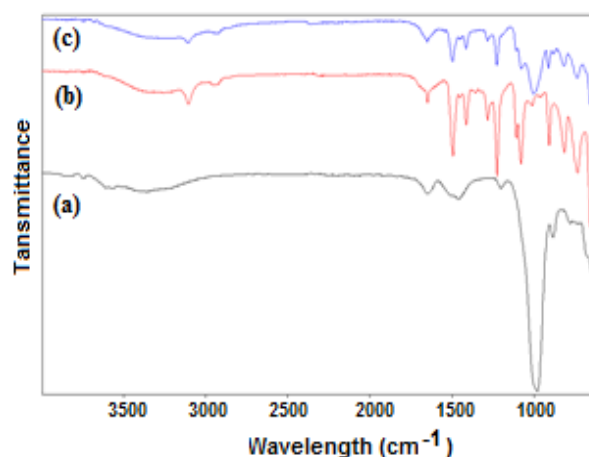


Figure 1. FTIR spectra of a) Sepiolite, b) PVI, and c) Sep-PVI composite.

In Figure 1a, the bands in the 4000–3000 cm^{-1} range is corresponding to Mg–OH bond vibrations⁴⁵, a band at 1655.06 cm^{-1} indicates the bending of zeolitic water, the bands in the 1200–600 cm^{-1} range is characteristic of silicate, the bands at 1202.83, 984.01 and 884.32 cm^{-1} can be attributed to the bonds of Si–O stretching vibration of the tetrahedral sheet^{45,46} and the bands at 782.20, 682.52 and 646.05 cm^{-1} are related to Mg–OH bond vibrations (deformation at 782.20 cm^{-1} and bending at 682.52 and 646.05 cm^{-1}).^{47,48} As shown in Figure 1b, the bands at 3106.57 cm^{-1} and 2953.40 cm^{-1} are corresponding to C–H (ring) and C–H (chain) stretching, respectively.⁴⁹ The bands appeared at 1497.02 cm^{-1} , 911.07 cm^{-1} and 816.24 cm^{-1} are correspond to C=N and

C=C stretching of imidazole rings, respectively. The absorption band at 660.64 cm^{-1} can be ascribed to bending vibration.^{49,50}

For Sep-PVI sample (Figure 1c), the bands observed at 3111.44 and 821.11 cm^{-1} can be ascribed to the stretching vibration of the C–H and C=N of imidazole rings, respectively. The characteristic peaks of PVI were appeared in the spectrum of Sep-PVI composite, and confirmed that the composite has been produced.

4.1.2. XRD Analysis

The XRD patterns in the range of $2\theta = 5^\circ\text{--}50^\circ$ for the sepiolite, the Sep-PVI composite and PVI are given in Figure 2. Figure 2a shows that the characteristic diffraction peak of sepiolite was found in the diffraction pattern at about $2\theta = 6.966^\circ$ (110), related to the reflections of internal channel.⁴⁵ The d-spacing of the characteristic diffraction peaks for sepiolite ($d_{110} = 12.68\text{ nm}$) and Sep-PVI composite ($d_{110} = 12.71\text{ nm}$) are very similar. One main reason is that unlike smectite clays, sepiolite exhibits a structure where TOT layers are mightily bonded by covalent bonds. Another possible reason is that the silanol groups attended to the polymerization are mainly presented on the whole external surface of sepiolite.⁵²

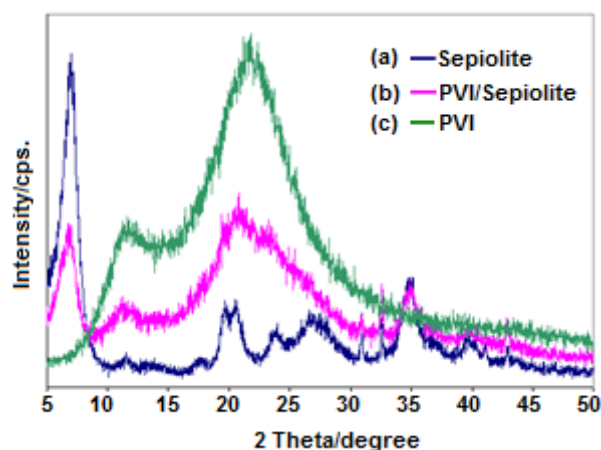


Figure 2. XRD patterns of the materials.

The diffraction intensity of Sep-PVI composite (Figure 2b) decreased when compared with sepiolite. The result was seen as an averment for substantially dispersion of sepiolite in PVI. Furthermore, some characteristic peaks of sepiolite were disappeared in the prepared composite. This may be ascribed to the homogenous dispersion of the sepiolite into PVI due to its bundles being generally delaminated to fiber sticks.⁵¹⁻⁵³

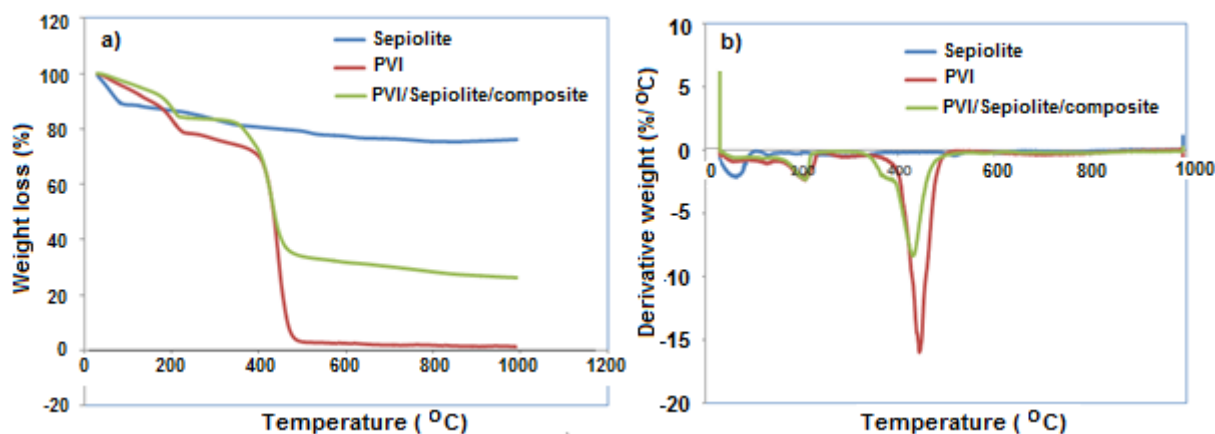


Figure 3. a) TGA, b) DTA curves of the materials.

4.1.3. TGA-DTA analysis

TGA and DTA curves of PVI, sepiolite and Sep-PVI composite are illustrated in Figure 3a and b. Figure 3a shows that the thermal decomposition of poly(vinylimidazole) is in one primary step and occurs in the temperature range of $340\text{--}500^\circ\text{C}$. In the TGA curve, the maximum of the decomposition temperature is determined at 450°C . The weight loss in the $340\text{--}500^\circ\text{C}$ temperature range is ascribed to PVI chain's decomposition.^{49,54,55} In the sepiolite thermogram, the

primary and first weight loss is near 100°C due to loss of zeolitic water that it is physically bonded to sepiolite in the structural channels and on the external surface.⁵⁶ Two of the four coordinated crystallization water molecules and the other two molecules of sepiolite are lost at about 300°C and at 520°C , respectively.^{46,57} Eventually, sepiolite lost hydroxyl groups or structural water around 750°C .⁴⁵ As can be seen from Figure 3a, the degradation temperature (429°C) of Sep-PVI composite prepared shifts to lower temperatures in compliance with PVI (444°C). The probable reason for these results may be

due to that the sepiolite catalyzes PVI degradation and/or the presence of sepiolite reducing the polymer chain stability via interparticular interactions.

4.1.4. SEM analysis

The surface morphology of the Sep-PVI composite was investigated by SEM analysis. Figure 4a-c shows the SEM images of sepiolite, PVI, and Sep-PVI composite respectively. SEM images in Figure 4a shows that sepiolite reveals stone-like aggregation. In SEM image of PVI, polymer showed spherical particulate structure. Additionally, PVI came into existence of particles with sizes $< 2\mu\text{m}$ (Figure 4b). It can be seen from Figure 4c, that the prepared Sep-PVI composite has a smooth and dense surface and sepiolite shows a good dispersion in PVI. Furthermore the surface of sepiolite is covered with PVI. A good adhesion was found between the PVI and the sepiolite due to strong hydrogen bonding between the silanol groups of sepiolite and PVI⁵⁸ and the high surface area of the sepiolite.⁵⁹

4.2. Effect of pH, initial concentration of Cu(II) ions and temperature on adsorption

The solution pH value makes a significant impact on the adsorption process due to protonation of functional groups in the adsorbent and the precipitation formation of

heavy metal ions.^{1-5,7,14} Considering the formation of Cu^{2+} hydroxide precipitate at higher pH values, the selected pH values in the batch experiments were set below 6.5 in this study. Also, the adsorption capacity of Sep-PVI composite for Cu^{2+} ions was investigated at the pH range of 2–6.5. It is found that the Cu^{2+} adsorption capacity of Sep-PVI composite increases with the initial pH increases from 2.0 to 6.5 and decreases when the initial pH is 6.0 (Figure is not shown). The optimal pH value for Cu^{2+} adsorption of by Sep-PVI composite is around 5. The imidazole groups of Sep-PVI composite are easily protonated at lower pH values, which means that more active sites are occupied by H^+ ions. When the initial solution pH value gradually increases, more active sites are deprotonated and the positive charge is reduced. This situation causes to a better affinity of the adsorbent to Cu(II) ions, resulting a higher adsorption capacity. Further as the pH value increases, hydroxide precipitate appears, and correspondingly the adsorption capacity declines. Thus, a pH value of 5 was selected for the following absorption studies.

The effect of different initial concentrations on adsorption of Cu(II) onto sepiolite and Sep-PVI composite is given in Figure 5. As can be seen in Figure 5, Cu(II) removal increases with an increase in the initial Cu(II) concentration. At higher Cu(II) concentration, this increase might be attributed to the increased contact probabilities between Cu(II) ions and the binding sites on the Sep-PVI composite.

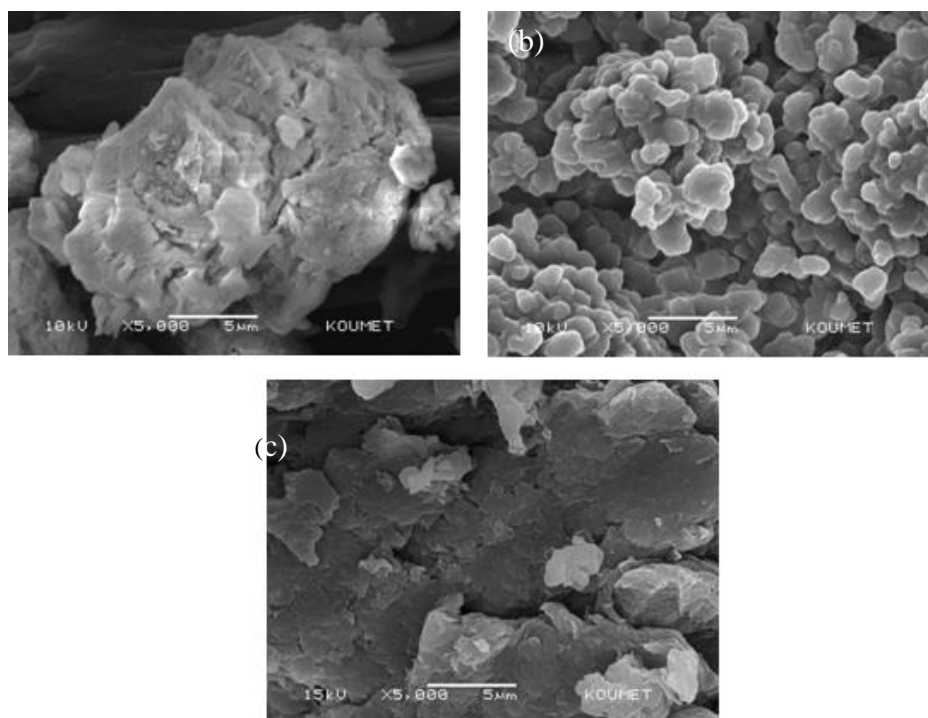


Figure 4. SEM photographs of: a) sepiolite, b) PVI and c) Sep-PVI composite.

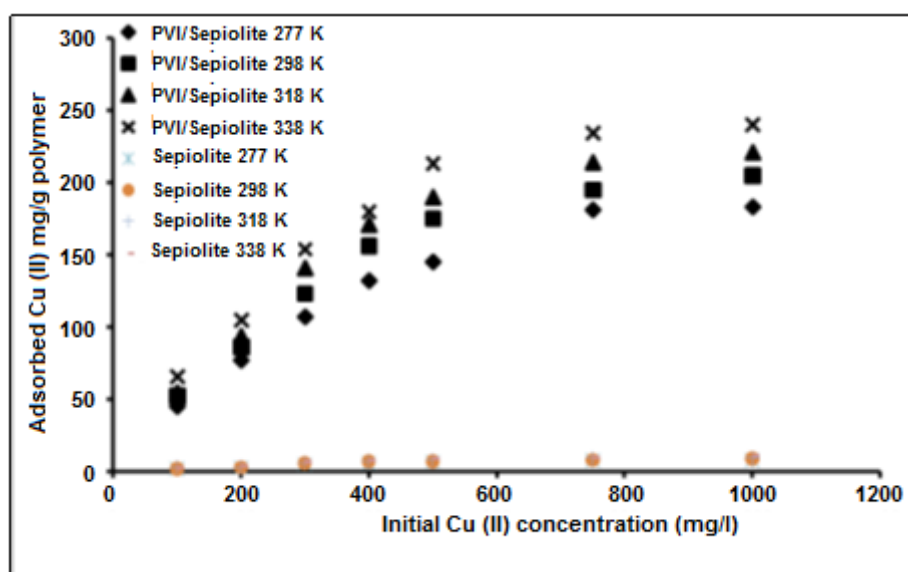


Figure 5. Effect of initial concentration of Cu(II) ions onto sepiolite and Sep-PVI composite.

In addition, the higher initial Cu(II) concentration provides an important driving force to overcome the mass transfer resistances between the Cu(II) aqueous solution and the Sep-PVI composite. As the binding sites are gradually occupied by Cu(II) ions, the adsorption process reaches the equilibrium. Also the Figure 5, for Cu(II) removal, shows that the adsorption capacity of prepared Sep-PVI composite is higher than that of sepiolite under the same adsorption conditions. The result can be explained with increase of the adsorption capacity of sepiolite for Cu(II) ions removal due to formation of composite with PVI. It is known that imidazole groups of PVI are complexed with divalent metallic ions catalyzed.¹⁹

The temperature effect on removal of Cu(II) ions by using sepiolite and Sep-PVI composite prepared was studied at different temperatures such as 277, 298, 318 and 338 K. The results obtained are shown in Figure 5. From this figure, it can be seen that the q_e values increase with increasing temperature. This situation may probably be attributed to higher collision frequencies at higher temperature.⁶⁰

4.3. Nonlinear isotherm analysis for adsorption

The parameters of the adsorption isotherm model were obtained by using nonlinear regression using SPSS (Ver.17). The fourteen isotherm models were used in

order to determine the characteristic parameters of the adsorption isotherm and predict the isotherms.

In the present study, the determination coefficient, R^2 was used to test the best-fitting isotherm to the experimental data:

$$R^2 = \frac{\sum_{i=1}^n (q_{meas} - \overline{q_{calc}})^2}{\sum_{i=1}^n (q_{meas} - \overline{q_{calc}})^2 + \sum_{i=1}^n (q_{meas} - q_{calc})^2} \quad (16)$$

In this equation, q_{calc} is the calculated the equilibrium solid phase concentration, $\overline{q_{calc}}$ is the average of q_{calc} and q_{meas} is the measured concentration of the equilibrium solid phase. If $R^2 = 1$, the fit is perfect for all points.

4.3.1. Single- and two-parameter isotherm models

The parameters of single- and two-parameter isotherm models are presented in Table 1. Figure 6 shows the predicted and experimental the single- and two-parameter isotherms by non-linear method for the adsorption of Cu(II) onto Sep-PVI composite.

Among the isotherm models, Henry's law has a single-parameter model and is the simplest one. Henry's law is feasible only in the lower range of adsorbate concentration.

Table 1. Isotherm parameters for the adsorption of Cu(II) onto Sep-PVI composite obtained by non-linear methods (single- and two-parameter isotherms)

Isotherm model	Equations	Equation No	Parameters			
			277 K	298 K	318 K	338 K
Henry	$q_e = K_{HE}C_e$	(2)	$K_{HE} = 0.299$ $R^2 = 0.834$	$K_{HE} = 0.347$ $R^2 = 0.773$	$K_{HE} = 0.388$ $R^2 = 0.738$	$K_{HE} = 0.436$ $R^2 = 0.738$
Freunlich	$q_e = K_F C_e^{1/n}$	(3)	$K_F = 9.8$ $n = 2.23$ $R^2 = 0.947$	$K_F = 14.55$ $n = 2.45$ $R^2 = 0.918$	$K_F = 18.25$ $n = 2.58$ $R^2 = 0.901$	$K_F = 24.24$ $n = 2.79$ $R^2 = 0.914$
Langmuir	$q_e = \frac{q_m K_L C_e}{(1 + K_L C_e)}$	(4)	$K_L = 0.00404$ $q_m = 247.52$ $R^2 = 0.990$	$K_L = 0.00525$ $q_m = 261.91$ $R^2 = 0.982$	$K_L = 0.00613$ $q_m = 277.84$ $R^2 = 0.981$	$K_L = 0.00744$ $q_m = 291.93$ $R = 0.978$
Dubinin-Radushkevich	$q_e = q_m \exp(-B[RT \ln(1 + 1/C_e)]^2)$	(5)	$B = 0.000728$ $q_m = 144.3$ $R^2 = 0.719$	$B = 0.000469$ $q_m = 162.9$ $R^2 = 0.722$	$B = 0.000375$ $q_m = 179.83$ $R^2 = 0.758$	$B = 0.00017$ $q_m = 190.78$ $R^2 = 0.663$
Temkin	$q_e = \frac{RT}{b} \ln(K_T C_e) = B_1 \ln(K_T C_e)$	(6)	$K_T = 0.0366$ $B_1 = 56.24$ $R^2 = 0.982$	$K_T = 0.0473$ $B_1 = 59.35$ $R^2 = 0.969$	$K_T = 0.0544$ $B_1 = 62.87$ $R^2 = 0.965$	$K_T = 0.0801$ $B_1 = 61.72$ $R^2 = 0.961$
Halsey	$q_e = (K_H C_e)^{1/n_H}$	(7)	$K_H = 162.34$ $n_H = 2.23$ $R^2 = 0.947$	$K_H = 706.34$ $n_H = 2.45$ $R^2 = 0.918$	$K_H = 1795$ $n_H = 2.58$ $R^2 = 0.901$	$K_H = 7291.9$ $n_H = 2.79$ $R^2 = 0.914$

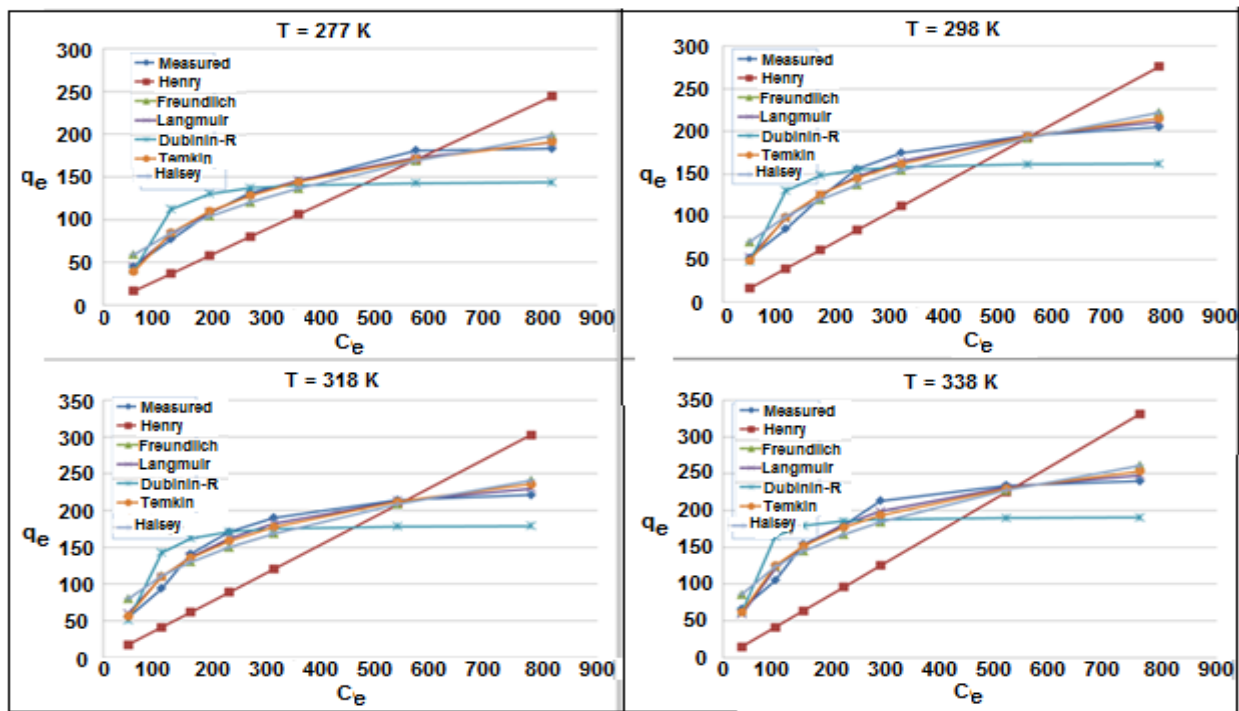


Figure 6. Single- and two-parameter isotherms obtained using the non-linear methods for the adsorption of Cu(II) onto Sep-PVI composite.

Therefore, it can be seen from Figure 6 and Table 1 that this model (R^2 varies from 0.738 to 0.834) completely fails to predict the adsorption equilibrium isotherm in this study.

For two-parameter isotherm models, the Langmuir isotherm model (R^2 varies from 0.978 to 0.990) provides a good fit to the experimental data for all temperatures whereas the Freundlich, Dubinin-Radushkevich, Temkin and Halsey values are considerably lower. The Langmuir equation is given in Eq. (4) (Table 1) where, q_m (mg g^{-1}) is the monolayer adsorption capacity of the composite, q_e (mg g^{-1}) is the equilibrium adsorption capacity, K_L (L g^{-1}) is the Langmuir constant related to the enthalpy of adsorption which is calculated by using the van't Hoff equation, and C_e is the equilibrium concentration (mg l^{-1}) of Cu(II).⁶¹ It can be deduced that surface of Sep-PVI composite is homogenous for the adsorption of Cu(II) ions by monolayer adsorption and all adsorption sites are equal. As shown in Table 1, the maximum adsorption values are 247.52, 261.91, 277.84 and 291.93 mg g^{-1} at 277, 298, 318 and 338 K, respectively. The parameter K_L is related to the affinity of adsorbate-adsorbent.⁶² K_L represents the equilibrium adsorption constant.⁶³ It was found that the adsorption process was more favorable at higher temperatures, and hereby the process is endothermic. According to the results, the best-fitted adsorption isotherm models were in the order: Langmuir

> Temkin > Freundlich = Halsey > Dubinin-Radushkevich.

4.3.2. Three-, four- and five-parameter isotherm models

The parameters of three-, four- and five-parameter isotherm models are presented in Table 2. Figure 7 shows the predicted and experimental the three-, four- and five-parameter isotherms by non-linear methods for the adsorption of Cu(II) onto Sep-PVI composite. The Khan and Toth isotherms have similar and high determination coefficients when compared to Radke-Prausnitz, Sips, Koble-Corrigan and Redlich-Peterson isotherms (Table 2). Although the R^2 values of the Khan isotherm model is satisfactory (0.986 to 0.995), the predicted values of q_m by the isotherm model do not match the experimental equilibrium data (Figure 7). Therefore, the Toth isotherm shows a better fit to the adsorption data for the adsorption of Cu(II). The coefficients of correlation of the Toth isotherm model are good (R^2 varied from 0.981 to 0.994) for all the tested systems. The order of the equilibrium constant, b_T , of Toth isotherm is similar to the equilibrium constant K_L of Langmuir. Therefore, Toth isotherm model is better precise for the experimental equilibrium data compared to other three-parameter isotherm models

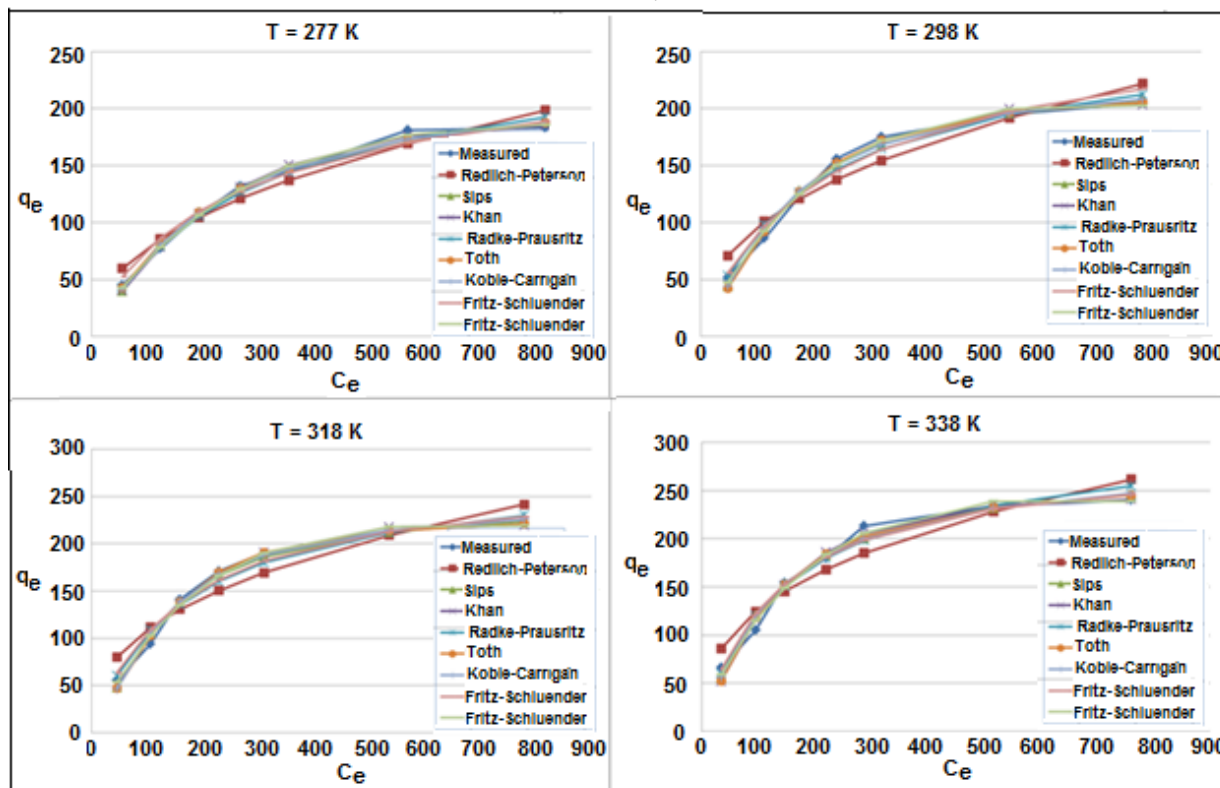


Figure 7. Three-, four- and five-parameter isotherms obtained using the non-linear methods for the adsorption of Cu(II) onto Sep-PVI composite

Table 2. Isotherm parameters for the adsorption of Cu(II) onto Sep-PVI composite obtained by non-linear methods (three-, four- and five-parameter isotherms)

Isotherm model	Equations	Equation No	Parameters			
			277 K	298 K	318 K	338 K
Redlich-Peterson	$q_e = \frac{K_R C_e}{1 + a_{RP} C_e^\beta}$	(8)	$K_R = 75.9$ $a_{RP} = 7.39$ $\beta = 0.56$ $R^2 = 0.949$	$K_R = 109.9$ $a_{RP} = 7.26$ $B = 0.598$ $R^2 = 0.919$	$K_R = 131.48$ $a_{RP} = 7.01$ $\beta = 0.616$ $R^2 = 0.903$	$K_R = 161.71$ $a_{RP} = 6.48$ $\beta = 0.646$ $R^2 = 0.915$
Sips	$q_e = q_m \frac{(K_S C_e)^\gamma}{1 + (K_S C_e)^\gamma}$	(9)	$q_m = 225.3$ $K_S = 0.00489$ $\gamma = 1.173$ $R^2 = 0.992$	$q_m = 233.9$ $K_S = 0.00655$ $\gamma = 1.263$ $R^2 = 0.987$	$q_m = 244.17$ $K_S = 0.00774$ $\gamma = 1.333$ $R^2 = 0.99$	$q_m = 281.2$ $K_S = 0.00806$ $\gamma = 1.081$ $R^2 = 0.979$
Khan	$q_e = \frac{q_m b_K C_e}{(1 + b_K C_e)^{a_K}}$	(10)	$q_m = 729.2$ $b_K = 0.00113$ $a_K = 1.98$ $R^2 = 0.995$	$q_m = 880.5$ $b_K = 0.00122$ $a_K = 2.12$ $R^2 = 0.992$	$q_m = 878.9$ $b_K = 0.00149$ $a_K = 2.00$ $R^2 = 0.993$	$q_m = 569.2$ $b_K = 0.0031$ $a_K = 1.42$ $R^2 = 0.986$
Radke-Prausnitz	$q_e = \frac{a_R r_R C_e^{\beta_R}}{a_R + r_R C_e^{\beta_R - 1}}$	(11)	$a_R = 238.28$ $r_R = 0.94$ $\beta_R = 0.01143$ $R^2 = 0.988$	$a_R = 231.72$ $r_R = 1.41$ $\beta_R = 0.0183$ $R^2 = 0.980$	$a_R = 229.5$ $r_R = 1.75$ $\beta_R = 0.028$ $R^2 = 0.977$	$a_R = 212.91$ $r_R = 2.28$ $\beta_R = 0.051$ $R^2 = 0.974$
Toth	$q_e = \frac{q_m b_T C_e}{(1 + (b_T C_e)^{n_T})^{1/n_T}}$	(12)	$q_m = 224.11$ $b_T = 0.00392$ $n_T = 1.219$ $R^2 = 0.992$	$q_m = 215.34$ $b_T = 0.00416$ $n_T = 1.965$ $R^2 = 0.992$	$q_m = 227.21$ $b_T = 0.0047$ $n_T = 2.132$ $R^2 = 0.994$	$q_m = 267.38$ $b_T = 0.00633$ $n_T = 1.332$ $R^2 = 0.981$
Koble-Carrigan	$q_e = \frac{A_{KC} B_{KC} C_e^{n_{KC}}}{1 + B_{KC} C_e^{n_{KC}}}$	(13)	$A_{KC} = 229.6$ $B_{KC} = 0.00234$ $n_{KC} = 1.131$ $R^2 = 0.992$	$A_{KC} = 234.8$ $B_{KC} = 0.00177$ $n_{KC} = 1.26$ $R^2 = 0.987$	$A_{KC} = 245.1$ $B_{KC} = 0.00125$ $n_{KC} = 1.373$ $R^2 = 0.99$	$A_{KC} = 283.7$ $B_{KC} = 0.00571$ $n_{KC} = 1.07$ $R^2 = 0.979$
Fritz-Schlunder	$q_e = \frac{A C_e^{\alpha_{FS}}}{1 + B_{FS} C_e^{\beta_{FS}}}$	(14)	$A = 2.5$ $B_{FS} = 0.0083$ $\alpha_{FS} = 0.81$ $\beta_{FS} = 0.82$ $R^2 = 0.986$	$A = 2.7$ $B_{FS} = 0.0052$ $\alpha_{FS} = 0.82$ $\beta_{FS} = 0.89$ $R^2 = 0.973$	$A = 3.35$ $B_{FS} = 0.00327$ $\alpha_{FS} = 0.805$ $\beta_{FS} = 0.97$ $R^2 = 0.98$	$A = 4.18$ $B_{FS} = 0.00577$ $\alpha_{FS} = 0.817$ $\beta_{FS} = 0.934$ $R^2 = 0.98$
Fritz-Schlunder	$q_e = \frac{\alpha_1 C_e^{\beta_1}}{\alpha_1 + \alpha_2 C_e^{\beta_2}}$	(15)	$\alpha_1 = 107.9$ $\alpha_1' = 59.1$ $\alpha_2 = 0.00223$ $\beta_1 = 0.793$ $\beta_2 = 1.519$ $R^2 = 0.996$	$\alpha_1 = 145.9$ $\alpha_1' = 79.5$ $\alpha_2 = 0.00712$ $\beta_1 = 0.847$ $\beta_2 = 1.464$ $R^2 = 0.993$	$\alpha_1 = 113.3$ $\alpha_1' = 51.22$ $\alpha_2 = 0.0066$ $\beta_1 = 0.845$ $\beta_2 = 1.433$ $R^2 = 0.993$	$\alpha_1 = 285.14$ $\alpha_1' = 53.80$ $\alpha_2 = 0.00257$ $\beta_1 = 0.686$ $\beta_2 = 1.515$ $R^2 = 0.99$

As can also be seen from Table 2, Fritz-Schlunder (four-parameter) model unable to describe the data because of low determination coefficients, compared to Fritz-Schlunder (five-parameter) model. The high determination coefficients (R^2 varies from 0.990 to

0.996) for Fritz-Schlunder (five-parameter) model were obtained for the all studied systems. As a result, the increased number of constants in the isotherm model equations would be able to simulate the model variations more accurately. However, the maximum capacities of

adsorption determined using the Fritz-Schlunder (five-parameter) model was compared to experimental data and it was found that the values are lower than those for the Langmuir and Toth isotherm models.

4.4. Adsorption thermodynamics

The van't Hoff equation can be used to determine the thermodynamic parameters because of temperature dependence of the equilibrium constant (K_L). This equation can be integrated as:⁶¹

$$\ln K_L = \frac{\Delta S^0}{R} - \frac{\Delta H^0}{R} \left(\frac{1}{T} \right) \quad (17)$$

in this equation, R is the universal gas constant ($\text{J mol}^{-1} \text{K}^{-1}$) and T the absolute temperature (K). ΔS^0 and ΔH^0 are the entropy and enthalpy changes of the adsorption process. They were determined from the intercept and slope of the plot of $\ln K_L$ versus $1/T$, respectively (Figure 8).

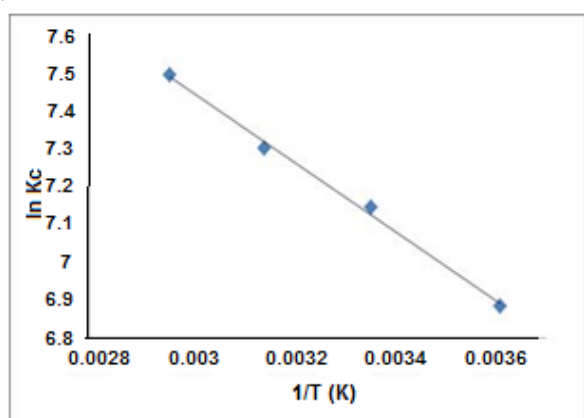


Figure 8 The plot of $\ln K_L$ versus $1/T$ for the determination of the thermodynamic parameters for the adsorption of Cu(II) onto Sep-PVI composite.

The equation of free energy for all studied temperature is obtained as:⁶¹

$$\Delta G^0 = \Delta H^0 - T\Delta S^0 \quad (18)$$

From Eq. (18), the Gibbs free energy change (ΔG^0) was calculated as -15.869, -17.651, -19.348 and -21.045 kJ mol^{-1} at 277, 298, 318, and 338 K, respectively (Table 3). According to the negative ΔG^0 values, the adsorption process is spontaneous and thermodynamically feasible. ΔG^0 values change usually between -20 and 0 kJ mol^{-1} for physisorption, whereas the values are often in the range of -80 to -400 kJ mol^{-1} for chemisorption.⁶⁴ In this study, the ΔG^0 values obtained indicate that the adsorption is physisorption. The enthalpy (ΔH^0) and entropy (ΔS^0) changes were calculated as +84,853 $\text{J mol}^{-1} \text{K}^{-1}$ and +7,635 kJ mol^{-1} , respectively (Table 3).

The ΔH^0 has positive value, which indicates endothermic adsorption process. From positive value of ΔS^0 , it can be said that the randomness at the solid-solute interface increases during the adsorption process.

Table 3. The thermodynamic values of the Cu(II) adsorption onto Sep-PVI composite at different temperatures

Temperature (K)	ΔG^0 (kJ mol^{-1})	ΔH^0 (kJ mol^{-1})	ΔS^0 ($\text{J mol}^{-1} \text{K}^{-1}$)
277	-15.869		
298	-17.651	+7.635	+84.853
318	-19.348		
338	-21.045		

4.5. Comparison of the adsorption capacities of different adsorbents for Cu(II)

For Cu(II) removal, a summary of the adsorption capacities of other adsorbents in the literature and Sep-PVI composite are given in Table 4. As can be seen from Table 4 that the maximum adsorption capacity of the Sep-PVI composite prepared in this study is found as 261.91 mg g^{-1} . The value is much higher than those of other adsorbents. These results indicate that the Sep-PVI composite synthesized is a promising adsorbent for removal of the Cu(II) ions from aqueous solutions.

5. CONCLUSIONS

A novel Sep-PVI composite for the removal of Cu(II) ions were prepared by in-situ polymerization from sepiolite and 1-vinyl imidazole. The obtained composite was characterized by XRD, FTIR, TGA and SEM. The removal of Cu(II) ions onto the Sep-PVI composite was studied at different temperatures, and the equilibrium data were modelled using Henry's law, Langmuir, Freundlich, Temkin, Dubinin-Radushkevich, Halsey, Redlich-Peterson, Khan, Sips, Radke-Prausnitz, Koble-Corrigan, Toth, Fritz and Schlunder (four-parameter) and Fritz and Schlunder (five-parameter) isotherm models. Among two-parameter models, the Langmuir model better described the isotherm data with high R^2 . In the case of three-parameter models, the Toth model was found to provide closest fit to the equilibrium experimental data even better than Langmuir model. The maximum adsorption capacity of Sep-PVI composite was in very well consistent with the experimental data. The high determination coefficients for Fritz-Schlunder (five-parameter) model were obtained for the all studied systems. However, the maximum capacity of adsorption determined using the Fritz-Schlunder (five-parameter) model was compared to experimental data and it was found that the values were lower than those of the

Table 4. Comparison of the adsorption properties of various adsorbents for the removal of Cu(II)

Adsorbents	T (°C)	pH	q _m (mg g ⁻¹)	Ref.
Crosslinked chitosan-coated bentonite beads	25	4.0	9.43	(3)
Non-crosslinked chitosan-coated bentonite beads	25	4.0	12.21	(3)
Chitosan–zeolite composites (CZ-2)	25	5.0	14.75	(13)
Chitosan–zeolite composites (CZ-0)	25	3.0	25.61	(13)
Chitosan–zeolite composite	25	3.0	25.96	(4)
Chitosan-tripolyphosphate beads	27	4.5	26.06	(9)
EDTA functionalized Fe ₃ O ₄ magnetic nano-particles	25	6.0	46.27	(5)
Chitosan–zeolite composites (CZ-1)	25	3.0	51.32	(13)
Sulfonated magnetic graphene oxide composite	30	5.0	56.86	(15)
Poly(N-isopropylacrylamide-co-acrylic acid) hydrogels	30	5.0	67.25	(7)
PVA/silica/MPTMS	25	6.0	70.01	(14)
Humic acid-immobilized polymer/bentonite composite	30	5.0	106.2	(16)
Fish bones	20	4.5	124.5	(1)
Mesoporous adsorbents prepared with fly ash	20	4.5	221	(2)
Sep-PVI composite	25	5.0	261.91	In this study

Langmuir and Toth isotherm models. Additionally, the study reveals that the more isotherm parameters provide a better fitting of the adsorption equilibrium data. Adsorption capacity of Sep-PVI composite for Cu(II) increased with an increase in temperature from 277 to 338 K, indicating an endothermic adsorption. Adsorption experiments showed that Sep-PVI composite was an effective adsorbent and could be used for the removal of Cu(II) from wastewater.

ACKNOWLEDGEMENTS

Authors thank to Kocaeli University and Uludağ University for continuous motivation. The authors also thank to METU Central Laboratory for analytical characterization support.

Nomenclature

a_K	Khan model exponent
a_R	Radke-Prausnitz isotherm constant
a_{RP}	Redlich-Peterson model constant, l mg ⁻¹
A	Fritz-Schlunder four-parameter model constant
A_{KC}	Koble-Carrigan isotherm constant
b_K	Khan isotherm constant
b_T	Toth isotherm constant
B	Heat of adsorption constant, J mol ⁻¹
B_1	Constant in Temkin adsorption isotherm, J mol ⁻¹
B_{FS}	Constant in Fritz-Schlunder four-parameter model
B_{KC}	Koble-Carrigan isotherm constant
C_e	Equilibrium concentration of adsorbate in solution, mg l ⁻¹
E	Mean free energy, kJ mol ⁻¹
K_F	Freundlich isotherm constant, mg ^{1-(1/n)} l ^{1/n} g ⁻¹
K_{HE}	Henry's law constant, l mg ⁻¹
K_H	Halsey isotherm constant
K_L	Langmuir isotherm equilibrium binding constant, l mg ⁻¹
K_R	Redlich-Peterson isotherm constant, l mg ⁻¹
K_S	Sips isotherm constant, l mg ⁻¹
K_T	Temkin isotherm constant
n	Exponent in Freundlich isotherm
n_H	Halsey equation exponents
n_{KC}	Koble-Carrigan model exponent
n_T	Toth model exponent
q_e	Amount of adsorption at equilibrium, mg g ⁻¹
q_m	Maximum adsorption capacity, mg g ⁻¹
r_R	Radke-Prausnitz isotherm constant
R	Universal gas constant, 8.314 J mol ⁻¹ K ⁻¹
R^2	Correlation coefficient
T	Absolute temperature, K
α	Radke-Prausnitz isotherm constant
α_1	Fritz-Schlunder five-parameter model sorption capacity, mg g ⁻¹
α_1'	Fritz-Schlunder five-parameter model constant
α_2	Fritz-Schlunder five-parameter model constant
α_{FS}	Fritz-Schlunder four-parameter model exponent
β	Constant in Dubinin-Radushkevich model
β_1	Fritz-Schlunder five-parameter model exponent
β_2	Fritz-Schlunder five-parameter model exponent
β_{FS}	Fritz-Schlunder four-parameter model exponent
β_R	Radke-Prausnitz model exponent
β_{RP}	Redlich-Peterson isotherm constant
ε	Polanyi potential
γ	Sips model exponent

Conflict of interest





Authors declare that there is no a conflict of interest with any person, institute, and company, etc.

REFERENCES

- Kizilkaya, B.; Tekinay, A. A.; Dilgin, Y. *Desalination* **2010**, 264, 37–47.
- Wu, X.-W.; Ma, H.-W.; Zhang, L.-T.; Wang, F.-J. *Appl. Surf. Sci.* **2012**, 261, 902–907.
- Dalida, M.L.P.; Mariano, A.F.V.; Futralan, C.M.; Kan, C.-C.; Tsai, W.-C.; Wan, M.-W. *Desalination* **2011**, 275, 154–159.
- Wan Ngah, W.S.; Teong, L.C.; Toh, R.H.; Hanafiah, M.A.K.M. *Chem. Eng. J.* **2012**, 209, 46–53.
- Liu, Y.; Chen, M.; Hao, Y. *Chem. Eng. J.* **2013**, 218, 46–54.
- Pellera, F.-M.; Giannis, A.; Kalderis, D.; Anastasiadou, K.; Stegmann, R.; Wang, J.-Y.; Gidarakos, E. *J. Environ. Manag.* **2012**, 96, 35–42.
- Chen, J.J.; Ahmad, A.L.; Ooi, B.S. *J. Environ. Chem. Eng.* **2013**, 1, 339–348.
- Karapinar, N.; Donat, R. *Desalination* **2009**, 249, 123–129.
- Wan Ngah, W.S.; Fatinathan, S. *J. Environ. Manag.* **2010**, 91, 958–969.
- Serencam, H.; Ozdes, D.; Duran, C.; Senturk, H.B. *Desalin. Water Treat.* **2014**, 52, 3226–3236.
- Ibrahim, H.S.; Ammar, N.S.; Ghafar, H.H.A.; Farahat, M. *Desalin. Water Treat.* **2012**, 48, 320–328.
- Nadaroglu, H.; Kalkan, E.; Demir, N. *Desalination* **2010**, 251, 90–95.
- Wan Ngah, W.S.; Teong, L.C.; Toh, R.H.; Hanafiah, M.A.K.M. *Chem. Eng. J.* **2013**, 223, 231–238.
- Keshtkar, A.R.; Irani, M.; Moosavian, M.A. *J. Taiwan Inst. Chem. Eng.* **2013**, 44, 279–286.
- Hu, X.-J.; Liu, Y.-G.; Wang, H.; Chen, A.-W.; Zeng, G.-M.; Liu, S.-M.; Guo, Y.-M.; Hu, X.; Li, T.-T.; Wang, Y.-Q.; Zhou, L.; Liu, S.-H. *Sep. Purif. Technol.* **2013**, 108, 189–195.
- Anirudhan, T.S.; Suchithra, P.S. *Chem. Eng. J.* **2010**, 156, 146–156.
- Yu, Y.; Qi, S.; Zhan, J.; Wu, Z.; Yang, X.; Wu, D. *Mater. Res. Bull.* **2011**, 46, 1593–1599.
- Kavas, H.; Baykal, A.; Senel, M.; Kaynak, M. *Mater. Res. Bull.* **2013**, 48, 3973–3980.
- Tekin, N.; Kadıncı, E.; Demirbaş, Ö.; Alkan, M.; Kara, A. *J. Colloid Interf. Sci.* **2006**, 296, 472–479.
- Gurbuz, O.; Sahan, Y.; Kara, A.; Osman, B. *Hacettepe J. Biol. Chem.* **2009**, 37, 353–357.
- Caner, H.; Yilmaz, E.; Yilmaz, O. *Carbohydr. Polym.* **2007**, 69, 318–325.
- Bergaya, F.; Jaber, M.; Lambert, J. F.; Galimberti, M. *Rubber-Clay Nanocomposites: Science, Technology, and Applications. (1. Clay and Clay Minerals)*. Wiley, 2011.
- Fukushima, K.; Tabuani, D.; Camino, G. *Mater. Sci. Eng. C.* **2009**, 29, 1433–1441.
- Kara, A.; Demirbel, E.; Sözeri, H.; Küçük, İ.; Ovalıoğlu, H. *Hacettepe J. Biol. Chem.* **2014**, 42, 299–312.
- Ho, Y.S. *Carbon* **2004**, 42, 2115–2116.
- Kumar, K.V. *J. Hazard. Mater. B.* **2006**, 136, 197–202.
- Tekin, N.; Kaya, A.U.; Esmer, K.; Kara, A. *Appl. Clay Sci.* **2012**, 57, 32–38.
- Al-Degs, Y.S.; Abu-El-Halawa, R.; Abu-Alrub, S.S. *Chem. Eng. J.* **2012**, 191, 185–194.
- Freundlich, H.M.F. *Z. Phys. Chem.* **1906**, 57, 385–471.
- Rengaraj, S.; Yeon, J.-W.; Kim, Y.; Jung, Y.; Ha, Y.-K.; Kim, W.-H. *J. Hazard. Mater.* **2007**, 143, 469–477.
- Langmuir, I. *J. Am. Chem. Soc.* **1916**, 38, 2221–2295.
- Dubinina, M.M. *Chem. Rev.* **1960**, 60, 235–266.
- Kundu, S.; Gupta, A.K. *Chem. Eng. J.* **2006**, 122, 93–106.
- Halsey, G. *J. Chem. Phys.* **1948**, 16, 931–937.
- Redlich, O.; Peterson, D.L. *J. Phys. Chem.* **1959**, 63, 1024.
- Sips, R.J. *J. Chem. Phys.* **1948**, 16, 490–495.
- Foo, K.Y.; Hameed, B.H. *Chem. Eng. J.* **2010**, 156, 2–10.

38. Khan, A.R.; Ataullah, R.; Al-Haddad, A. *J. Colloid Interf. Sci.* **1997**, 194, 154–165.
39. Liu, Y.; Liu, Y.-J. *Sep. Purif. Technol.* **2008**, 61, 229–242.
40. Vijayaraghavan, K.; Padmesh, T.V.N.; Palanivelu, K.; Velan, M. *J. Hazard. Mater. B.* **2006**, 133, 304–308.
41. Toth, J. *Acta Chem. Acad. Sci. Hungaria.* **1971**, 69, 311–317.
42. Koble, R.A.; Corrigan, T.E. *Ind. Eng. Chem.* **1952**, 44, 383–387.
43. Basha, S.; Murthy, Z.V.P.; Jha, B. *Ind. Eng. Chem. Res.* **2008**, 47, 980–986.
44. Fritz, W.; Schlunder, E.U. *Chem. Eng. Sci.* **1974**, 29, 1279–1282.
45. Rangabhashiyam, S.; Anu, N.; Nandagopal, M.S.G.; Selvaraju, N. *J. Environ. Chem. Eng.* **2014**, 2, 398–414.
46. Beauger, C.; Lainé, G.; Burr, A.; Taguet, A.; Otazaghine, B.; Rigacci, A. *J. Membr. Sci.* **2013**, 130, 167–179.
47. Alkan, M.; Tekin, G.; Namli, H. *Micropor. Mesopor. Mat.* **2005**, 84, 75–83.
48. Wan, C.; Chen, B. *Nanoscale.* **2011**, 3, 693–700.
49. Unal, H. I.; Erol, O.; Gumus, O.Y. *Colloids and Surfaces A: Physicochem. Eng. Aspects.* **2014**, 442, 132–138.
50. Chen, Z.; Yang, J.; Yin, D.; Li, Y.; Wu, S.; Lu, J.; Wang, J. *J. Membrane Sci.* **2010**, 349, 175–182.
51. Soheilmoghaddam, M.; Wahit, M.U.; Yussuf, A.A.; Al-Saleh, M.A.; Whye, W.T. *Polym. Test.* **2014**, 33, 121–130.
52. Lu, P.; Xu, J.; Liu, K. *J. Appl. Polym. Sci.* **2011**, 119, 3043–3050.
53. Killeen, D.; Frydrych, M.; Chen, B. *Mater. Sci. Eng. C.* **2012**, 32, 749–757.
54. Jang, J.; Kim, H. *J. Appl. Polym. Sci.* **1995**, 56, 1495–1504.
55. Fodor, C.; Bozi, J.; Blazsoi, M.; Ivain, B. *Macromolecules* **2012**, 45, 8953–8960.
56. Frost, R.L.; Kristof, J.; Horvath, E. *J. Therm. Anal. Calorim.* **2009**, 98, 749–755.
57. Serna, C.; Ahlrichs, J.L.; Serratos, J.M. *Clay Miner.* **1975**, 23, 452–457.
58. Tartaglione, G.; Tabuani, D.; Camino, G.; Moisis, M. *Compos. Sci. Technol.* **2008**, 68, 451–460.
59. Bidsorkhi, H.C.; Soheilmoghaddam, M.; Pour, R.H.; Adelnia, H.; Mohamad, Z. *Polym. Test.* **2014**, 37, 117–122.
60. Ghasemi, Z.; Seif, A.; Ahmadi, T.S.; Zargar, B.; Rashidi, F.; Rouzbahani, G.M. *Adv. Powder Technol.* **2012**, 23, 148–156.
61. McKay, G.; Mesdaghinia, A.; Nasser, S.; Hadi, M.; Aminabad, M.S. *Chem. Eng. J.* **2014**, 251, 236–247.
62. Oubagaranadin, J.U.K.; Murthy, Z.V.P. *Appl. Clay Sci.* **2010**, 50, 409–413.
63. Kumar, K.V. *Dyes Pigments.* **2007**, 74, 595–597.
64. Özcan, A.; Ömeroğlu, Ç.; Erdoğan, Y.; Özcan, A.S. *J. Hazard. Mater.* **2007**, 140, 173–179.

ORCID

-  0000-0002-9390-9875 (A. Kara)
-  0000-0003-3560-2995 (M. Kılıç)
-  0000-0003-0141-5817 (N. Dinibütün)
-  0000-0003-0141-5817 (A. Şafaklı)



Synthesis and characterization of alkyd resin based on soybean oil and glycerin using zirconium octoate as catalyst

Mohamed E. ELBA, Elsayed M. ABDEL REHİM, Ramadan E. ASHERY*

Damanhour University, Faculty of Science, Department of Organic Chemistry, Egypt

Received: 30 October 2017, Revised: 07 April 2018; Accepted: 11 April 2018

*Corresponding author's e-mail address: ramadansayed66@yahoo.com (R.E. Ashery)

ABSTRACT

A one pot synthesis of alkyd resins based on the soybean oil and glycerin with the zirconium octoate (zirconium 2-ethyl hexanoate) as a new renewable raw material was performed. The alcoholysis reaction of soybean oil and glycerin carried out in absence of nitrogen gas inlet in the presence of zirconium octoate. The alkyd resin was obtained from polycondensation of the alcoholysis products with phthalic anhydride at 250 °C. The structure confirmed by FT-IR and ¹H-NMR spectroscopy. Flexibility, drying time, hardness, adhesion test, impact resistance, gloss test and chemical resistance of synthesized alkyd resins was investigated. The prepared resin was formulated in white lacquer and yellowing resistance tested with commercial resins.

Keywords: Phthalic anhydride, soybean oil, zirconium octoate, alkyd resin.

1. INTRODUCTION

Alkyd resins make an important group of commercial synthetic polymers and are used widely in coating and paint industry. They have become essential raw material in the production of metals, wood and wood-based materials like furniture and floors, cement, cement-lime and gypsum plasters. The commonly used raw materials for the production of alkyd resins, besides plant oils like soybean oil and linseed oil, are synthetic pentaerythritol, glycerin and phthalic anhydride which are toxic.¹ Alkyd resins can be defined in brief as polyesters modified with fatty acids, fatty oils or higher synthetic carboxylic acids. The molecules consist of a polyester backbone, which may be scarcely moderately branched depending on the raw material selected, and fatty acid groups as side

Kataliz olarak zirkonyum oktoat kullanarak soya fasulyesi ve gliserin esaslı alkid reçinenin sentezi ve karakterizasyonu

ÖZ

Yeni bir yenilenebilir hammadde olarak soya fasulyesi yağı ve gliserin ile zirkonyum oktoat (zirkonyum 2-etil heksanoat) içeren alkid reçinelerinin tek bir saksı sentezi gerçekleştirilmiştir. Soya fasulyesi yağı ve gliserinin alkoliz reaksiyonu azot gazı olmaksızın zirkonyum oktoat varlığında yapıldı. Alkid reçinesi 250 °C' de alkoliz ürünlerinin ftalik anhidrit ile polikondenzasyonundan elde edildi. Yapı FT-IR ve ¹H-NMR spektroskopisi ile teyit edildi. Sentezlenen alkid reçinelerinin esneklik, kuruma süresi, sertlik, yapışma testi, darbe direnci, parlaklık testi ve kimyasal mukavemet özellikleri araştırıldı. Hazırlanan reçine beyaz lakürde formüle edildi ve sararma direnci ticari reçineler ile test edildi.

Anahtar Kelimeler: Ftalik anhidrit, soya fasulyesi yağı, zirkonyum oktoat, alkid reçinesi.

chains excess (free) hydroxyl and residual carboxyl groups are also present. An alkyd resin consisting of oil solely, additional glycerol and ortho – phthalic acid represented in simplified form have produced industrially in 1930. Alkyd resins rapidly developed into the most important type of synthetic resin for coating chemistry. Even today they still occur over 40% of world production of synthetic coating resins. The huge success of alkyd resins can be attributed—in short—to an ideal combination of polyester and oil properties. The polyester component is responsible for physical (surface) drying and weather resistance (gloss retention, freedom from yellowing, etc). The oil component is important for the suppleness of the films (internal plasticization) and the suppleness of the films (internal plasticization) and all for the capability of oxidative crosslinking.

The strength of alkyd resins, such as self curing at room temperature as one component system provides very broad compatibility and solubility spectrum, virtually unlimited variability of properties by appropriate choice of raw material and synthetic condition, good pigment wetting, attractive flow properties leading to good spreadability of paints and relatively low cost.² The oil type selected for the production of usually alkyds has a profound effect on the properties of the finished alkyd. The presence of fragments derived from unsaturated fatty acids in the polymer structure gives them the ability to cure solubility chemically in the solvents used to manufacture varnishes. The ability to blend with other film-forming substance alkyd resins is cured due to intermolecular reaction of unsaturated bonds contained in the fatty acid chains and hydroxyl groups derived from polyols under the influence of oxidative polymerization initiators. The chain polymerization processes occur in alkyd resins to yield cross linking intermolecular bonds C-C and C-O-C.³⁻⁴ However, the high numbers of unsaturated bonds in the fatty acid chains cause that not all unsaturated bonds react in the alkyd curing process. The presence of surplus unsaturated bonds in the cured coating leads to its yellowing following oxidation after exposure to atmospheric oxygen.. The coating chemistry generally classifies alkyd resins on the basis of their oil content or their fatty acid content calculated as triglyceride content, type of oil or fatty acid (linseed oil alkyd, soybean oil alkyd, etc) classification according to the oil content (triglyceride content). The resin is based on the following nomenclature as (1) less than 40% oil: short oil alkyd, (2) 40–60% oil: medium oil alkyd, (3) over 60 to 70% oil: long oil alkyd, and (4) over 70-85% oil: very long oil alkyd.

Long oil alkyd always dry by oxidation, and their high oil content provides good flow, high flexibility and easy manual processing. But also they lead to relatively slow drying, if conjugate oils or acids are used in the resin synthesis. Faster drying long oil alkyd resins are produced based on soybean oil used as sole film former for decorator paint.² Polyester amide and alkyd resins⁵ have applications in different fields such as painting, coating, adhesives and binders for composites. The vegetable oils and other green renewable raw materials are common sources used in the organic coating industry especially for the synthesis of alkyd resin in preference to petroleum products due to increased worldwide awareness of environmental concerns.⁶ Alkyd resins have acquired great importance because of their economy, availability of raw materials, biodegradability, durability, flexibility, good adhesion and ease of application.⁷

The traditional oils such as soybean⁸ oil, linseed oil⁹, sunflower oil¹⁰ and coconut oil¹¹ are used in the synthesis of alkyd resin. This paper describes the synthesis of alkyd resins which are based on the new renewable raw material catalyst zirconium octoate (zirconium 2-ethyl hexanoate) as a new catalyst which act as base-catalyzed alcoholysis of soybean oil. The

zirconium octoate in alcoholysis reaction prevent oxidation of oil so the formation of monoglyceride by using zirconium octoate as catalyst in this synthesis useful for the color of monoglyceride. In the present work, the physico-chemical and film performance properties of the synthesized alkyd resins were studied and compared with commercial resins.

2. MATERIALS AND METHOTDS

2.1. Materials

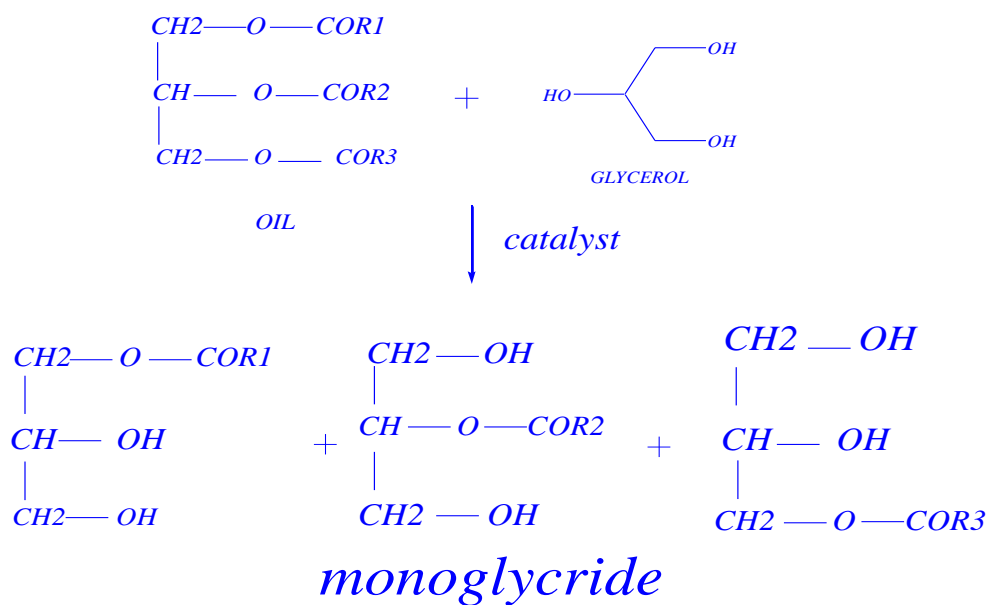
The soybean oil was provided from from oil technology company (purity 99.8%). Phthalic anhydride (99.9%), glycerin (99.8%), xylene (99.7%), methanol (99.6%), potassium hydroxide (100%), phenolphthaline (99.3%) were obtained from the Elgomhoria company. Lithium hydroxide (98.8%) was received from Dr Shahin chemicals, and cobalt octoate (99.8%), zirconium octoate (18% in mineral spirit), mineral spirit (99.5%) were purchased from a trade company.

2.2. Methods

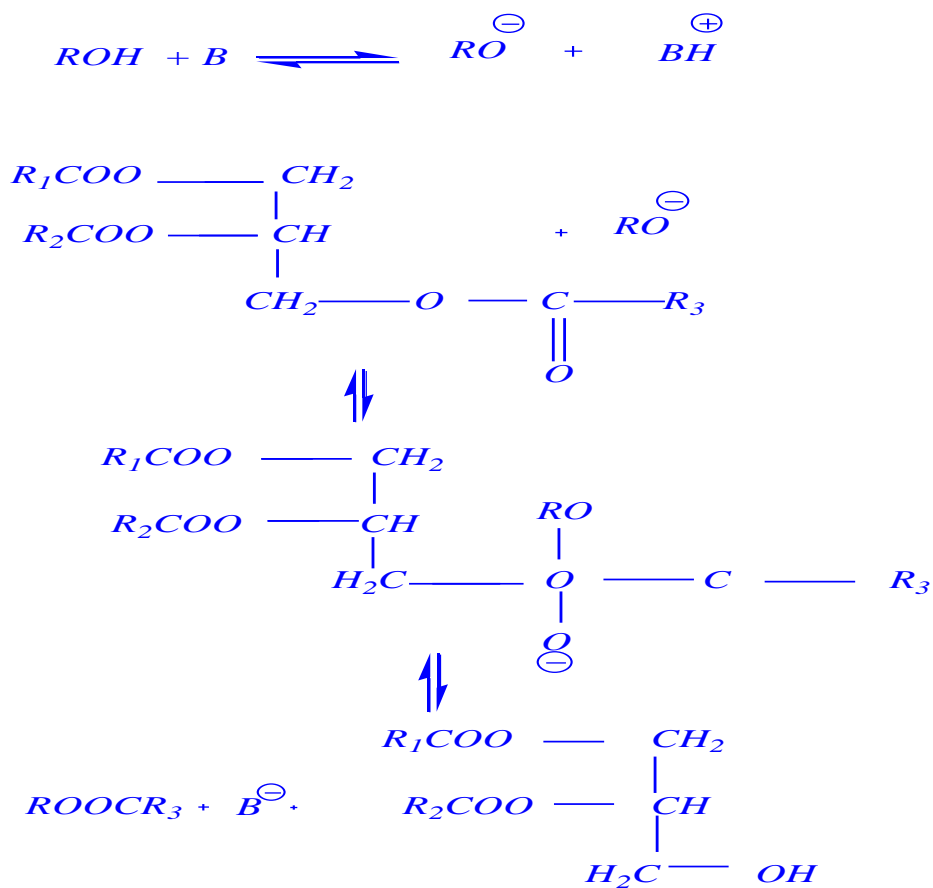
2.2.1. Alkyd resin synthesis

Alkyd resins were synthesized using monoglyceride fusion technique,¹² for this reason soybean oil, glycerin and lithium hydroxide (as catalyst) were charged into a four neck round bottom 1000 ml flask equipped with a mechanical stirrer, condenser and thermometer. The temperature was raised by slow heating to 290-300°C. The monoglyceride is formed by the alcoholysis process as seen in [Scheme 1](#). The mechanism of the base-catalyzed alcoholysis of soybean oil for monoglyceride formation is depicted in [Scheme 2](#).¹³⁻¹⁴ The completion of monoglyceride process was monitored by testing the solubility of one volume of sample dissolve with two volume of methanol to give clear solution where the triglyceride can not dissolve in methanol but monoglyceride can dissolve in methanol. Then the reaction mixture was cooled to 180°C and phthalic anhydride was added the monoglyceride mixture. Then, the temperature was raised to 240-250°C and maintained at this range. The reaction was monitored by periodic determination of acid value (AV) of the mixture to desired number (10-14) mg KOH/g of the resin. The alkyd resin synthesis is shown in [Scheme 3](#). The constituents of two resins along with some necessary characteristics are shown in [Table 1](#).

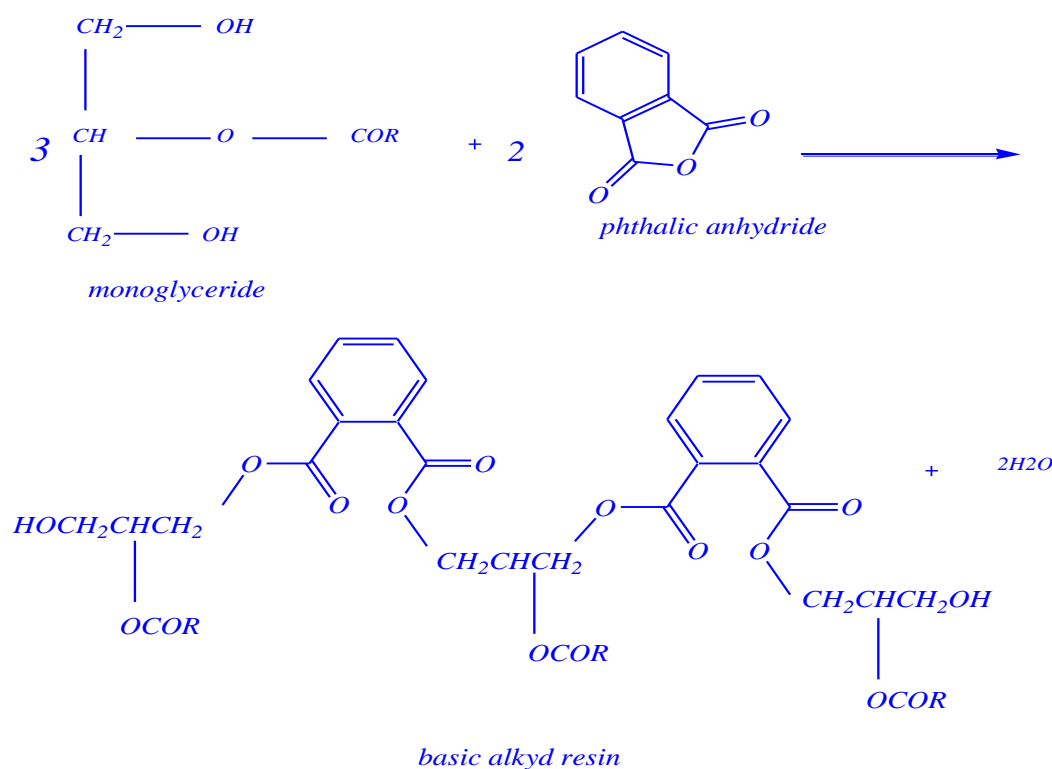
This process was repeated with zirconium octoate as catalyst but the temperature used in the preparation of monoglyceride was 290-300°C, and there was not nitrogen gas inlet. There was not nitrogen gas inlet. But nitrogen gas was used only in the stage of addition of ophthalmic anhydride to aid removal of water from reaction. In case of using lithium hydroxide as catalyst, nitrogen gas inlet was used in all stages of reaction.



Scheme 1. Transesterification of vegetable oil by glycerin for synthesizing alkyd resin.



Scheme 2. The base-catalyzed mechanism of alcoholysis reaction of vegetable oil.



Scheme 3. The synthesis of alkyd resin.

Table 1. The constituents of alkyd resins

Raw material (W %)	Alkyd resin A	Alkyd resin B
Soybean oil	54.9	54.9
Glycerin	16.22	16.22
Phthalic anhydrid	26.63	26.63
Lithium hydroxide	-	0.00816
Zirconium Octoate 18%	0.199	-
Xylene	0.02	0.02
Properties		
Acid value (100% solid) mg KOH/g	14	14
Solid content (%)	98	98
Viscosity (55% in WS) (cpoise)	2500	2900

2.2.2. The preparation of coating films

In order to study drying time, hardness, gloss and chemical resistance, two alkyd resins were applied onto

cleand glass plates of 100 mmx100 mm x 3mm. The application was confirmed by applicator with slot width of 120 μm . The sample was prepared at 55% solution of each blend in the described solvent system with drying catalyst in the following amount (100 gm of resin dissolved in mineral spirit (cobalt octoate, zirconium octoate). Adhesion, mechanical were carried out on coated steel substrate. The cleand steel plates were used for this purpose. All coated plates were kept under stander conditions.

2.3. Characterization

2.3.1. The drying time test

The drying time was determined by "set-to-touch" and " tack-free" stages at regular interval of time. The test was confirmed according to ASTM D 1640(1995).

2.3.2. The hardness test

Two resins were applied on glass plates and were allowed to dry for one week of application. The test was confirmed according to ASTM D 4366(1997).

2.3.3. The adhesion test

The cross-hatch adhesion test was performed on the coated steel plates after one week of application. The test was confirmed according to ASTM D 3359(1997).

2.3.4. The flexibility test

The flexibility of the dried films was evaluated using the mandrel test according to ASTM D 1737. The coated steel film after a week of application was placed over the 118 in mandrel with the uncoated side in contact with mandrel, and was bent 180 degree around it. The bended plate was examined visually for cracks or loss of adhesion. If the film passed through in mandrel then it was accepted to pass the flexibility test.

2.3.5. The impact resistance test

The impact resistance was measured by falling weight impact procedure according to ASTM D 2794. The test was accomplished on the coated steel plates after a week of film application.

2.3.6. The gloss test

The test was confirmed according to ASTM D 523 (1989). The sixty-degree gloss reading was taken on each of the films after the application in white lacquer.

2.3.7. The chemical resistance test

The chemical resistance test was accomplished according to ASTM D 1647(1996), D870(1997) and D1308(1998) on coated glass and steel plates after a week from the application. Alkali and acid resistance tests were accomplished on glass substrate immersed vertically in separate beakers containing distilled water, dilute HCl (10%), aqueous NaCl (10%) and KOH (4N) solutions at room temperature. The samples checked by eye. The appearance of the film at regular intervals within 1 day became changes.

2.3.8. The FT-IR and $^1\text{H-NMR}$ analysis

The structure of two resin were confirmed according to the FT-IR and $^1\text{H-NMR}$ spectra for resin at 500 MHz NMR spectrometer using CDCl_3 as the deuterated solvent.

3. RESULT AND DISCUSSION

3.1. The synthesis of alkyd resin

The alkyd resins were synthesized using lithium hydroxide and zirconium 2-ethylhexanoate by alcoholysis process where soybean oil undergoes transesterification when heated with glycerol at 250 °C in case of lithium hydroxide as catalyst. Also, the alkyd resins were synthesized with nitrogen gas inlet until

monoglyceride forms in case of the using of zirconium octoate.¹³⁻¹⁴ The soybean oil undergoes transformation to the monoglyceride by heating at temperature 290-300°C without any further oxidation and there was not nitrogen gas inlet. Then esterification was carried out with addition of ophthalmic anhydride. The nitrogen gas inlet was used as inert blanket when catalyst was lithium hydroxide to prevent the oxidation of oil. The nitrogen gas inlet was used in the second stage with zirconium octoate with addition of phthalic anhydride which facilitates the removal of water produced during mm condensation reaction. The reaction was controlled by measuring acid value at different intervals of time. The reaction was stopped as soon as the desired level of acid value was attained.

3.2. The structural analysis of the alkyd resins (A, B)

The FT-IR spectra of alkyd resins (A, B) are shown in Figures 1 and 2, respectively. These spectra indicate indicate the presence of important linkage of ester group, olefinic double bonds and other characteristic peaks. Characteristic peaks in FT-IR spectra of alkyd resins (A, B) are listed in Table 2.

Table 2. Characteristic peaks in FT-IR spectra of alkyd resin (A, B)

Peaks of resin A (cm^{-1})	Peaks of resin B (cm^{-1})	Functional groups
3472.55	3514.28	O-H stretching vibration
3008.8	3007.27	Olefinic C-H stretching vibration
2925.65	2925.77	C-H aliphatic stretching vibration
2854.38	2857.13	
1735.1	1737.14	C=O stretching frequency of ester
1599.45	1590.97	C=C stretching frequency of alkene an aromatic band
1580.28		
1489.18	1455.8	Symmetric and asymmetric bending of methyl groups
1377.7	1373.16	
1280.77	1275.5	C-O-C stretching vibrations attached with aliphatic and aromatic moiety
1041.64	1071.89	
742.65	740.84	Out of plane aromatic C-H bending vibration
705.98	570.33	

For alkyd resin (A), the peak for C=O appears at 1735 cm^{-1} in case of synthesized resin. The peak at 3472 cm^{-1} indicates the presence of hydroxyl group. For alkyd resin (B), the polyesterification reaction is confirmed by FT-IR analysis and C=O observed at 1737 cm^{-1} . The peak at 3514 indicate the presence of O-H group, the peak at 1590 cm^{-1} indicates C=C stretching for unsaturation of fatty acids and aromatics.

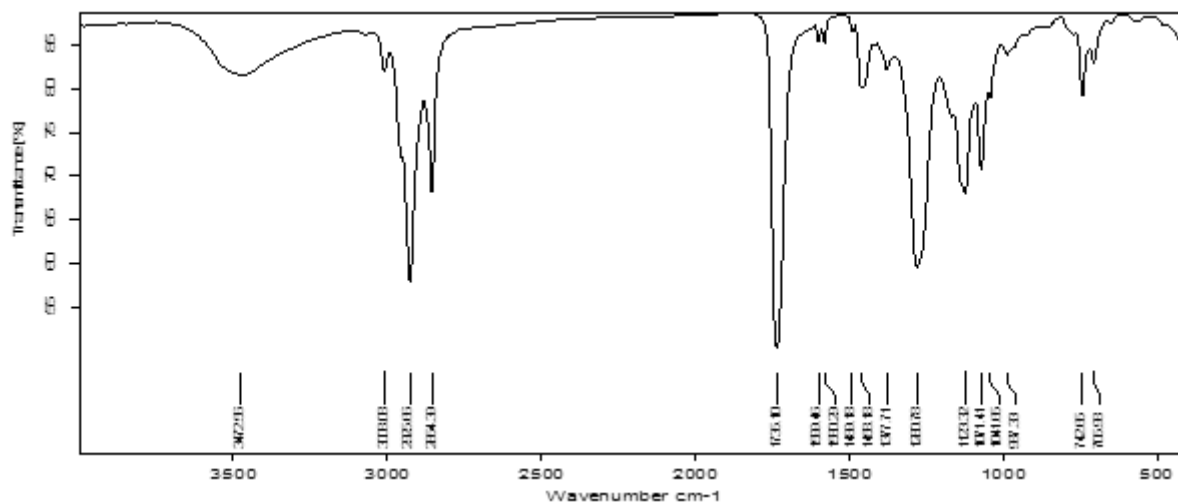


Figure 1. FT-IR spectra of alkyd resin (A) using Lithium hydroxide as catalyst.

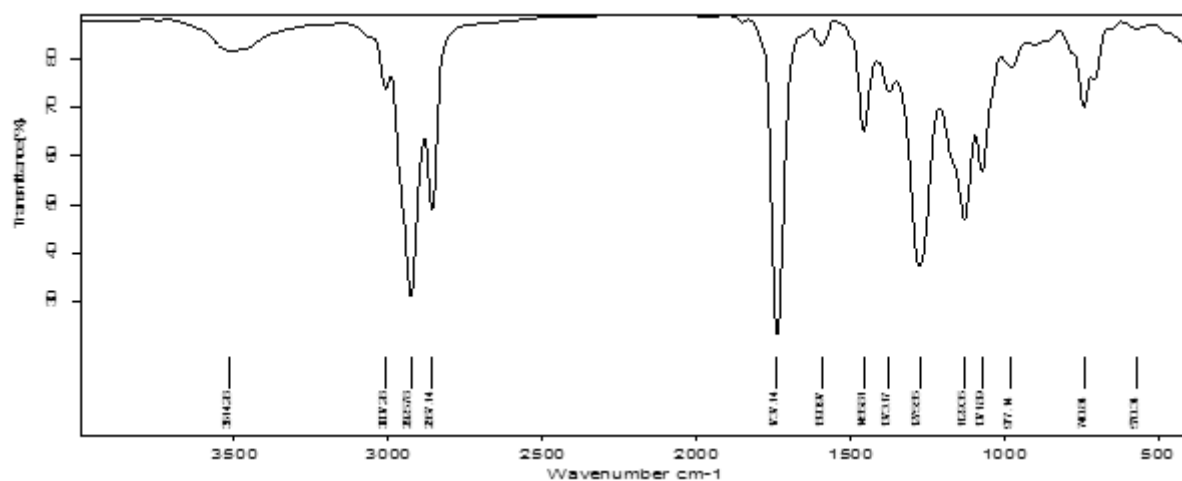


Figure 2. FT-IR spectra of alkyd resin (B) using zirconium 2-ethylhexanoate as catalyst

$^1\text{H-NMR}$ spectra of the alkyd resin A using lithium hydroxide (LiOH) as catalyst is shown in [Figures 3](#). Peaks appeared at δ 0.96 ppm for the protons of terminal methyl groups of fatty acids was confirmed by this peak. The peaks next to that at δ 1.35 ppm are due to protons of all $-\text{CH}_2$ present in the chain of fatty acids. The peak at δ 5.42 ppm resonance due to the unsaturated carbon (olefinic hydrogen in the fatty acid chain). The proton of aromatic ring and xylene solvent used to dissolve resin can be depicted by peaks at the rang δ 7.00-7.78 ppm. The peaks appeared at δ 6.95-6.97 ppm for $-\text{CH}$ present in glycerol molecule linkage to oxygen of the ester group. This may be due to the presence of anhydride groups which results in deshielding effect. The peaks appeared at δ 3.45-3.9 ppm for $-\text{CH}_2$ present in glycerol moiety attached to $-\text{OH}$ group in the resin. The peaks appeared at δ 4.23-4.65 ppm for $-\text{CH}_2$ present in glycerol moiety attached (phthalic moiety). Peaks appeared at δ 2.3-2.4 ppm for $-\text{CH}_3$ attached to aromatic ring this due to xylene solvent present in sample resin. $^1\text{H-NMR}$ analysis for resin B which the zirconium 2-ethylhexanoate used as catalyst for preparation the alkyd

resin are shown in [Figure 4](#). The proton of terminal methyl groups of fatty acids was confirmed by the peak δ 1.02 ppm. The peak next to that at δ 1.40 ppm are due to protons of all $-\text{CH}_2$ present in the fatty acid chain. The peak at δ 5.48 ppm are due to the unsaturated carbon (olefinic hydrogen in the fatty acid chain). The proton of aromatic ring of phthalic moiety and proton of aromatic ring of xylene moiety at the range δ 7.15-7.83 ppm. The peaks appeared at δ 4.26-4.70 ppm for $-\text{CH}_2$ present in glycerol moiety attached to (phthalic moiety). The peak appeared at δ 1.72 ppm are depicted to $-\text{CH}_2$ group attached to ester group of zirconium 2-ethylhexanoate catalyst. The peaks appeared at the range δ 2.32-2.44 ppm for $-\text{CH}_3$ attached to aromatic ring this due to xylene solvent present in sample resin. The peaks appeared at δ 7.05-7.08 ppm for $-\text{CH}$ present in glycerol molecule linkage to oxygen of the ester group. This may be due to the presence of anhydride groups which results in deshielding effect. The peaks appeared at δ 2.68-2.91 ppm for $-\text{CH}_2$ present in glycerol moiety attached to $-\text{OH}$ group in the resin.

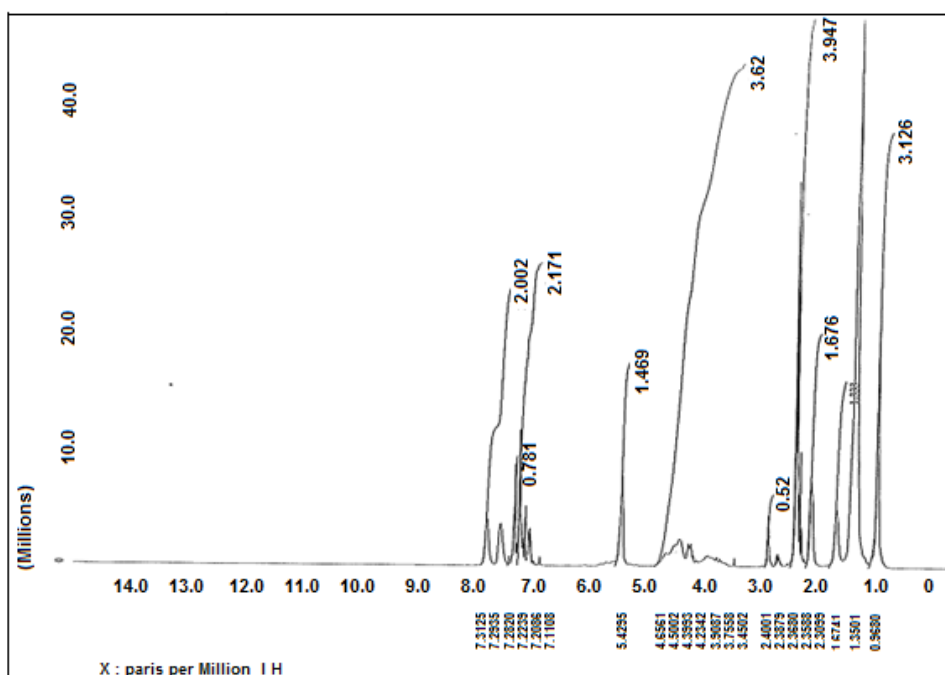


Figure 3. The ^1H -NMR spectra of alkyd resin A using lithium hydroxide (LiOH) as catalyst.

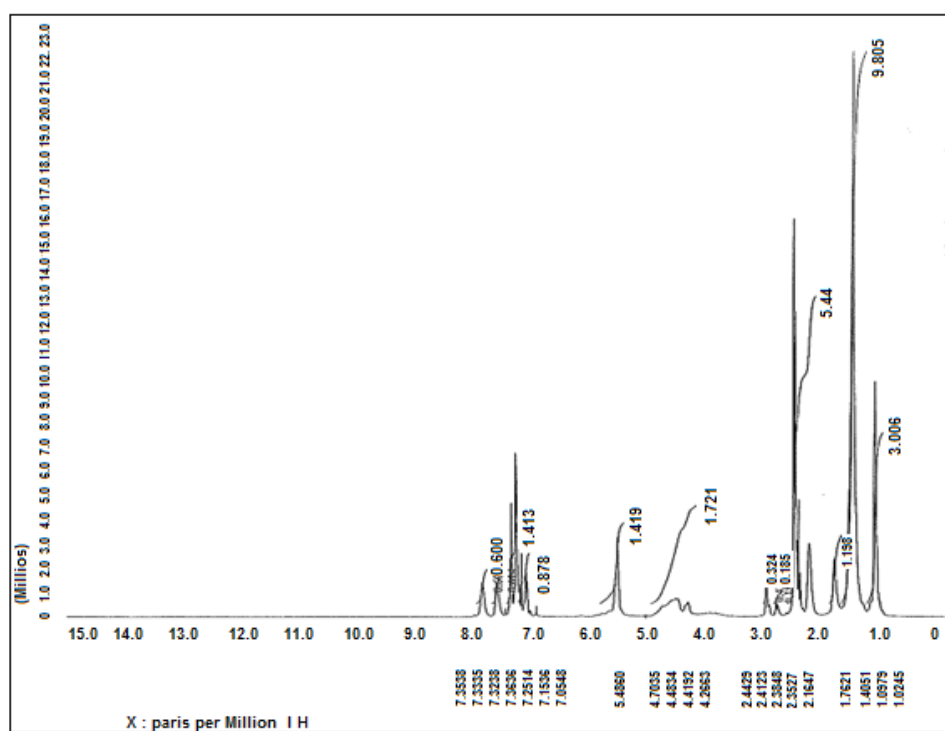


Figure 4. The ^1H -NMR spectra of alkyd resin B using zirconium 2-ethylhexanoate as catalyst.

3.3. The drying time for resins (A, B)

Table 3 describes the time required to two resin dried where the first is set-to-touch and the hard drying of resin was tack free time. The alkyd resin film driers by auto-oxidation process.²³ due to intake of oxygen from atmosphere mechanistic studies of autoxidation drying process of coating based on alkyd resin have concentrated on methylene interrupted fatty acids²⁴, but there are many other theoretical and empirical findings that are valid for other compounds .it is likely that a carbonyl group kinetically facilitates insertion of a transition metal ion into α -carbon-carbon bond.²⁵ The hydrogen atoms attached to carbon atoms in α -position of carbonyl group are more active(acidic)compared to ordinary alkyl hydrogen and similar that hydrogen atoms attached to ester group in alkyd resin , these hydrogen atoms are deprotonated by zirconium octoate salt, providing an enolate anion (Michael donor), the enolate anion then reacts an addition to olefin of the fatty acids emerged during the oxidative crosslinking of alkyd resin by Russell mechanism.²⁶⁻²⁷ All these interesting possibilities speed up the network formation and result in lower drying times.

3.4. The adhesion test for resin (A, B)

Results are given in Table 3. The results showed a desired adhesion for resins (A, B) where two resin prepared from the same oil (soybean oil) and glycerin which give the same polyester component which responsible for adhesion.

Table 3. Adhesion and hardness test results of alkyd resins

	Set-to-touch (min)	Tack free time (min)	Hardness (s)	Adhesion %
Resin A	75	360	14	100
Resin B	80	350	16	100

3.5. The hardness

Results are given in Table 3. The results show the hardness increases by using the zirconium catalyst than toward the use of lithium hydroxide catalyst in the synthesis of resin. This indicates when alkyd resin prepared using zirconium catalyst and zirconium octoate used in drying resin with octoate cobalt, the hardness of dried film increases with small amount of hydrocarbone resin in varnish industry. The film hardness depends on crosslinking density of the surface of the film, but presence of stable and rigid aromatic moiety in the backbone chain of phthalic anhydride – based film also

showed the property zirconium octoate as drier which made resin B gave good hardness than resin A. But the two values of hardness are close to each others.²¹⁻²²

3.6. The flexibility

Table 4 gives the flexibility test results. Two samples passed the test and no cracking or peeling was observed. This may be due to the oil content in the prepared alkyd resin

Table 4. Flexibility, impact resistance, gloss test results of alkyd resins

	Flexibility	Impact resistance cm	Gloss 60°, %
Resin A	passed	125	86
Resin B	passed	135	87

3.7. The impact resistance

The impact resistance results are given in Table 4. Two resin prepared using lithium hydroxide and zirconium 2-ethylhexanoate catalyst dried films show significant improvements in impact resistance. The resin prepared from zirconium catalyst gives a good impact resistance due to the zirconium element.

3.8. The gloss

Results of gloss test are given in Table 4. The gloss values of resins prepared from zirconium catalyst and lithium hydroxide is like approximately each other, which means the two resin contains the same percentage of oil and polyester component responsible for gloss retention.

3.9. The chemical resistance

Chemical resistance of dried film are given in Table 5. The resin A and resin B was good resistance to distilled water this due to low hydroxyl value present in alkyd resin and more cross-linked network results and two resin completely unaffected with NaCl 10% for the same reason. Poor alkali resistance of alkyd resin is due to the presence of alkali hydrolysable ester linkages and the alkyd resin containing free acid groups which react with alkali. Two alkyd resin unaffected with HCl 10% this due to two resin contain acid number and ester linkages poor affected by HCl 10%. The poor rsistivity to alkali is probably due to hydrolsable ester group present in the two resin.²⁰

Table 5. Chemical resistance test results of alkyd resins

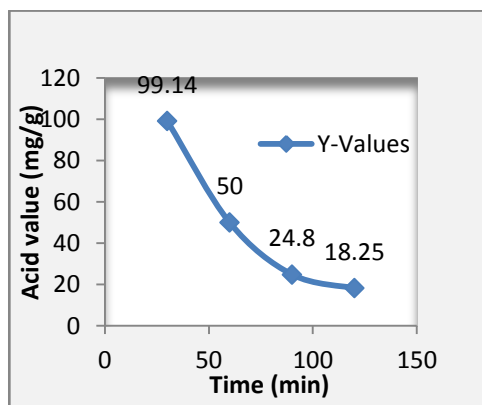
	Distilled water	NaCl (10%)	KOH (4 N)	HCl (10%)
Resin A	Completely unaffected	Completely unaffected	Completely affected	Unaffected
Resin B	Completely unaffected	Completely unaffected	Completely affected	Unaffected

3.10. The yellowing resistance

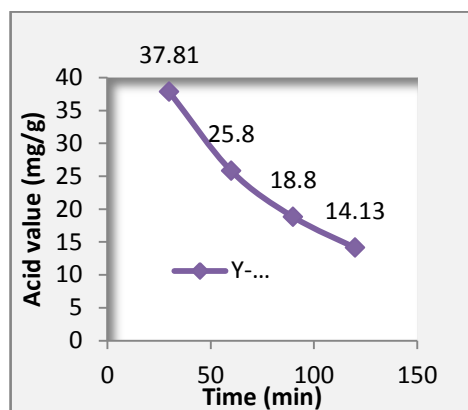
The tendency for alkyd based coatings to yellowing is a common concern all over the organic coatings industry.¹⁵⁻¹⁶ The oils containing linolenic acid are subject to discoloration because it is known this acid is the main cause of discoloration.¹⁷⁻¹⁸ The soybean oil contains 54% linoleic acid, therefore, soybean oil is good yellowing resistance where soybean oil is widely used around world. The aim of this work the tendency of lowering yellowing across the preparation of monoglyceride using zirconium octoate to prevent autoxidation of oil and production of alkyd resin transparent after application on glass blend. The alkyd resin prepared from zirconium catalyst when applied in white lacquer was given good color and high yellowing resistance than white lacquer prepared from commercial resin.¹⁹

3.11. The acid value with time

For the polyesterification reaction, the acid value change with time are shown in Figures 5 and 6.

**Figure 5.** Acid value determined using zirconium octoate as catalyst.

The acid value and hydroxyl number are important parameters. The hydroxyl and carboxylic group concentration is also quite important parameters. For air drying alkyds, the concentration of these groups affects their drying properties. Set-to-touch drying time of resin A took lower time than resin B, but resin B was prepared from zirconium -2- ethylhexanoate which gave tack free time in drying process lower than resin A according to Table 3.

**Figure 6.** Acid value determined using LiOH as catalyst.

Of course this is not the only parameter that determines the properties of the resins. Many other factors also affect their properties. In this work although acid value of resin B takes more time to adjust like resin A. Because the resin A is prepared from strong base which reacted with carboxylic groups and lowered acidity, but the drying time and yellowing resistance finally of resin prepared from zirconium octoate is better than resin prepared from lithium hydroxide.

4. CONCLUSIONS

The results obtained in the present work showed the ability of zirconium octoate salt to synthesized the monoglyceride from soybean oil and glycerin by alcoholysis reaction and prevent the oxidation of oil at high temperature where the monoglyceride formed in the absence of nitrogen gas inlet this is best result was obtained by this catalyst since the catalyst reduce the cost in the production alkyd resin and protected the reaction from oxidation which take place during the preparation of resin. The zirconium octoate salt can act as base-catalyzed transformation of triglyceride by glycerin to form monoglyceride under high temperature. The structure of alkyd resin was confirmed by FT-IR and H^1 -NMR spectroscopy and comparable with the alkyd synthesized LiOH catalyst. The physico-chemical characteristics referred to the resin prepared from zirconium octoate salt was good yellowing resistance when formulated in white lacquer. The other properties were good at drying time, gloss. The zirconium octoate catalyst gave the best results in yellowing processe since the alkyd resin prepared could resist the yellowing for along time compared resins prepared from other catalysts.

Conflict of interest

Authors declare that there is no a conflict of interest with any person, institute, and company, etc.

REFERENCES

- Gandini, A. *Green Chem.* **2011**, 13 (5), 1061-1083.
- European Coatings Handbook*, Brock., T.; Groteklaes, M.; Mischke, P. 2000, 16-85.
- Erhan, S.Z. *Industrial uses of vegetable oil*. AOCs publishing, 2005.
- Tuck, N. Wiley, CV. \sit A ser. *Technol.* 2000.
- Gaykar, D.V. *Paint India* 7. **2001**, 55-60.
- Pramanik, S.; Sagar, K.; Konwar, B.K.; Karak, N. *Prog. Org. Coat.* **2012**, 75 (4), 569-578.
- Turner, G.P.A. *Introduction to paint chemistry and principles of paint technology*, 3rd ed.; Champman and Hall, London, 1988.
- Kyenge, B.A.; Anhwange, B.A.; Ageh, J.T.; Igbum, G.O. *Int. J. Mod. Org. Chem.* **2012**, 1 (2), 66-71.
- Solomon, D.H.; Swift, J.D. *J. Oil Colour Chem. Assoc.* **1966**, 49, 915-927.
- Aydin, S.; Akcay, H.; Evren, O.; Seniha Guner, F.; Tuncer Erciyas, A. *Prog. Org. Coats.* **2004**, 51(4), 273-279.
- Wholf, R.H. Coconut oil modified alkyd reirns and copolymers There of witr an alkyl acrylate. U.S. Patent 3, 374, 194, Mar. 19, 1968.
- Wicks, Z.; Jones, F.; Pappas, S.P. *Organic Coating Science and Technology*. John Wiley & Sons, New York, 1999.
- Taft Jr, R.W.; Newman, M.S.; Verhoek, F.H. *J. Am. Chem. Soc.* **1950**, 72, 4511-4519.
- Guthrie, J.P. *J. Am. Chem. Soc.* **1991**, 113, 3941-3949.
- Lazzari, M.; Chiantore, O. *Polym. Degrad. Stabil.* **1999**, 65 (2), 303-313.
- Köckritz, A.; Martin, A. *Eur. J. Lipid Sci. Tecno.* **2008**, 110, 812-824.
- Warwel, S. Rusch gen Klass, M. *Lipid Technol.* **1997**, 9, 10-14.
- Dobson, G.; Christie, W.W.; Sebedio, J.L. *J. Chromatogr.* **1996**, 723, 349-354.
- Asemani, H.R.; Ahmadi, P.; Sarabi, A.A.; Eivaz Mohammadloo, H. *Prog. Org. Coat.* **2016**, 94, 18-27.
- Singha Mahapatra, S.; Karak, N. *Prog. Org. Coat.* **2004**, 51, 103-108.
- Deligny, P.K.T.; Tuck, N. Alkyds and polyesters. In *Resins for Surface Coatings*; Oldring, P.K.T., Ed.; John Wiley & Sons, New York, 2000. Vol 2, p. 15.
- Sharma, B.; Dolui, S.K.; Sharma, A.K.. *J. Sci. Ind. Res.* **2001**, 60, 153-158.
- Privett, O.S. *J. Am. Oil Chem. Soc.* **1959**, 36 (10), 507-512.
- Porter, N.A.; Wujek, D.G. *J. Am. Chem. Soc.* **1984**, 106 (9), 2626-2629.
- R usina, A.; Vlcek, A.A. *Nature* **1965**, 206, 295-296.
- Stenberg, C.; Svensson, M.; Johansson, M. *Ind. Crop. Prod.* **2005**, 21 (2), 263-272.
- Russell, G.A. *J. Am. Chem. Soc.* **1957**, 79 (14), 3871-3877.


 0000-0003-1604-1790 (R.E. Ashery)

Note: ORCID numbers of Elba and Abdel Rehim were not sent.



The magnetic fructose imprinted polymer for determination of fructose from apple juice

Burcu Okutucu*

Ege University, Faculty of Science, Department of Biochemistry, 35100, Bornova-Izmir, Turkey

Received: 02 February 2018, Revised: 26 April 2018, Accepted: 30 April 2018

*Corresponding author's e-mail address: burcu.okutucu@ege.edu.tr

ABSTRACT

Molecularly imprinted polymers (MIP) are synthetic receptors that have an ability to recognize and select its template molecule from complex matrix. Nowadays many new approaches of MIPs are researched. One of them is the preparing of magnetic MIPs. Magnetic molecularly imprinted polymer (MMIP) nanoparticles can be a candidate for solid phase extraction adsorbent by the porous morphology, narrow size distribution, stable chemical and thermal property. The aim of this study is to prepare MMIP nanoparticles for solid phase extraction of fructose from apple juice. The PEG treated Fe_3O_4 magnetic nanoparticles surface was coated with monosaccharide (fructose) imprinted polymer. The monomer acrylamide, cross-linking agent ethylene glycol dimethacrylate (EGDMA), initiator azobisisobutyronitrile (AIBN), the porogen dimethylsulfoxide were used for fructose imprinting. The structural characterization of MMIP was performed by FT-IR, and the imprinting characteristics of polymer were also studied by adsorption experiment and Scatchard analysis. The 65% of fructose was recognized with fructose MMIP from apple juice using only an external permanent magnet without filtration/centrifugation.

Keywords: Nanoparticles, magnetic molecularly imprinted polymers, fructose, apple juice.

1. INTRODUCTION

Molecularly imprinted polymers (MIP) are synthetic receptors that have a highly specific recognition ability for target molecule. MIPs are produced by target molecule, monomer(s), crosslinker together with in the porogen by thermal or UV polymerization. After the target molecule is removed, the cavities of polymer can rebind target molecule on size, shape and functionality¹. Nowadays the widespread use of molecularly imprinted polymer in separation, chemical catalysis, chemical sensing has increased, and also to combine them with

Manyatik fruktoz baskılanmış polimer ile elma suyundan fruktoz tayini

ÖZ

Moleküler baskılanmış polimerler (MIP) karışık ortamlardan kendi kalıp molekülünü tanıma ve ayırt etme yeteneğine sahip sentetik reseptörlerdir. Günümüzde MIP'in bir çok yeni uygulaması araştırılmaktadır. Bunlardan birisi manyatik MIP'lerin hazırlanmasıdır. Manyatik moleküler baskılanmış polimerler (MMIP) poroz yapıları, belirli boyut aralıkları, stabil kimyasal ve termal özelliklerinden dolayı iyi bir katı faz ekstraksiyon adsorbantı için iyi bir aday olabilir. Bu çalışmanın amacı, elma suyundan fruktozun katı faz ekstraksiyonuyla elde edilmesi için MMIP nanopartiküllerini hazırlamaktır. Bunun için çalışmada PEG ile kaplanan Fe_3O_4 manyatik nanopartiküllerinin yüzeyi monosakkarit (fruktoz) baskılanmış polimer ile kaplandı. Monomer akrilamid, çapraz bağlayıcı etilen glikol dimetakrilat, insiyatör azobisisobutirilonitril ve porojen olarak dimetilsülfoksit fruktoz bakılama için kullanıldı. MMIP'in yapısal karakterizasyonu FT-IR tarafından gerçekleştirildi ve polimerlerin baskı özellikleri de adsorpsiyon deneyi ve Scatchard analizi ile incelendi. Fruktozun % 65'i, filtrasyon/santrifüjleme olmaksızın sadece bir harici sabit mıknatıs kullanılarak elma suyundan fruktoz MMIP ile tanındı.

Anahtar kelimeler: Nanopartikül, manyatik moleküler baskılanmış polimerler, fruktoz, elma suyu.

different materials is an interesting and attractive area. Magnetic nanoparticles were one of these materials. There are many different possible approaches that magnetic nanoparticle MIP can be used. The usage of magnetic nanoparticles as solid phase extraction (SPE) adsorbents are very widespread. The advantages of using magnetic adsorbents in SPE are removing of any desired molecules from complex sample matrices by applying an external magnetic field. This process is very rapid and convenient. When some magnetic nanoparticles are used with MIPs as a core, the magnetic MIPs (MMIPs) are occurred. These materials can have not only magnetically

characteristic, but also selectivity for the guest molecule. And also they have a controllable rebinding process because of the characteristics of the molecularly imprinted polymers. The usage of MMIPs provides a separation faster and easier because of removing by an external magnetic field without centrifugation or filtration. Recently, magnetic polymers have many areas that can be used especially in medicine, biotechnology, and environment.²⁻¹⁰

Magnetic iron oxide or magnetite, Fe_3O_4 , is used commonly as the magnetical component in molecularly imprinted polymer technique because of its low toxicity, ease of preparation (even if in large-scale production), ease of operation (the magnetic particles can be removed easily from the bulk solution by applying an external magnetic field), ease of surface modification with different functional groups, excellent dispersibility in aqueous solution and low cost.¹¹

The preparation of magnetic MIPs is done by self-polymerization of monomers with target molecules at the surface of the magnetic nanoparticle core. The most important point is the choice of monomers. Because the aim is the preparation of a thin MIP layer on the surface of magnetic nanoparticles. Mostly acrylamide and methacrylic acids are used. The acrylamide provides multiple hydrogen-bonding sites as well as hydrophilicity, thus imprinted polymer template-monomer complexation can be formed by hydrogen bonds, which is the most found in imprinted polymers.¹²⁻¹⁵ Molecular recognition of the template molecule in imprinted polymer is based on intramolecular interaction between the template and functional groups in the polymer which is found by the polymerization of monomer and crosslinker. So, crosslinker have to be used to contribute to template complexation and polymer morphology.

In this study, Fe_3O_4 magnetic imprinted polymers were prepared for fructose. It was acrylamide used as a monomer, ethylene glycol dimethacrylate as a crosslinker and DMSO as a porogen. Characterization studies and Scatchard analysis were also done.

2. MATERIALS AND METHOTDS

2.1. Materials

Acrylamide, fructose, ethylene glycol dimethacrylate (EGDMA), methanol (MeOH), polyethylene glycol (PEG), chloroform (CHL), dimethylsulfoxide (DMSO), ammonium hydroxide (25%) were obtained from Sigma (USA). Azobisisobutyronitrile (AIBN) was purchased from Wako Pure Chem. Ind. (Japan). Sulfuric acid was taken from Fluka. All other chemicals and reagents were of the highest available purity and used as purchased.

2.2. Preparation of magnetic fructose imprinted polymeric nanoparticles

The preparation of magnetic fructose imprinted polymeric nanoparticles was divided into two steps. The first step is the synthesis of PEG- Fe_3O_4 magnetic nanoparticles by co-precipitation method. 1 mol l^{-1} $\text{FeCl}_3 \cdot 4\text{H}_2\text{O}$ and 0.75 mol l^{-1} $\text{FeCl}_2 \cdot 6\text{H}_2\text{O}$ and 80 ml distilled water was placed into three-necked flask (clear yellow solution). The mixture was stirred at 500 rpm and 80°C for two hours under N_2 pressure. After two hours 0.4 M ammonium hydroxide (28%, in percent weight) was added dropwise to the solution and (the color of the solution was turned to black) continuing to stir at 500 rpm for 30 minutes.¹⁶ The magnetic nanoparticles were separated from the solution by magnetic separator. The resulting magnetic nanoparticles were washed with 3 times distilled water and 2 times methanol. After washing, magnetic nanoparticles were obtained and dried under vacuum at 45°C for further usage. For surface modification, 500 mg of magnetic nanoparticles were put in 2g PEG / 20 ml distilled water and stirred for two hours. To obtain homogeneous PEG- Fe_3O_4 nanoparticles, the solution was put into the ultrasonic bath for 45 minutes and centrifuged at 5000 rpm for 20 minutes.

The second step is imprinting process. The prepolymerization solution acrylamide (30 mg) and fructose (20 mg) was dissolved in DMSO (5 ml) and waited for 30 minutes for prepolymerization. The PEG- Fe_3O_4 nanoparticles were placed into three-necked flask and firstly prepolymerization solution (monomer-template) was added to the flask and then EGDMA (0.9 ml) and 10 mg AIBN were added and stirred. To obtain fructose imprinted PEG- Fe_3O_4 nanoparticles, the mixture was stirred under N_2 pressure at 800 rpm for 30 minutes, and then continued to stir 500 rpm for 4 hours at 60°C and for 20 hours at 25°C in the same speed. By the help of magnetic separator, fructose imprinted PEG- Fe_3O_4 nanoparticles were taken from the solution and was ready for subsequent usage. The magnetization of magnetic fructose imprinted polymer obtained is shown in [Figure 1](#). The control magnetic nanoparticles were prepared without fructose (NMMIP). The MMIP and NMMIP were used directly for extraction without grinding or sorted by size.



Figure 1. Magnetization of magnetic fructose imprinted polymer.

2.2.1. Elution of template (fructose)

The resultant fructose imprinted PEG-Fe₃O₄ nanoparticles were washed repeatedly with methanol:acetic acid (4:1) solution and 2 times methanol at 25°C to remove the fructose. The complete removal of fructose from the fructose imprinted PEG-Fe₃O₄ nanoparticles was confirmed by o- cresol: H₂SO₄ assay.¹⁷ The standard range of fructose was between 1 and 300 μmol ml⁻¹.

2.3. Binding experiments

2.3.1. Static adsorption experiments

Adsorption experiments were performed to evaluate the recognition properties of MMIPs at different conditions (pH, substrate concentration, polymer content, etc.). The adsorption capacity of magnetic imprinted nanoparticles towards fructose was assayed with rebinding experiments. Briefly, 10 mg of magnetic polymers (template removed) was mixed with different concentration of fructose (1-50 μmol ml⁻¹) in 1 ml of methanol in an eppendorf tube and shaken for 2 h at orbital rotator and at room temperature. After that time, the magnetic polymers were centrifuged at 5000 rpm for 5 minutes and the concentration of the remaining or unbound fructose in the solution was determined by o- cresol: H₂SO₄ assay. The NIP was used as a control to determine the non-specific binding. The amount of fructose (Q; μg g⁻¹) bound to the polymers was calculated by subtracting the amount of free substrate from the initial concentration. The amount of fructose that is imprinted is defined by Eq. (1).

$$Q = (C_0 - C_t) \times V / W \quad (1)$$

Where W (g) is the weight of the magnetic nanoparticles, V (l) is the volume of solution (methanol), C₀ (μmol l⁻¹) (initial concentration of the fructose) and C_t (μmol l⁻¹) (concentration of fructose at the supernatant) respectively. All of the measurements were carried out in triplicate, and the average values were calculated.

2.3.2. Scatchard analysis

To evaluate binding sites of fructose imprinted polymer (scatchard plot analysis) was used in a batch mode. Briefly, 5 μmol ml⁻¹ of fructose concentration were studied with different amount of imprinted and non-imprinted magnetic nanoparticles (10-100 mg) in 1 ml methanol and was shaken for 2 hours. After that time, the tubes were centrifuged and the supernatant was analyzed by o- cresol: H₂SO₄ assay.

The binding parameter of fructose imprinted magnetic nanoparticles was estimated by Scatchard analysis by using Eq. (2).

$$Q_e / C_e = (Q_{max} - Q_e) / K_d \quad (2)$$

Where K_d (μmol ml⁻¹) is the equilibrium dissociation constant, C_e (μmol ml⁻¹) is the equilibrium concentration of fructose, Q_{max} (μmol g⁻¹) and Q_e (μmol g⁻¹) are the apparent maximum adsorbed amount and the equilibrium adsorbed amount of fructose, respectively.

2.4. The application of fructose MMIP to real sample

The preparation of apple juice for fructose analysis with MMIP is studied. The apple is an important fruit for children and adults. As known, it is a rich source of sugars and biologically active compounds. The sugars presented in apple (juice) are fructose 5-15% (w/w), glucose 1-14% (w/w), sucrose 1-5% (w/w).¹⁸ The traditional gravimetric, chemical and instrumental methods for carbohydrate analysis are destructive, expensive, sophisticated and time-consuming. Magnetic MMIPs are a good alternative for fructose in a complex medium. The apple sample was prepared for fructose magnetic MMIP. The apple was ground and then the juice was extracted using a fruit juice extractor. The liquid was filtered through Whatman No.54 paper. The fructose content was determined by o- cresol: H₂SO₄ assay (6.56 g ml⁻¹).

To evaluate the specific recognition ability of fructose MMIP; 1 ml of apple juice was immersed with 20 mg of MMIP for 10 minutes. After the treatment of magnetic nanoparticles with the external field, the upper solution was analyzed (Unbound). The MMIP was washed with methanol and, the bound content was analyzed. The all fructose samples were tested with o- cresol: H₂SO₄ assay.

3. Results and Discussion

3.1. The preparation of fructose imprinted magnetic nanoparticles

The most common method for preparing Fe₃O₄ particles were chemical co-precipitation method. This method has many advantages as mentioned in the following: For example, this method is the simplest and most effective way of obtaining homogeneous nanoparticles, and also magnetic nanoparticles can be coated or grafted with starch, dextran, PEG, PVA, and so on. If the magnetic nanoparticles are not coated with surface coating material, their surface becomes

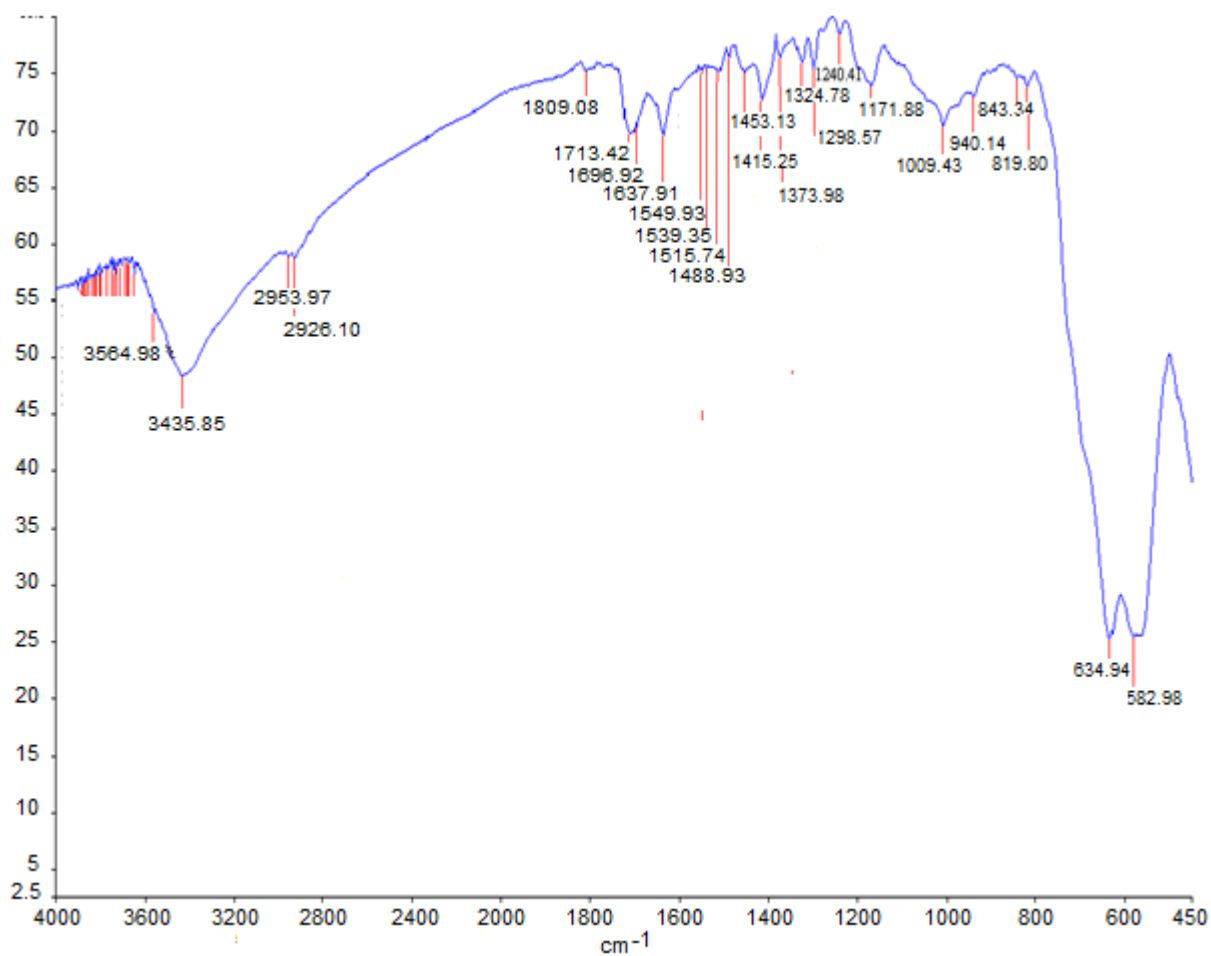


Figure 2. FT-IR of MMIP.

hydrophobic. As a result of this hydrophobicity, the particles agglomerate and form large clusters (increased particle size leads to lose of the magnetic properties, etc). The advantages of coating are to prevent aggregation, and this also renders the nanoparticles water soluble or oil-soluble, and provides functionalization for the conjugation of biomolecules. In this study, PEG was used as the surface coating material to introduce a polymeric chain on the surface of the magnetic nanoparticles. Molecular recognition of the template molecule in imprinted polymers is based on the intermolecular interaction between the template molecule and functional groups in the polymer chain. Many of the monomers were tested at different properties (acidic, neutral, basic), but the best result was obtained by acrylamide. The monomer selection is a very important part of preparing MMIPs. Because monomer directly affects the imprinted layer thickness, which has a significant influence on the imprinting factor. Also the apparent thickness was the sign of maximum rebinding capacity and imprinted sites. As known, a porogenic

solvent can affect the morphology and recognition capability of the MMIPs. Usually, polymerization is done in the low-polar solvent which has advantages. The magnetic imprinted polymers prepared using acrylamide with DMSO as porogenic solvent had better molecular recognition. When DMSO was used, good homogeneity and density of the resultant beads could be prepared reproducibly. Also fructose (template molecule) was solved in DMSO very well. The other important factor for the taken best imprinting factor was molar ratios between the functional monomer and cross-linker. The most effective ratio was the ratio of monomer to cross-linker of 1:2 (i.e. acrylamide: EGDMA ratio), which was found in the experiment, and also this ratio gives high adsorption capacity and selectivity for fructose MMIPs. It can be explained that if there is not enough crosslinker, effective imprinting sites cannot be formed. On the other hand, too much cross-linker will lead to the template molecules being embedded too deep and will reduce effective imprinting sites.

On the other hand, FT-IR analysis was performed to obtain better informed about the preparation of magnetic fructose MMIPs (Figure 2). Compared with Fe_3O_4 nanoparticles, the absorption band of Fe-O at 582 cm^{-1} in MMIPs proved that Fe_3O_4 was embedded in these materials. The characteristic peak of acrylamide was observed at 3435 cm^{-1} , indicating the N-H is stretching of acrylamide.

3.2. The adsorption graphs and Scatchard analysis

The rebinding of fructose on MMIPs was studied. As shown in Figure 3, the binding amount of fructose to the magnetic polymers increased until it reached a saturation level. The results are shown that the specific cavities to fructose is existed and to lead higher adsorption capacity.

In order to obtain the binding affinity of polymers and their theoretical number of binding sites for the template, the Scatchard equation was used. It is an effortless and straightforward way to recognize multiple classes of binding sites and provides a graphical presentation of binding data. The K_d and Q_{max} values were calculated with the help of Eq. (2). The K_{d1} $4.65\text{ }\mu\text{mol}^{-1}$, $Q_{\text{max}1}$ $29\text{ }\mu\text{mol ml}^{-1}$, and K_{d2} $37.6\text{ }\mu\text{mol}^{-1}$, Q_{max} $2.53\text{ }\mu\text{mol ml}^{-1}$ values were found, respectively.

The results of these values show that; the binding site configuration in the MMIP is heterogeneous, and indicates that the binding sites can be classified into two distinct groups with different specific binding properties. As seen from Figure 4, there are two distinct linear sections suggesting two binding sites. One is of high selectivity and the other is of low affinity. The origin of molecular recognition in MIPs can be generally attributed to both shape selectivity and pre-organization of functional groups, however external magnetic field also effected the contributions of these effects. Because of this reason; there are two different binding sites.

3.3. The selectivity study of fructose MMIP at apple juice

The selectivity of magnetic fructose imprinted polymer nanoparticles is tested with apple juice. The amount of initial fructose in apple juice was determined by o- cresol: H_2SO_4 assay. After applying the apple juice to MMIP and NMMIP, the solution was also tested with o- cresol: H_2SO_4 assay to determine the adsorbed amount of fructose. The ratio of C_p (the amount of fructose adsorbed on magnetic fructose MIP, as $\mu\text{mol g}^{-1}$) to C_s (the equilibrium concentration of fructose in solution, as $\mu\text{mol ml}^{-1}$) was the fructose that is determined by MMIP. As seen in Table 1, magnetic fructose MIP can recognize fructose by a 65% ratio from the complex matrix (i.e. apple juice). NMMIP can recognize only 10% of fructose because of surface functional groups of magnetic MIP.

Table 1. The selectivity of fructose with magnetic fructose imprinted polymer from apple juice

	Fructose Content (g ml^{-1})
Conventional method (o- cresol: H_2SO_4 assay)	6.56
Mangetic Fructose imprinted polymer	4.25
Non-imprinted polymer	0.6

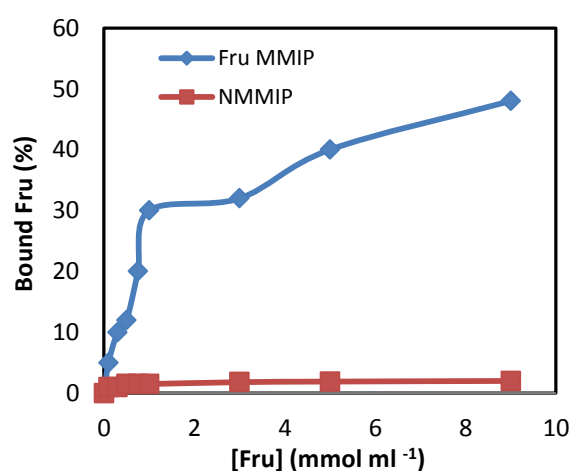


Figure 3. Adsorption graphs of magnetic fructose imprinted (Fru MMIP) and non-imprinted (NMMIP) polymer.

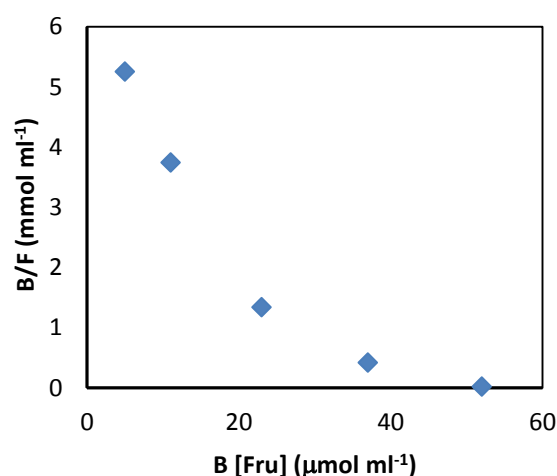


Figure 4. A Scatchard graph of magnetic fructose imprinted polymer.

The fructose of apple juice was also determined by conventional method (o- cresol: H₂SO₄ assay). However, before the assay applied, the apple juice was centrifuged, and then was filtered twice to get a clear solution with the aim to analyze. The results taken from MMIP were without centrifugation. By this result, fructose MMIP can be effectively used to analyze fructose from apple juice.

4. CONCLUSIONS

Molecularly imprinted polymers with magnetic properties are used as a cheaper and robust alternative to separate from complex media. The characterization of fructose imprinted magnetic polymers was done by FT-IR. The adsorption graphs and the real sample application were investigated. The results indicated that the prepared MMIPs showed a high adsorption capacity and good selectivity to fructose. The main advantage of this fructose MMIPs is the possibility to be stored and used at room temperature without any loss in separation capacity. In this study, the fructose can be analyzed from apple juice without any extra analytical methods such as filtration or centrifugation. It was shown that magnetic fructose MIP can be an alternative adsorbent for solid phase extraction.

ACKNOWLEDGEMENTS

This study was financially supported by Ege University Scientific Research Foundation (Project No: 2011 FEN 042).

Conflict of interest


Authors declare that there is no a conflict of interest with any person, institute, and company, etc.

REFERENCES

- Alexander, C.; Andersson, H.S.; Andersson, L.; Ansell, R.J.; Kirsch, N.; Nicholls, I.A.; O'Mahony, J.; Whitcombe, M.J. *J. Mol. Recog.* **2006**, 19, 106-180.
- Chen, L.; Li, B. *Anal. Methods* **2012**, 4, 2613-2621.
- Dan Chen, D.; Deng, J.; Liang, J.; Xie, J.; Huang, K.; Hu, C. *Anal. Methods* **2013**, 5, 722-728.
- Kan, X.; Geng, Z.; Zhao, Y.; Wang, Z.; Zhu, J. *Nanotechnol.* **2009**, 20, 165601-165608.

- Simón de Dios, A.; Díaz-García, M.E. *Anal. Chim. Acta.* **2010**, 666, 1-22.
- Changa, L.; Chena, S.; Li, X. *Appl. Surf. Sci.* **2012**, 258, 6660- 6664.
- Liua, Z.L.; Ding, Z.H.; Yao, K.L.; Tao, J.; Dua, G.H.; Lua, Q.H.; Wanga, X.; Gong, F.L.; Chen, X. *J. Magn. Magn. Mate.* **2003**, 265, 98-105.
- Philippova, O.; Barabanova, A.; Molchanov, V.; Khokhlov, A. *Eur. Polym. J.* **2011**, 47, 542-559.
- Zhang, Z.; Tan, W.; Hu, Y.; Li, G. *J. Chromatogr. A.* **2011**, 1218, 4275- 4283.
- Zhang, X.; Chen, L.; Xu, Y.; Wang, H.; Zeng, Q.; Zhao, Q. Ren, N.; Ding, L. *J. Chromatogr. B.* **2010**, 878, 3421-3426.
- Phutthawong, N.; Pattarawarapan, M. *Polym. Bull.* **2013**, 70, 691-705.
- Behrens, S. *Nanoscale* **2011**, 3, 877-892.
- Laurent, S.; Forge, D.; Port, M.; Roch, A.; Robic, C.; Elst Vander, L.; Muller, R.N. *Chem. Rev.* **2008**, 108, 2064-2110.
- Ma, Z.; Liu, H. *China Particuology* **2007**, 5, 1-10.
- Boyer, C.; Whittaker, M.R.; Bulmus, V.; Liu, J.; Davis, T.P. *NPG Asia Mater.* **2010**, 2, 23-30.
- Lerma-García, M.J.; Zougagh, M.; Ríos, A. *Microchim. Acta.* **2013**, 180, 363-370.
- Kumar, V.; Pattabiraman, T.N. *Indian J. Clin Biochem.* **1997**, 12, 95-99.
- Walker, R.W.; Dumke, K.A.; Goran, M. I. *Nutrition* **2014**, 30, 928-935.

ORCID

 0000-0002-0907-4175 (B. Okutucu)



Practical synthesis, characterization and photo-physical properties of metallophthalocyanines bearing benzhydryloxy substituents

Mehmet Salih AĞIRTAŞ*, Muhammed Yusuf ÖNDEŞ, Beyza CABİR

Department of Chemistry, Faculty of Science, Van Yüzüncü Yıl University, 65080, Van, Turkey

Received: 28 March 2018, Revised: 28 May 2018, Accepted: 29 May 2018

*Corresponding author's e-mail address: salihagirtas@hotmail.com (M. Salih Ağırtaş)

ABSTRACT

The aim of present study is to make practical synthesis of benzhydryloxy substituted phthalocyanines with high solubility. Therefore, the synthesis and characterization of benzhydryloxy substituted zinc and magnesium of phthalocyanines were performed. The characterization of the new compounds was clarified by spectra such as IR, NMR, UV and Mass spectra. Furthermore, fluorescence and aggregation behaviors of these new compounds were investigated. It was seen to be obtained the compounds more economically with the method used.

Keywords: Phthalocyanine, practical synthesis, characterization, aggregation.

Benzhidriloksi substituentlerini taşıyan metalloftalosiyaninlerin pratik sentezi, karakterizasyonu ve foto-fiziksel özellikleri

ÖZ

Bu çalışmanın amacı, yüksek çözünürlüğe sahip benzhidriloksi substitue ftalosiyaninlerin pratik sentezini yapmaktır. Bu nedenle, ftalosiyaninlerin benzhidriloksi substitueli çinko ve magnezyum sentezi ve karakterizasyonu gerçekleştirilmiştir. Yeni bileşiklerin karakterizasyonu, IR, NMR, UV ve Kütle spektrumları gibi spektrumlarla açıklandı. Ayrıca, bu yeni bileşiklerin floresan ve agregasyon davranışları araştırıldı. Kullanılan yöntemle bileşiklerin daha ekonomik olarak elde edildiği görüldü.

Anahtar Kelimeler: Ftalosiyanin, pratik sentez, karakterizasyon, agregasyon.

1. INTRODUCTION

Phthalocyanines (Pcs) are known to have been synthesized since a century. In addition to being used as dyes and pigments, they are also being used in different areas.¹⁻² Some of these areas can be listed as liquid crystals³, catalysts⁴, chemical sensors⁵, photovoltaic⁶, data storage⁷, semiconductors⁸, light-emitting diodes⁹, solar cell¹⁰, nonlinear optic material¹¹ and sensor for photodynamic therapy.¹² Innovations are added these areas depending on technological developments. At the beginning of the factors that limit the use of phthalocyanines in these areas lies low resolution and aggregating.¹³ Many studies with regard solubility of phthalocyanines are present in the literature.¹⁴⁻¹⁶ Factors that inhibit solubility are obstacles to other applications. For compounds of phthalocyanine, determining the behavior of aggregation also gives an idea of solubility.¹⁷ Aggregation also inhibits the solubility of phthalocyanine compounds.¹⁸ Thus aggregated

phthalocyanine compounds are ineffective as photosensitizers. Soluble and non-aggregated phthalocyanines are also needed to obtaine applicable photophysical data.¹⁹ As a result, phthalocyanine compounds are prevented from effectively using the optical and redox properties.²⁰ An important way to prevent this is to choose appropriate groups for peripheral and non-peripheral positions.²¹

In this study, we reported the synthesis and the characterization of new metallo phthalocyanines substituted with benzhydryloxy peripheral units. The reasons for choosing this functional group are that the bulky and Pcs core enhance the solubility in organic solvents and control the aggregation behavior in different concentrations. At same time, a significant advantage of these compounds is that they can dissolve in a wide range of solvent environments.

2. MATERIALS AND METHODS

2.1. Materials

Zinc(II) chloride (ZnCl_2), magnesium (II) chloride (MgCl_2), potassium carbonate (K_2CO_3), ethanol, methanol, ethyl acetate, acetonitrile, chloroform (CHCl_3), dichloromethane (CH_2Cl_2), tetrahydrofuran (THF), dimethyl sulfoxide (DMSO) were purchased from Merck and Sigma. The solvents were purified according to standard procedure²² and stored over molecular sieves (4 Å). All reactions were carried out under dry nitrogen atmosphere. Melting points were measured on an electro-thermal apparatus. Electronic spectra were recorded on a Hitachi U-2900 Spectrophotometer (Van YYU, Central Laboratory, Turkey). Routine FT-IR spectra were recorded on a Thermo Scientific FT-IR (ATR sampling accessory) spectrophotometer (Van YYU, Central Laboratory, Turkey). ^1H NMR spectra were recorded on an Agilent 400 MHz spectrometer (Van YYU, Central Laboratory, Turkey) with tetramethylsilane as internal standard. Mass spectra were recorded on a MALDI (matrix assisted laser desorption ionization) BRUKER Microflex LT.

2.2. Method

2.2.1. 4-(benzhydryloxy)phthalonitrile (3)

A mixture of diphenyl methanol **1** (0.532 g, 2.89 mmol) and 4-nitrophthalonitrile **2** (0.500 g, 2.89 mmol) in 15 mL dimethylformamide (DMF) was stirred at room temperature under nitrogen atmosphere. After stirring for 15 min, K_2CO_3 (1.27 g, 9.2 mmol) was added into the mixture over a period of 2 h. The reaction mixture was further stirred for 48 h, and then poured into cold water (150 mL) and stirred again. The precipitate was filtered, washed with water to neutralize, and then dried. The residue was recrystallized from ethanol. The product is soluble in ethyl acetate, acetonitrile, CHCl_3 , CH_2Cl_2 , dichloroethane, benzene, THF, DMF and DMSO. Yield: 0.40 g (45 %). Mp: 158-160°C. FT-IR spectrum (cm^{-1}): 3109, 3059, 3039 (Ar-CH), 2900 (CH), 2225 (CN), 1593, 1566, 1492, 1454, 1354, 1414, 1311, 1253, 1207, 1161, 1087, 1006, 879, 702. ^1H NMR (400 MHz, DMSO-d_6) δ ppm: 8.02, 8.00, 7.84, 7.47, 7.46, 7.36, 7.34, 7.29, 7.27, 6.83, 1.73.

2.2.2. 2, 10, 16, 24 – Tetrakis(benzhydryloxy phthalocyaninato) Zinc (II) (4)

A mixture of 4-(benzhydryloxy) phthalonitrile **3** (0.100 g) and ZnCl_2 (0.020 g) was powdered in a quartz crucible and heated in a sealed glass tube for 5 min under nitrogen at 270 °C. After cooling to room temperature, the product was washed with water, and was filtered. Then, the product washed with hexane, benzene and toluene again. The product was purified by column chromatography on silica with an eluent of THF. The product is soluble in CH_2Cl_2 , dichloroethane, ethanol, methanol, CHCl_3 , propanol, butanol, ethyl acetate, DMF, THF, and DMSO. The yield was 0.048 g (46 %). UV-Vis

(THF) λ_{max} (log ϵ : 680 (5.22), 614 (4.71), 350 (5.08). FT-IR spectrum (cm^{-1}): 3059, 2920, 1604, 1485, 1450, 1400, 1350, 1242, 1095, 1037, 941, 879, 744. MALDI-TOF MS: m/z $[\text{M}]^+$ calcd. for $\text{C}_{84}\text{H}_{56}\text{N}_8\text{O}_4\text{Zn}$: 1306.77; found $[\text{M}]^+$: 1306.79.

2.2.3. 2, 10, 16, 24 – Tetrakis (benzhydryloxy phthalocyaninato) Mg (II) (5)

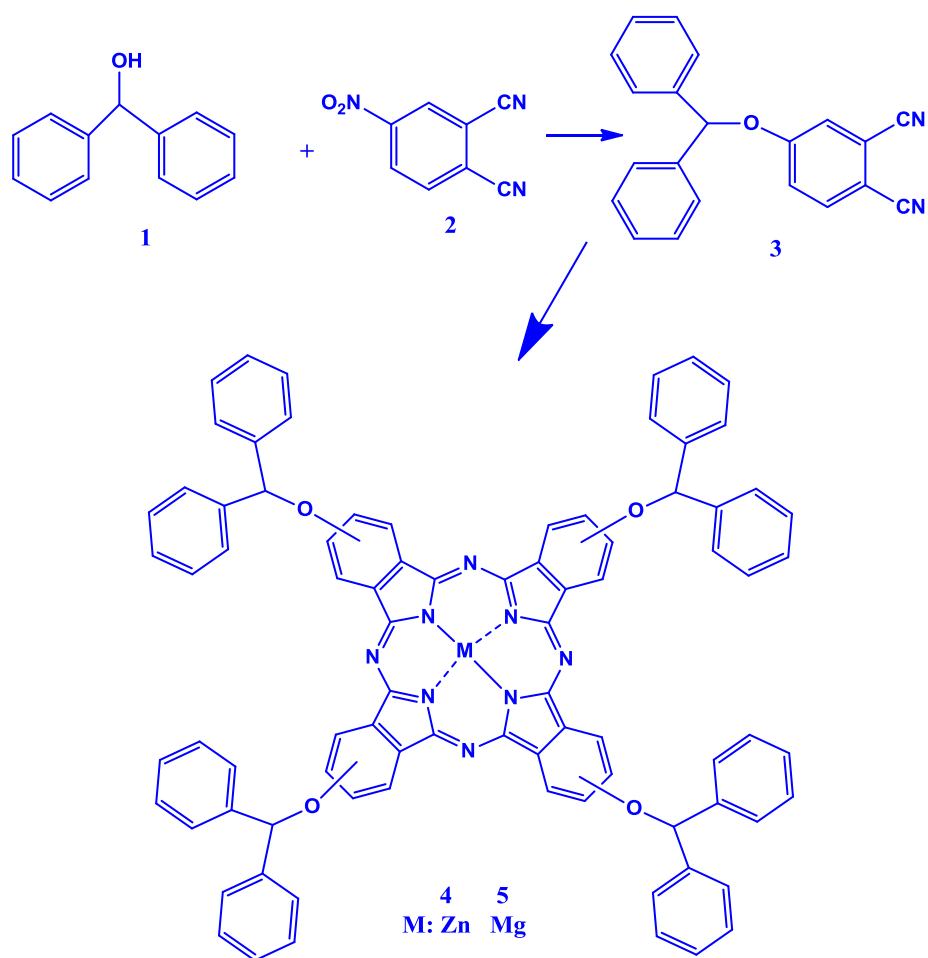
A mixture of 4-(benzhydryloxy) phthalonitrile **3** (0.100 g) and MgCl_2 (0.020 g) was powdered in a quartz crucible and heated in a sealed glass tube for 5 min under nitrogen at 270 °C. After cooling to room temperature, the product was washed with water, and was filtered. Then, the product washed with hexane, benzene, and toluene and diethyl ether again. The product is soluble in CH_2Cl_2 , dichloroethane, ethanol, methanol, CHCl_3 , propanol, butanol, ethyl acetate, DMF, THF, and DMSO. The yield was 0.032 g (31 %). UV-Vis (THF) λ_{max} (log ϵ : 690(5.25), 622(4.74), 354(4.98). FT-IR spectrum (cm^{-1}): 3024, 2924, 1600, 1492, 1450, 1338, 1261, 1095, 1026, 906, 802, 756. MALDI-TOF MS: m/z $[\text{M}]^+$ calcd. for $\text{C}_{84}\text{H}_{56}\text{MgN}_8\text{O}_4$: 1265.70; found $[\text{M}]^+$: 1265.17.

3. RESULTS AND DISCUSSION

3.1. Synthesis and Characterization

The synthetic recipe and the formulas of the 4-(benzhydryloxy) phthalonitrile (**3**) and metallophthalocyanines (**4-5**) are shown in Scheme 1. Synthesis of 4-(benzhydryloxy) phthalonitrile (**3**) was carried out in a similar way to our previous studies. Diphenyl methanol **2** and 4-nitrophthalonitrile **1** were added the reaction mixture in the presence of potassium carbonate to obtain the phthalonitrile derivative. The reaction was completed at room temperature under a nitrogen atmosphere for 48 hours. The phthalocyanines (**4-5**) were prepared by the reaction of 4-(benzhydryloxy) phthalonitrile (**3**) with ZnCl_2 , MgCl_2 under N_2 atmosphere. Spectra such as UV, IR, NMR and mass spectra were used in the elucidation of the structure of the newly prepared compounds.

Novel phthalocyanines (**4-5**) were purified by column chromatography after pre-purification (solvent washing). This purification is not to separate the isomers, but is for obtaining of the appropriate isomer mixtures. In the literature, such compounds are given as molecular symmetry as C_{4h} , C_{2v} , C_s , and D_{2h} . It is often not necessary to purify these isomers. If the separation of the isomers is necessary, different chromatographic methods can be used.²³ New phthalocyanines are easy soluble in ordinary organic solvents such as chloroform, dichloroethane, dichloromethane, tetrahydrofurane, dimethylformamide, dimethyl sulfoxide, ethanol, methanol, propanol, butanol, ethyl acetate. The high solubility of these compounds of phthalocyanine gives advantages in terms of applications.



Scheme 1. The route for the synthesis of compounds 3-5.

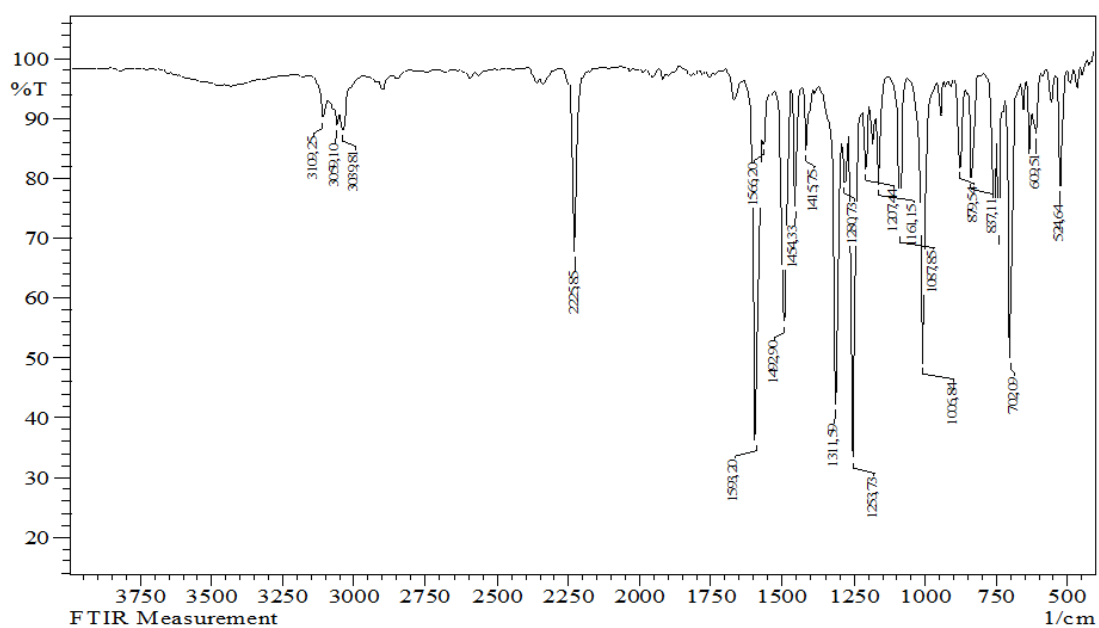


Figure 1. FT-IR spectrum of 4-(benzhydryloxy) phthalonitrile 3.

The IR spectrum gives information on the nitrile peak, which is regarded as a significant difference between phthalonitrile derivatives, and phthalocyanine compounds. This peak reveals the structural difference. It is not found in compounds of $2225(\text{CN})\text{ cm}^{-1}$ band phthalocyanine in 4- (benzhydryloxy) phthalonitrile compound. This confirms what is expected for the compounds. The FT-IR spectrum of compound **3** is shown in Figure 1. The complex compound **4** gives IR vibration bands at 702, 879, 1006, 1087, 1253(C-O-C), 1454-1492, and 1598(C=C) cm^{-1} . These data support what is expected. The Compound **5** shows similar bands except minor shift values.

The NMR spectrum used to elucidate the structure of organic compounds gives important information. The ^1H NMR spectrum of the 4- (benzhydryloxy) phthalonitrile compound having an organic structure in DMSO- d_6 gives the aromatic and aliphatic protons as 8.02, 8.00, 7.84, 7.47, 7.46, 7.36, 7.34, 7.29, 7.27, 6.83 (Ar-H), 1.73 ppm, respectively. Compounds **4** and **5** show slight shifts relative to the starting material. Complex **4** compound gives aromatic at 7.45, 7.29, 7.18, 7.06, 6.86, 6.62 (Ar-H) and aliphatic peaks at 1.37 ppm. Complex **5** shows 7.65, 7.31, 7.18, 6.86, 6.62, and 1.35 peaks.

The mass spectra of the compounds of phthalocyanine confirm the structures of the compounds. The 1306.79 ion peak value obtained for zinc phthalocyanine is equivalent to the calculated mass of 1306.77. This confirms the expected complex structure. A similar phenomenon has also been observed for the compound of magnesium phthalocyanine. It corresponds to the value of 1265.17 which is calculated at 1265.70 value.

3.2. Photophysical study

UV spectral studies provide some characteristic information by electronic structure of phthalocyanine compounds. One of them is the characteristic Q and B bands. These bands are basic indicators for molecular structure. At the same time, these bands provide information on whether or not the structural metal of the composite is connected. Absorption, excitation, and emission spectra play an important role in determining the structure and the photophysical properties of the compound when evaluated together. The tetrahydrofuran solvent was used for the spectral work. The $\pi\text{-}\pi^*$ transitions of Q and B bands of the synthesized phthalocyanine compounds are in accordance with the literature.²³ The numerical values of the UV absorption bands are given experimental limitations. Some parameters present that affect the void space between HOMO and LUMO for phthalocyanine compounds. This value gives information about whether phthalocyanine compound can be used as semiconductor or photosensor.²⁴ Current studies show that compounds of phthalocyanine are useful in the case of reddish absorption bands to be used as photosensors. When a compound meets these requirements, it can provide a

potential to be used therapeutically.²⁵ The values for the phthalocyanine compounds have been obtained at values of 680 and 690 nm which are much higher than the assumed value of 650 nm.

Aggregation studies for **4-5** compounds of phthalocyanine were carried out in THF. Aggregation studies for **4-5** compounds of phthalocyanine were carried out in THF. Absorption values were read in the UV spectrum against the increase of the amount of substance in the range of $5.74 \times 10^{-6}\text{M}$ - $3.22 \times 10^{-5}\text{M}$ concentration. The aggregation studies of compounds **4** and **5** are given in Figures 2 and 3, respectively. Aggregation studies show that these compounds are well suited to the Beer-Lambert law. These compounds are solubilized not only in THF, but also in solvents such as CH_2Cl_2 , dichloroethane, ethanol, methanol, CHCl_3 , propanol, butanol, ethyl acetate, DMF, and DMSO. Both non- aggregation and high resolution give advantages for applications.

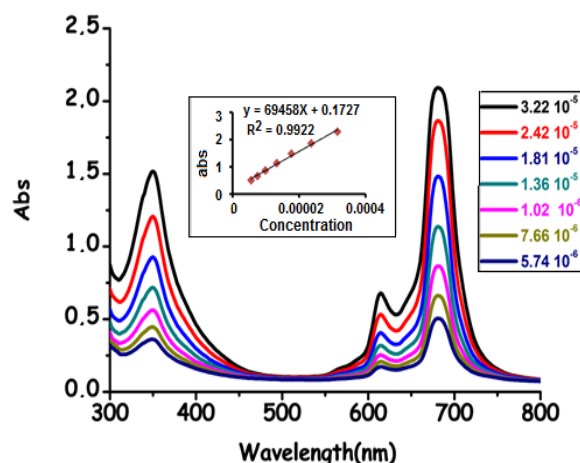


Figure 2. Aggregation study of compound **4** in THF (Concentrations: $3.22 \cdot 10^{-5}$, $2.42 \cdot 10^{-5}$, $1.81 \cdot 10^{-5}$, $1.36 \cdot 10^{-5}$, $1.02 \cdot 10^{-6}$, $7.66 \cdot 10^{-6}$, $5.74 \cdot 10^{-6}$ M).

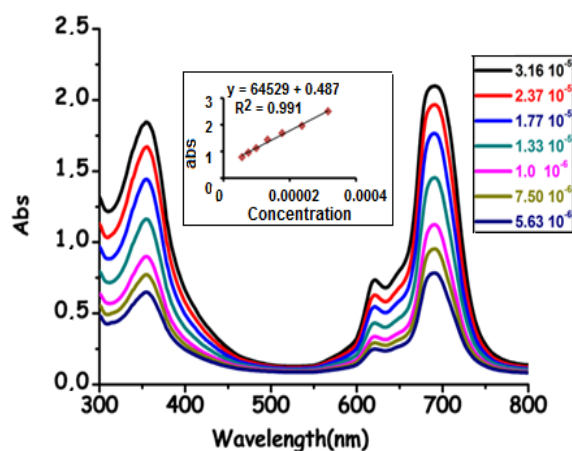


Figure 3. Aggregation study of compound **5** in THF (Concentrations: $3.16 \cdot 10^{-5}$, $2.37 \cdot 10^{-5}$, $1.77 \cdot 10^{-5}$, $1.33 \cdot 10^{-5}$, $1.0 \cdot 10^{-6}$, $7.50 \cdot 10^{-6}$, $5.63 \cdot 10^{-6}$ M).

As is known, fluorescence substances have an increasing interest day by day. This is why some of these materials are widely used. They are used in many applications such as DNA, sensors and many technological applications. The absorption, excitation and emission spectra for phthalocyanines **4** and **5** are shown in Figures 4 and 5. The Stoke's shifts are consistent with available data in the literature.²⁶⁻²⁷ Phthalocyanines are often obtained with sophisticated processes with low yields. Often the resolution is not as good as desired. For this reason, the synthesis of phthalocyanines which are easily designed and have high solubility is economically important.

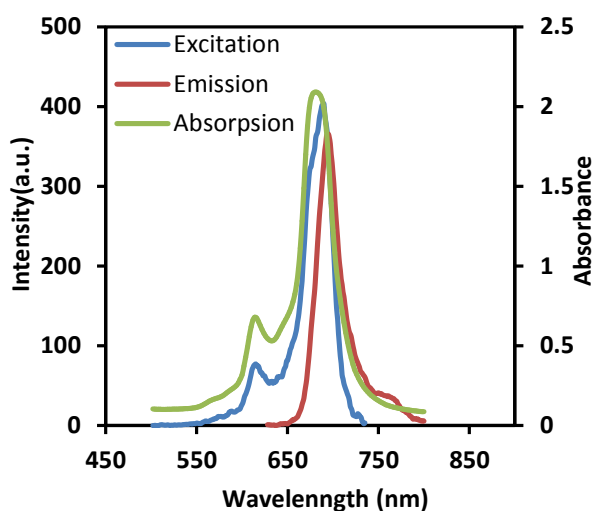


Figure 4. Electronic absorption, excitation and emission spectra of compound **5** in THF (Excitation wavelength = 693 nm).

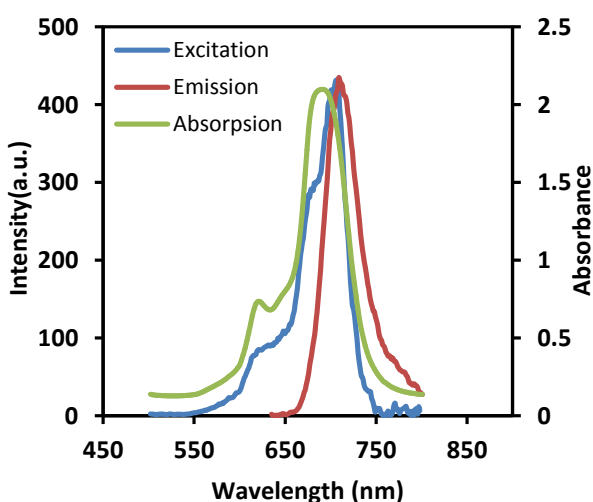


Figure 5. Electronic absorption, excitation and emission spectra of compound **6** in THF (Excitation wavelength = 647 nm).

4. CONCLUSIONS

Zinc (II) and magnesium (II) phthalocyanines (**4-5**) bearing benzhydryloxy groups were synthesized for the first time *via* the cyclotetramerisation reaction of new 4-(benzhydryloxy) phthalonitrile (**3**) in the presence of corresponding metal salt. New compounds were characterized by spectroscopic data (¹H NMR, MALDI-TOF, IR, and UV-vis). All the studied metal (II) phthalocyanines are soluble in most solvents chloroform, dichloroethane, dichloromethane, tetrahydrofuran, dimethylformamide, dimethyl sulfoxide, ethanol, methanol, propanol, butanol, ethyl acetate. These phthalocyanines have a significant advantage in solubility in a large number of solvents. In addition, these compounds may have potential for use in different areas due to their fluorescence, non-aggregation, and high-resolution properties.

ACKNOWLEDGEMENTS

The authors are grateful to the Office of Scientific Research Projects of Van Yüzüncü Yıl University for their financial support.

Conflict of Interest


Authors declare that there is no a conflict of interest with any person, institute, company, etc.


REFERENCES


- McKeown, N.B. *Phthalocyanine Materials: Synthesis, Structure and Function*, Cambridge University Press, Cambridge, 1998.
- Leznoff, C.C.; Lever, A.B.P. Eds. *Phthalocyanines: Properties and Applications*, vol. 4, VCH, New York, 1989.
- Garland, A.D.; Chambrier, I.; Cammidge, A.N.; Cook, M.J. *Tetrahedron* **2015**, 71, 7310-7314.
- Liang, Q.; Zhanga, M.; Liub, C.; Xua, S.; Li, Z. *Appl. Catal. A* **2016**, 519, 107-115.
- Shi, J.; Luan, L.; Fang, W.; Zhao, T.; Liu, W.; Cui, D. *Sens. Actuators B* **2014**, 204, 218-223.
- Sánchez-Díaz, A.; Pacios, R.; Muñecas, U.; Torres, T.; Palomares, E. *Org. Electron.* **2011**, 12: 329-335.
- Lile, J.R.D.; Heine, T.; Zhou, S. *Comp. Mater. Sci.* **2017**, 129, 24-36.

8. Shao, X.; Wang, S.; Li, X.; Su, Z.; Chen, Y.; Xiao, Y. *Dyes Pigments* **2016**, 132, 378-386.
9. Deng, Z.; Lü, Z.; Chen, Y.; Yin, Y.; Zou, Y.; Xiao, J.; Wang, Y. *Solid State Electron.* **2013**, 89, 22-25.
10. Ma, D.; Pan, S.; Zhang, T.; Huang, B.; Xie, S.; Yang, H.; Peng, Y. *Dyes Pigments* **2016**, 127, 78-86.
11. Sekhosana, K.E.; Nyokong, T. *J. Mol. Struct.* **2016**, 1117, 140-146.
12. Wang, A.; Gui, L.; Lu, S.; Zhou, L.; Zhou, J.; Wei, S. *Dyes Pigments* **2016**, 126, 239-250.
13. Erdoğan, A.; Arıcı, M. *J. Fluorine Chem.* **2014**, 166, 127-133.
14. Ağırtaş, M.S. *Dyes Pigments* **2008**, 79, 247-51.
15. Ağırtaş, M.S. *Inorg. Chim. Acta* **2007**, 360, 2499-502.
16. Bandera, Y.; Burdette, M.K.; Shetzline, J.A.; Jenkins, R.; Creager, S.E.; Foulger, S.H. *Dyes Pigments* **2016**, 125, 72-79.
17. Palewska, K.; Sworakowski, J.; Lipinski, J. *Opt. Mater.* **2012**, 34, 1717-1724.
18. Chen, J.; Zhang, T.; Wang, S.; Hu, R.; Li, S.; Ma, J.S.; Yang, G. *Spectrochim. Acta A.* **2015**, 149, 426-433.
19. Nyokong, T., Antunes, E. *Photochemical and Photophysical Properties of Metallophthalocyanines. Handbook of Porphyrin Science*, 2010, pp. 247-357.
20. Claessens, C.G.; Hahn, U.; Torres, T. *Chem. Rec.* **2008**, 8, 75-97.
21. Tillo, A.; Stolarska, M.; Kryjewski, M.; Popenda, L.; Sobotta, L.; Jurga, S.; Mielcarek, J.; Goslinski, T. *Dyes Pigments* **2016**, 127, 110-115.
22. Armarego, W.L.F.; Chai, C.L.L. *Purification of laboratory Chemicals*, 7nd ed., Butterworth-Heinemann, Oxford, 2013.
23. Saka, E.T.; Kobak, R.Z.U.; Alp, H.; Sarkı, G.; Koca, A.; Kantekin, H. *Synthetic Met.* **2016**, 217, 295-303.
24. Fukuda, T.; Kobayashi, N. In: Kadish KM, Smith KM, Guillard R, editors. *Handbook of porphyrin science with applications to chemistry, physics, materials science, engineering, biology and medicine*, Singapore: World Scientific Publishing Co. Pte. Ltd, vol. 9, 2010.
25. Mehraban, N.; Freeman, H.S. *Materials* **2015**, 8, 4421-4456.
26. Saka, E.T.; Durmuş, M.; Kantekin, H. *J. Organomet. Chem.* **2011**, 696, 913-924.
27. İşçi, Ü.; Beyreis, M.; Tortik, N.; Topal, S.Z.; Glueck, M.; Ahsen, V.; Dumoulina, F.; Kiesslich, T.; Plaetzer, K. *Photodiagn. Photodyn.* 2016, 13, 40-47.

ORCID

 0000-0003-1296-2066 (M.S. Ağırtaş)

 0000-0002-4593-3694 (M.Y. Öndeş)

 0000-0003-4735-4511 (B. Cabir)



Biosorption of methylene blue and acid red 88 from wastewater by using peanut shell

Onur YEL

TEV Inanc High school, 44100, Gebze/Kocaeli

Received: 16 April 2018, Revised: 29 May 2018, Accepted: 31 May 2018

*Corresponding author's e-mail address: onuryel77@gmail.com (O. Yel)

ABSTRACT

This study represents the removal of harmful dye substances from wastewaters by using a waste and cheap biosorbent. For this aim, peanut shell was used as a biosorbent for the removal of methylene blue and acid red 88 dyes. The effects biosorbent amount, initial dye concentration, pH, temperature, contact time and dye type on biosorption were studied. In the study, the highest removal of acid red 88 was found as 88% using dye solution of 200 ppm with 5.0 grams of peanut shell at contact time of 300 minutes. The highest removal of methylene blue was determined as 99% using dye solution of 200 ppm with 4.0 grams of peanut shell at contact time of 60 minutes. As a result of dye type, methylene blue which has a linear geometric structure has demonstrated a high removal than acid red 88. Biosorption isotherms for both dyes were found more consistent with the Langmuir model according to Freundlich model.

Keywords: Biosorption, peanut shell, methylene blue, acid red 88.

Yer fıstığı kabuğu kullanarak atıksudan metilen mavisi ve asit kırmızısı 88 boyasının biyosorpsiyonu

ÖZ

Bu çalışma atık ve ucuz bir biosorbent kullanarak atık sularadan zararlı boyar maddelerin uzaklaştırılmasını temsil etmektedir. Bu amaçla, yer fıstığı kabuğu metilen mavisi ve asit kırmızısı 88 boyalarının uzaklaştırılması için bir biosorbent olarak kullanıldı. Biyosorpsiyon üzerine biosorbent dozu, başlangıç boyar madde konsantrasyonu, pH, sıcaklık, temas süresi ve boya tipinin etkileri incelendi. Çalışmada, asit kırmızısı 88' in en yüksek uzaklaştırılması 300 dakikalık temas süresinde yer fıstığı kabuğunun 5 gramı ile 200 ppm'lik boya çözeltisi kullanılarak % 88 olarak bulundu. Metilen mavisinin en yüksek uzaklaştırılması ise 60 dakikalık temas süresinde yer fıstığı kabuğunun 4 gramı ile 200 ppm'lik boya çözeltisi kullanılarak % 99 olarak belirlendi. Boya tipinin bir sonucu olarak lineer bir geometrik yapıya sahip olan metilen mavisi, asit kırmızısı 88' den daha yüksek bir uzaklaştırma göstermiştir. Her iki boya için biyosorpsiyon izotermi Freundlich modeline göre Langmuir modeliyle daha tutarlı bulundu.

Anahtar Kelimeler: Biyosorpsiyon, yer fıstığı kabuğu, metilen mavisi, asit kırmızısı 88.

1. INTRODUCTION

Water is the most important vital resource for living beings in terms of life's existence in the earth. When the establishment and expansion places of the ancient civilizations were investigated, a water edge has been always preferred. As a result of the significance of water resources, wars have come to the fore, and the importance of freshwater resources has once again been revealed.¹ Due to both industrialization and rapid population growth in the world, existing water sources are subject to anthropogenic contamination. The damages caused by this pollution can cause non-reversible damages to the environment. One such way of water

pollution is a result of the dyes used in textile factories.² With the consumption of these dyestuffs, an enormous pollution can occur in the environment that can disrupt the ecological balance. Dyes are used for the colorization process of objects such as fabric and fibers in the textile industry. Moreover, these dyes are decomposed by biodegradable methods due to their molecular structure. Synthetic dyestuffs are used widely in textile, paint, paper and printing industries. Today, over 100,000 synthetic dyes are used commercially and 700,000 tons of dyes is produced annually.³ When the amount of dye production and remaining waste of dye after its usage are considered, it is evident that the removal of the colored wastewaters is essential for the preservation of the

environment. Beside the primary harm of the dyestuff pollution, there are many other side effects of the polluted colored wastewaters where the water resource becomes unfit for use as nourishment.⁴ Some dyes have mutagenic and / or carcinogenic effects. The lack of photosynthesis causes the amount of dissolved oxygen in the water to derogate so that the anaerobic microorganisms outcompete aerobic microorganisms, which results in the formation of malodorous compounds in the growth of anaerobic microorganisms in the environment. In addition, the lack of oxygen can create a significant danger for the lives of other living things that require oxygen.⁵⁻⁷ Many biological, physical and chemical methods are used for the treatment of wastewater containing dyestuffs. These methods can be listed as; anaerobic treatment⁸, coagulation–flocculation⁹, adsorption¹⁰, biosorption¹¹, ultrafiltration¹², electrocoagulation¹³, and ion exchange.¹⁴ The most common and most important of these methods is adsorption. It is based that certain molecules dissolved in liquid phase cling onto the surface of a solid substance. According to other conventional methods, adsorption technique have attracted interest in recent years because it provides an effective removal the pollutants from environment. Adsorption is economically reasonable and provides high quality product formation.¹⁵ The most used raw material in adsorption process is activated carbon also known as the widest adsorbent.¹⁶ As it has a highly porous structure, it has an adsorption capacity of between 500 and 1200 m² per gram of surface of activated carbon. For this reason, in many industrial processes, the activated carbon is seen to be used.¹⁷ However, active carbon is an economically disadvantaged adsorbent and it challenges researchers to find new, cheap, natural, and local adsorbents as alternatives to activated carbon. One of these alternatives, as proposed in this study, is peanut shell. Peanut is make peanut oil, butter, flour, and as a vegetarian protein resource, and are commonly harvested in global market to be consumed for nutritional purpose. Its annual production was over 43.9 million tons in 2014.¹⁸ Peanuts have a covering shell which is not appropriate for nutritional usage where it appears as a waste in the industries using peanuts.¹⁹ Hence, in this study, peanut shells are used as low-cost biosorbent material.

2. MATERIALS AND METHODS

In this study, a low-cost peanut shell was used as an biosorbent. Upon removal of methylene blue and acid red 88 dyes from the wastewaters by the usage of biosorbent, the effect of the biosorbent amount, contact time, dye concentration, pH, temperature, dyes type parameters were investigated. The results were calculated by measuring a UV-Visible spectrophotometer. The operations carried out in this aim are as follows:

2.1. Biosorbent preparation

The biosorbent which is in a state of waste after the consumption of peanuts, was firstly subjected to a washing process to minimize its chromaticity and then was applied to a drying process at 50°C in a thermal G11320SD oven. The dry peanut shells obtained after the dehydration process (there was a reduction in size), by the aid of emery paper, was pulverized in the context of expanding the surface area. In this direction, the biosorbent, which has become smaller in size, has been preserved by transferral into nylon plastic bags.

2.2. Preparation of colored wastewaters

First of all, artificial wastewaters are prepared in this direction. Distilled water was used as a solvent in the solutions, since water pollution is being investigated. For this reason, the stock solutions of methylene lue and acid red 88 of 800 ppm were prepared. Then, 50, 100, 200, 300 ppm solutions of methylene blue and acid red 88 dyes from the stock solutions were were prepares by diluting from stoch solutions. preserved in 100 mL HDPE containers for interaction with the biosorbent. methylene blue and acid red 88 were supplied from the local textile industry, AK-KIM Textile Industry in Yalova, Turkey. Their molecular structures are shown in Figures 1 and 2.

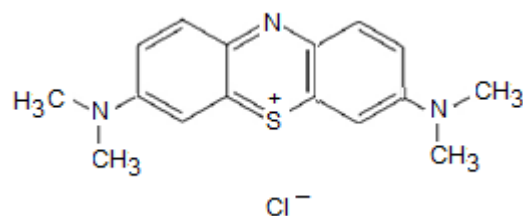


Figure 1. Methylene blue.

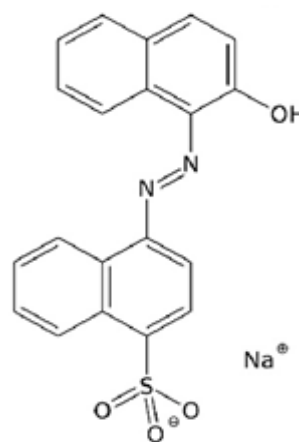


Figure 2. Acid red 88.

2.3. Application of adsorption experiments

In the case of carrying out the adsorption experiments, the previously prepared methylene blue dye and acid red 88 solution were interfaced with the biosorbent designated as Peanut Shell dust, which is stocked in plastic packages. 0.1, 0.25, 0.5, 1, 2, 4, 5 grams of adsorbents were used in the adsorption process. In the case of more homogenous dispersion of the mixture contained in 100 ml HDPE containers, the mixture was allowed to stand for 5 minutes as standard in all experiments. Then, all the solutions were rinsed at 110 rpm on a Thermal N11340 shaker at a variety of interaction time (0.25, 0.5, 1, 2, 4, 5 hours). Samples taken from the dye solution were initially centrifuged in Yuda 800D Centrifuge at 110 rpm to eliminate the residue particles and the samples were collected in closed test tubes. Then supernatants were analysed using UV-Vis spectrophotometer.

2.4. Analysis of experimental results

Shimadzu UV-Vis-2600 spectrophotometer was used to perform spectral scanning for methylene blue and acid red 88 dyes. As it is shown in Figure 3, the maximum absorbance values were read at 502 nm for acid red 88 and at 654 nm for methylene blue.

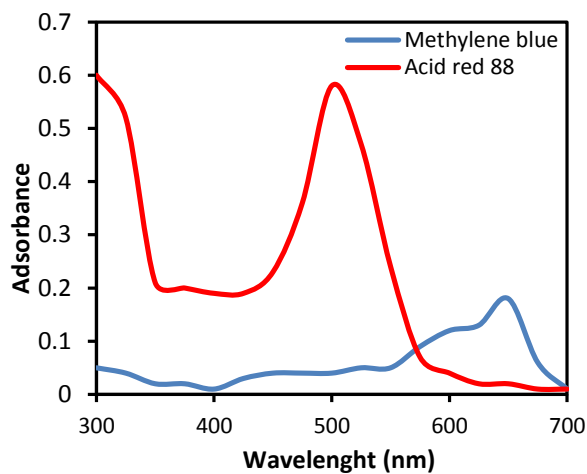


Figure 3. UV-Vis spectra of dyes.

In addition, in the measurements made with standard stock solutions, the R^2 value are found to be more than 0.99 as shown in Figures 4 and 5. Standard graphics in Figures 4 and 5 were used to determine the amounts of dyes removed by biosorbent.

2.4.1. Calculation of the biosorption capacity of biosorbent

When the system is in equilibrium during the adsorption process, the amount of substance adsorbed by

unit mass of biosorbent material was calculated as a function of temperature, and concentration. The amounts of dye adsorbed were estimated by using Eq. (1).

$$q_e = (C_0 - C_e) V / m \quad (1)$$

where q_e is the adsorption capacity of biosorbent (mg g^{-1}), C_0 is the initial concentration of dye (mg l^{-1}), C_e is the concentration of the dye adsorbed at the equilibrium (mg l^{-1}), V is the volume of solution (l), and m is the mass of the biosorbent (g).

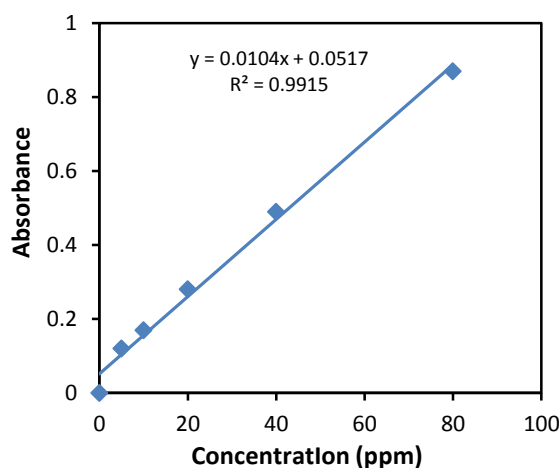


Figure 4. Standard absorbance graph of methylene blue.

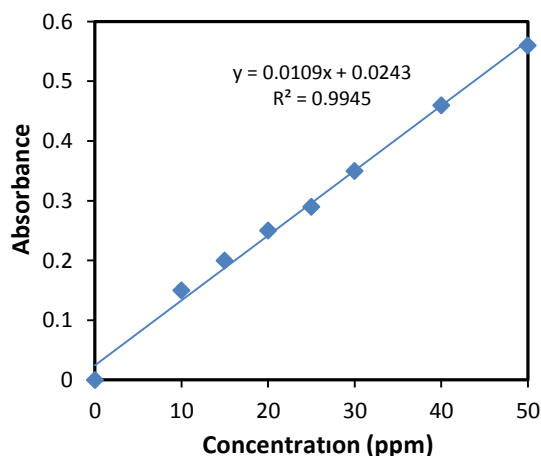


Figure 5. Standard absorbance graph of acid red 88.

2.4.2. Biosorption isotherms

The biosorption isotherm was studied according to the Langmuir and Freundlich isotherm models, which are used commonly.

The linear form of the Langmuir isotherm equation which indicates a homogenous adsorption, is given in Eq. (2),

$$C_e/q_e = 1/q_m K_L + C_e/q_m \quad (2)$$

In the equation, q_m is the maximum adsorption capacity (mg g^{-1}), C_e is the equilibrium concentration of dye in liquid phase (mg l^{-1}), K_L is Langmuir isotherm constant indicating adsorption energy. From the slope and intercept of the plot of C_e/q_e vs C_e , the values of q_m and K_L are obtained respectively.

The linear form of Freundlich isotherm equation which indicates a heterogeneous adsorption can be expressed in Eq. (3),

$$\ln q_e = \ln k + 1/n \ln C_e \quad (3)$$

In this equation, C_e is the equilibrium concentration of dye remained in liquid phase (mg l^{-1}), and q_e is amount of dye that is adsorbed by unit biosorbent (mg g^{-1}). k and n are the Freundlich isotherm constants. k indicates biosorption capacity (mg g^{-1}), n indicates the intensity of biosorption. From the slope and intercept of the plot of $\ln q_e$ vs $\ln C_e$, the values of n and k are obtained respectively.

3. RESULTS AND DISCUSSION

3.1. The effect of dye type on biosorption

In order to determine the efficacy of the different type of the dyes, the working conditions was kept constant at room temperature, $\text{pH} = 7$, 4 grams of the biosorbent, and dye concentration of 200 ppm. When the graph in Figure 6 is examined, a higher removal rate is observed in the methylene blue dye than in the acid red 88 dye.

The most acceptable reason for the high removal of methylene blue that it has a more appropriate geometric shape than acid red 88. Molecular structures of the dyes are shown in the Figures 1 and 2. Due to its linear structure, methylene blue molecules have the ability to demonstrate better biosorption into the pores of the biosorbent.

On the other hand, methylene blue and acid red 88 have different wavelengths, where blue color has a larger wavelength than the red color. Thus, the color difference is a considerable factor to the removal difference between the dye samples. The concentration which reduced below near-zero levels in experiments with methylene blue reveals that the peanut shell dust has a great potential of adsorbing ability. According to Figure 6, this high removal rate take places at an interaction time of about 30 min. At this point, the interaction time should be kept in 30-60 minutes period in order to prevent the loss of energy.

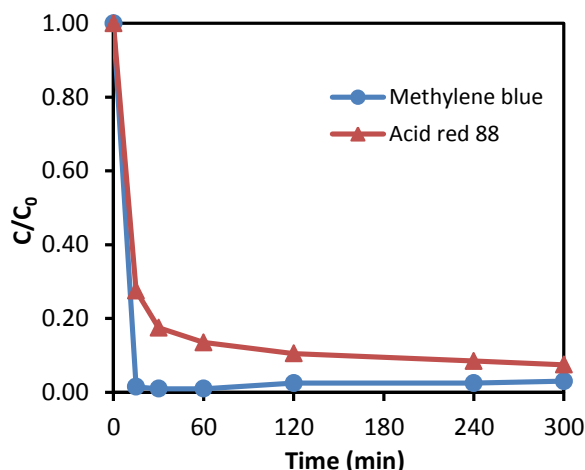


Figure 6. The effect of dye type on the biosorption of dyes (Dye concentration: 200 ppm, biosorbent amount: 4 gram).

3.2. The effect of initial dye concentration on biosorption

To examine the effect of the dye concentration on biosorption, the experimental conditions was kept constant at $\text{pH} = 7$, at room temperature, at the interaction time of 60 minutes, and 4 grams of biosorbent. According to Figure 4, the removal curve for acid red 88 dye stays at a lower level than the methylene blue removal curve. Therefore, when the type of dyes is examined, it appears that methylene blue dye has a higher adsorbing property. As a result of the interaction of the dyes with the peanut shell according to Figure 7, the highest removal is seen at 200 ppm for acid red 88, and 50 ppm for methylene blue.

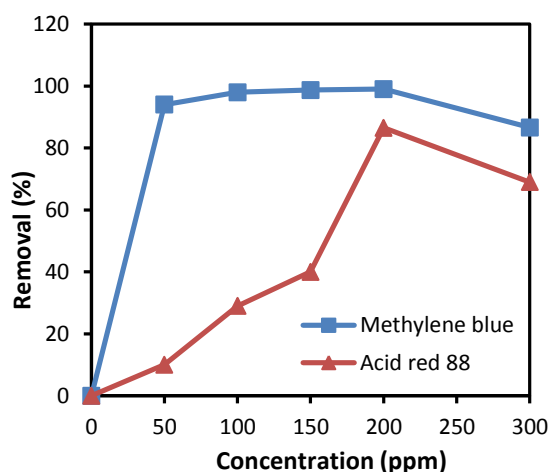


Figure 7. The effect of initial concentration on the biosorption of dyes (Dye concentration: 200 ppm, contact time: 60 minutes, biosorbent amount: 4 gram).

Biosorption for the same amount of grams for methylene blue is observed for all the concentrations at high removal percentages. Higher percentages of removal were obtained in the initial concentration of 200 ppm for acid red 88. When the other results of acid red 88 are examined, it is seen that this removal rate of the dye has also decreased after a rise. At this point, methylene blue also draws the same curve in a micro size. This is the cause of the parabolic curve, which first increases until its peak point and then decreases. This decrease can be explained by the insufficient pores of biosorbent due to the abundance of the dye concentration.

3.3. The effect of the amount of biosorbent on biosorption

To measure the effect of the amount of biosorbent on the removal of the dyes, the experimental conditions were selected as the dye solutions of 200 ppm, the interaction time of 60 min, the pH = 7, and room temperature. As can be seen in Figure 8, the increase in the amount of dyes per gram of biosorbent indicates that the remaining concentration decreases.

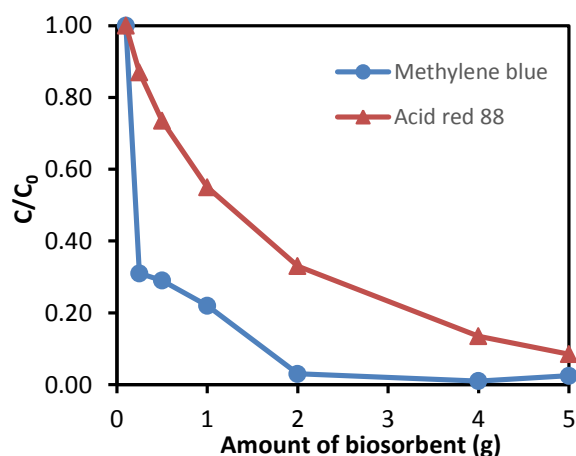


Figure 8. The effect of biosorbent amount of on the biosorption of dyes (Dye concentration: 200 ppm, contact time: 60 minutes).

According to the biosorption results of the two dyes, the increase in mass of biosorbent i generally leads to higher removal. When the test results for the methylene blue dye is examined, very similar removal rates are observed after a period of 1-2 grams. It can be understood that 1-2 grams of biosorbent can be used as the optimum amount of removal.

3.4. The effect of temperature change on biosorption

In order to measure the effect of temperature change on biosorption, the experimental results were obtained at pH 7, 200 ppm of dye concentrations, 120 minutes of

interaction time and 2 grams of biosorbent quantities. As can be seen from Figure 9, an increase in temperature slightly increases biosorption. Therefore, the energy consumption due to increased temperature does not encounter its cost. The slightly increased removal with additional temperature is not cost effective for the biosorption process. Hence, room temperature level has is the optimum because of the huge loss of energy for a slight increase in removal in higher temperatures.

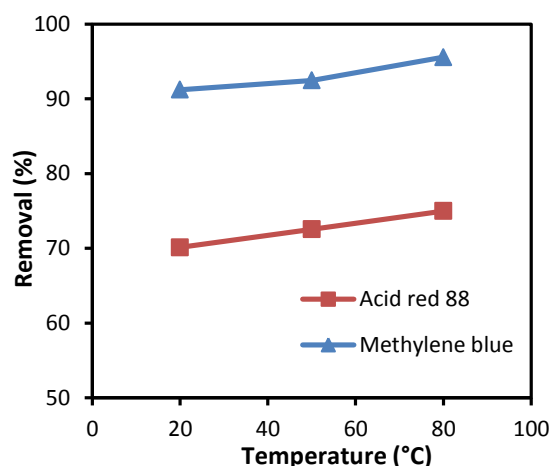


Figure 9. The effect of temperature on the biosorption of dyes (Dye concentration: 200 ppm, contact time: 120 minutes, biosorbent amount: 2 gram).

3.5. The effect of pH on biosorption

The effect of pH change on biosorption was carried out under the conditions initial dye concentration of 200 ppm, 120 minutes of interaction time and 2 grams of biosorbent. As can be seen in Figure 10, the best biosorption is obtained at pH 7. The same findings are also observed in the literature studies.²⁰

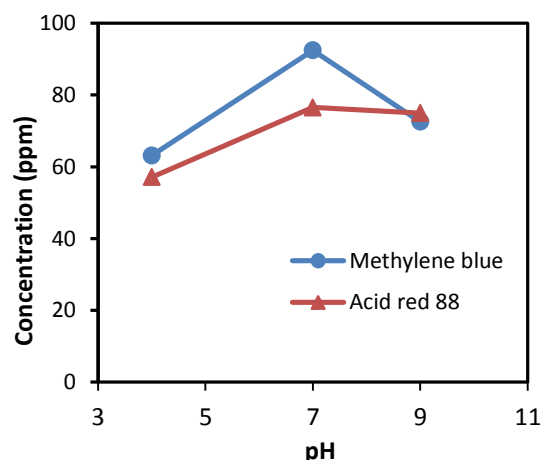


Figure 10. The effect of pH on the biosorption of dyes (Dye concentration: 200 ppm, contact time: 120 minutes, biosorbent amount: 2 gram).

All additional changes in pH level also affects the concentration of solution with the effect of H^+ or OH^- ions. Therefore, those additional hydronium or hydroxide ions can place into the empty pores of biosorbent instead of dye molecules. As can be seen in Figure 10, the optimum level of pH for biosorption is 7, indicating that no pH change is necessary to increase the removal of dye. Since the water is pure in its neutral pH range in the environment, it does not offer any additional action to achieve higher removal rates.

3.6. Biosorption isotherms

The biosorption isotherms of methylene blue and acid red 88 are studied according the Langmuir and Freundlich models in Equations (2) and (3), respectively. Isotherms were obtained for initial concentrations between 50 and 300 ppm for both dyes. The obtained isotherm parameters are given in Tables 1 and 2.

Table 1. Isotherm parameters of biosorption of methylene blue

	Methylene blue		
	Langmuir	Freundlich	
q_m	19.685	k	6.1854
K_L	0.5353	n	1.8761
R^2	0.8616	R^2	0.76

Table 2. Isotherm parameters of biosorption of acid red 88

	Acid red 88		
	Langmuir	Freundlich	
q_m	4.4091	k	0.1905
K_L	0.0181	n	1.6869
R^2	0.9898	R^2	0.9578

As can be seen from these Tables, Langmuir biosorption capacity (q_m) are found as 19.68 and 4.4091 $mg\ g^{-1}$ for methylene blue and acid red 88, respectively. The values of K_L which indicate biosorption energy were determined to be 0.5353 and 0.0181 $l\ g^{-1}$ for methylene blue and acid red 88, respectively.

The values of Freundlich biosorption capacity (k) isotherm are estimated as 6.1854 and 0.1905 $mg\ g^{-1}$ for methylene blue and for acid red 88, respectively. The values of n which indicate biosorption intensity were found as 1.8761 and 1.6869 $g\ l^{-1}$ for methylene blue and acid red 88, respectively. With the correlation coefficients of 0.86 and 0.9998 for methylene blue and acid red 88, the consistency to Langmuir isotherm was more good than Freundlich isotherm.

4. CONCLUSIONS

The wastewaters discharged to nature by the textile industry are rapidly becoming a globally increasing problem. These non-biodegradable dyes bring problems to the environment due to their toxic contents. For this reason, it is necessary to concentrate on the studies about the recovery of such wastes and toxic water. In this study, the removal of methylene blue and acid red 88 dyes that are used in the textile industry was investigated using peanut shell. In order to enlarge the surface area of the peanut shell, the pulverization process was made. The effects of biosorbent amount, contact time, initial dye concentration, pH, temperature, and type of dyes were investigated on the removal of the dyes by the biosorbent. At the result of the experiments, the highest removals for acid red 88 and methylene blue dyes were found as 88% and 99% under the experimental conditions studied, respectively. Biosorption isotherm followed best the Langmuir for both dyes. Because of the high removal rates obtained, the usage of peanut shell as an biosorbent can be a considerable alternative. These shells which can be easily obtained in most countries, are cheap and do not require industrial processing in any way, thus providing an alternative solution for the removal of contaminants from water. It is also possible that the peanut shell which are not subjected to any chemical treatment compared to activated carbon, can be supplied directly from the natural environment, and it can be used in an industrial context as a result of this work.

ACKNOWLEDGEMENTS

The author thanks for the financial assistance provided by Gebze Technical University.

Conflict of interest


Author states that there is no conflict of interest with any person, institute, company, etc.

REFERENCES

- Gleick, P. H. *Environment: Sci. Policy Sustainable Development* **2010**, 36(3), 6-42.
- Kant, R. *Nat. Sci.* **2012**, 4, 22-26.
- Karapinar, I.; Kargı, F. *Turk. J. Engin. Environ. Sci.* **2000**, 24, 161-169.
- Banat, I. M.; Nigam, P.; Singh, D.; Marchant, R. *Bioresour. Technol.* **1996**, 58, 217-227.

5. Gregorio, C. *Bioresour. Technol.* **2006**, 97, 1061-1085.
6. Wasif, A. I.; Kone, C. D. *Text. Eng. I.* **1996**, 1-15.
7. Chang, M. W.; Chern, J. M. *J. Taiwan Inst. Chem. E.* **2010**, 41 (2), 221-228.
8. Karapınar, I.; Alparslan, S. *Enzyme Microb. Tech.* **2005**, 36 (2), 273-279.
9. Selçuk, H.; Meriç, S. *Global NEST J.* **2006**, 8 (2), 95-102.
10. El-Geundi, M. S. *Water Res.* **1991**, 25 (3), 271-273.
11. Kargı, F.; Ozmiçlı, S. *Enzyme Microb. Tech.* **2004**, 35 (2-3), 267-271.
12. Marcucci, M.; Nosenzo, G.; Capannelli, G.; Ciabatti, I.; Corrieri, D. *Desalination* **2001**, 75-82.
13. Bayramoglu, M.; Kobya M.; Can O. T.; Sozbir M. *Sep. Purif. Technol.* **2004**, 37 (2), 117-125.
14. Raghu, S.; Basha, C. A. *J. Hazard. Mater.* **2007**, 149 (2), 324-330.
15. Kocaer, F. O.; Alkan, U. *Uludag University Eng.-Architecture Faculty J.* **2002**, 7(1), 47-55.
16. Kumar, M.; Kumar, D.; Pandey, L.; Gaur, P. J. *Chem. Eng. Commun.* **2010**, 197(11), 1435-1444.
17. Zhou, H. *Adv. Mat. Res.* **2012**, 573-574.
18. Varshney, R. K.; Pandey, M.; Puppala, N. *Springer, Cham*, **2017**. 1-6.
19. Etoriki, A. M.; Massoudi, F. M. *Oriental J. Chem.* **2011**, 27(3), 875-884.
20. Namasivayam, C.; Kavitha, D. *Dyes and pigments.* **2002**, 54(1), 47-58.

ORCID

 ID 0000-0002-3706-4062 (O. Yel)



Co-immobilization of pullulanase, glucoamylase and glucose isomerase together with cross-linked enzyme aggregates: Fructose conversion from three enzymes and starch in one step

Yakup AKKOÇ^{1,*}, S. Seyhan TÜKEL²

¹Department of Medical Techniques, Posof Vocational School, Ardahan University

²Department of Chemistry, Faculty of Science-Literature, Cukurova University

Received: 03 May 2018, Revised: 07 June 2018; Accepted: 10 June 2018

* Corresponding author's e-mail address: yakupakkoc@gmail.com

ABSTRACT

In this study, in order to obtain fructose syrup from starch, pullulanase (PUL), glucoamylase (GA) and glucose isomerase (GI) were immobilized together with cross-linked enzyme aggregates (CLEAs), and named as 'combi-CLEAs'. The values of V_{max} and K_m from the kinetic parameters of combi-CLEAs [(GA + PUL) + GI] were found as 12 U g⁻¹ and 0.1157 mg ml⁻¹ in optimum conditions, respectively. After 50 uses, it was observed that the remaining activity of combi-CLEAs [GA + PUL + GI] was preserved at 46%. The thermal stability of combi-CLEAs [GA + PUL] + GI] was observed to be 44% and 30%, respectively, at 60 and 80 °C after 24 hours. At the end of 30 days, the storage stabilities of combi-CLEAs [(GA + PUL) + GI] was determined as 56% and 13% at the temperatures of 4 and 25°C, respectively.

Keywords: Combi-CLEAs, fructose syrup, enzyme immobilization.

Pullulanaz, glukoamilaz ve glukozimerazın çapraz bağlı enzim agregatları ile beraber immobilizasyonu: Tek basamakta üç enzim ile nişastadan fruktoz dönüşümü

ÖZ

Bu çalışmada nişastadan fruktoz şurubu elde etmek için pullulanaz (PUL), glukoamilaz (GA) ve glukozimeraz (GI) çapraz bağlı enzim agregatları (CLEAs) ile beraber immobilize edildi ve 'combi-CLEAs' olarak isimlendirildi. Combi-CLEAs [GA + PUL] + GI'nin optimum şartlardaki V_{max} and K_m değerleri sırasıyla 12 U g⁻¹ ve 0,1157 mg ml⁻¹ olarak bulundu. Combi-CLEAs [GA + PUL] + GI'nin 50 kullanımdan sonra kalan bağlı aktivitesinin % 46' da koruduğu gözlemlendi. 24 saat sonunda, 60 ve 80 °C' de Combi-CLEAs [GA + PUL] + GI'nin termal kararlılığının sırasıyla % 44 ve % 30 olduğu gözlemlendi. 30 günün sonunda, Combi-CLEAs [GA + PUL] + GI'nin 4 ve 25 °C' deki depolama kararlılığı ise sırasıyla % 56 ve % 13 olarak belirlendi.

Anahtar Kelimeler: Combi-CLEAs, fruktoz şurubu, enzim immobilizasyonu.

1. INTRODUCTION

Pullulanase (pullulan 6-glukanohidrolaz, EC 3.2.1.41) is an enzyme which hydrolyzes the pullulan, starch, amylopectin, and β -limit dextrin, α -1,6 glycosidic bonds.¹ Whereas glucoamylase converts starch into glucose, glucose isomerase converts glucose into fructose.²

In the food industry, in order to obtain fructose syrup, first the glucose syrup is obtained from starch, and then fructose syrup is obtained from glucose syrup. In the industry, this process is done in three stages. In the first stage, the starch is gelatinized by using alpha amylase

(EC 3.2.1.1) or pullulanase (EC 3.2.1.41). In the second stage, glucose syrup is obtained by using glucoamylase (EC 3.2.1.3). In the third stage, fructose syrup is obtained from glucose by using glucose isomerase.³

Free enzymes used commercially are for single use and have limited usage areas. With using of enzymes multiple times, the enzyme immobilization technology provides great financial advantages for the industrialists in terms of economic sense.

Recently, several studies related to the immobilization of two or three enzymes by combi-CLEAs (combined cross-linked enzyme aggregates) have been conducted.⁴⁻⁸ In the combi-CLEAs, the product ge-

nerated by an enzyme is substrate of another enzyme.

Generally in combi-CLEAs, by using inorganic salts and organic solvents, two or more enzymes are precipitated together without denaturation. Then, using dialdehyde or glutaraldehyde, the aggregates are connected.⁹

In the literature, there are some studies in which the enzyme has been immobilized by using different methods to obtain fructose syrup.^{4,11-13} For example, in the previous studies focusing on immobilization of enzyme to obtain fructose syrup, there has been no data related to storage stability, thermal stability and residual relative activity from the number of reuse, so far.^{4,12,13} In this study, it was aimed to obtain fructose syrup from starch by obtaining co-immobilization of pullulanase (PUL), glucoamylase (GA) and glucose isomerase (GI) together with CLEAs. Moreover, the storage stability and thermal stability of combi-CLEAs [(GA + PUL) + GI] and residual relative activity from the number of reuse were investigated. Because, it is very important that the immobilized enzymes to be used in industry are economical, reusable, able to be stored for a long time, and resistant at high temperatures.

2. MATERIALS AND METHODS

2.1. Materials

The mixture of glucoamylase and pullulanase enzymes and *Streptomyces Rubiginosus* Glucose Isomerase were taken from Sonar Company as a gift. All reagents used in the research were analytical purity and were taken from Merck or Sigma (St. Louis, MO) companies.

2.2. Methods

2.2.1. Preparation of combi-CLEAs [(GA + PUL) + GI]

The different amounts of (GA + PUL) and GI enzymes were mixed and dissolved in phosphate buffer, and then precipitated by adding ammonium sulphate. After the precipitation, glutaraldehyde was added, and it was kept in the water bath. Then, combi-CLEA [(GA + PUL) + GI] was washed and stored at 4°C for later use.

2.2.2. Determination of the relative activity of CLEAs [(GA + PUL) + GI]

The relative activity of combi-CLEAs [(GA + PUL) + GI] was calculated by measuring the amount of fructose in the relative activity of glucose isomerase. This was determined by measuring the amounts of fructose occurring in the reaction according to Resorcinol-HCl method used by Tolsma.⁷ One unit (U)

was calculated as the amount of enzyme that converts 1 μ mol glucose into fructose in 1 min.

2.2.3. Determination of the optimum temperature of combi-CLEAs [(GA + PUL) + GI]

The activities of combi-CLEAs [(GA + PUL) + GI] were measured by preparing at five different temperatures of 40, 50, 60, 70 and 80°C, and the temperature showing the maximum relative activity was determined.

2.2.4. Determination of thermal stability of combi-CLEAs [(GA + PUL) + GI]

Combi-CLEAs [(GA + PUL) + GI] was incubated for different time intervals (1, 3, 5, 7, 9, 11, 13, 15, 17, 19 and 24) at 60 and 80°C and remaining activities were determined.

2.2.5. Determination of storage stability of combi-CLEAs [(GA + PUL) + GI]

After the initial activities were determined, the samples of combi-CLEAs [(GA + PUL) + GI] were kept at 5 and 25°C for 1 month and their remaining activities were measured at regular intervals.

2.2.6. Determination of reuse stability of combi-CLEAs [(GA + PUL) + GI]

2 ml of starch solution of 1.5% was added to the column having different amounts of combi-CLEA [(GA + PUL) + GI] and after 30 minutes, the column was drained by opening the underlying tap. The relative activity of the enzyme was calculated by measuring the amount of the emerging fructose. After 20 second following the draining of the column, 2 ml of substrate solution was added to the column, and the relative activity was determined in the same manner. The remaining relative activity was calculated as the percentage of the relative activity in the first usage.

3. RESULTS AND DISCUSSION

In this study, pH, temperature, thermal stability and reuse parameters of combi-CLEA [(GA + PUL) + GI] were investigated.

3.1. Optimization of immobilization conditions of combi-CLEAs [(GA + PUL) + GI]

Optimization of immobilization conditions were performed so that combi-CLEAs [(GA + PUL) + GI] could show maximum relative activity. The immobilization environment, in which the final concentration of ammonium sulphate used as a precipitation to determine the optimum concentration of

ammonium sulphate was prepared as 20%, 30%, 40%, 50%, 60%, and 70% (w/v). The ammonium sulphate concentration showing the highest relative activity was determined as 40% (w/v). The results obtained are shown as relative activity (%) in Figure 1.

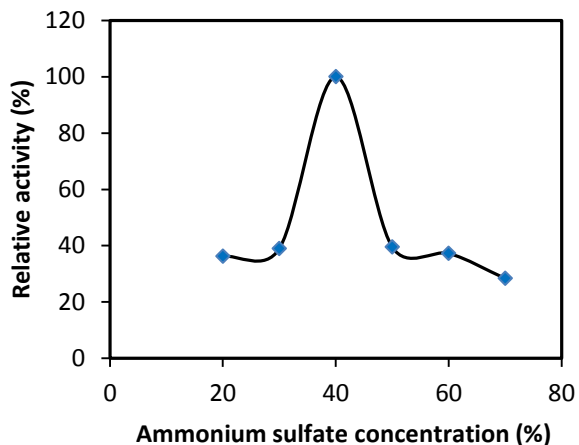


Figure 1. Relationship between the ammonium sulphate concentration in the immobilization medium and the activities of combi-CLEAs [(GA + PUL) + GI].

In order to identify the optimum immobilization time of combi-CLEAs [(GA + PUL) + GI], at the end of 1-24-hours immobilization process, combi-CLEAs were prepared. The immobilization time showing the highest combi-CLEA [(GA + PUL) + GI] relative activity was obtained was determined as 5 hours. The results obtained are shown as relative activity (%) in Figure 2.

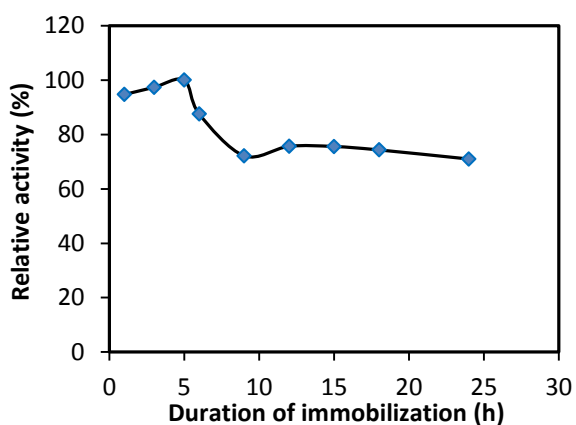


Figure 2. The effect of immobilization time on combi-CLEAs [(GA + PUL) + GI].

In order to identify the optimum glutaraldehyde concentration, the samples of combi-CLEAs [(GA + PUL) + GI] were prepared by using glutaraldehyde at the levels of 12.5%, 25%, 30%, 40% and 50%. The glutaraldehyde concentration indicating the highest combi-CLEAs [(GA + PUL) + GI] relative activity was

determined as 25%. The results obtained are shown as relative activity (%) in Figure 3.

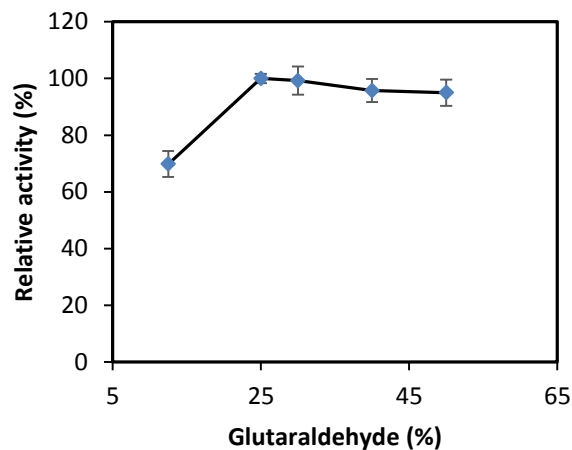


Figure 3. Relationship between glutaraldehyde concentration in the immobilization medium and the activities of combi-CLEAs [(GA + PUL) + GI].

The change of combi-CLEAs [(GA + PUL) + GI] relative activity depending on pH was measured by using buffers in different pH values at 60°C. The pH value showing the maximum relative activity of combi-CLEAs [(GA + PUL) + GI] was determined as 6. The results obtained are shown as relative activity (%) in Figure 4.

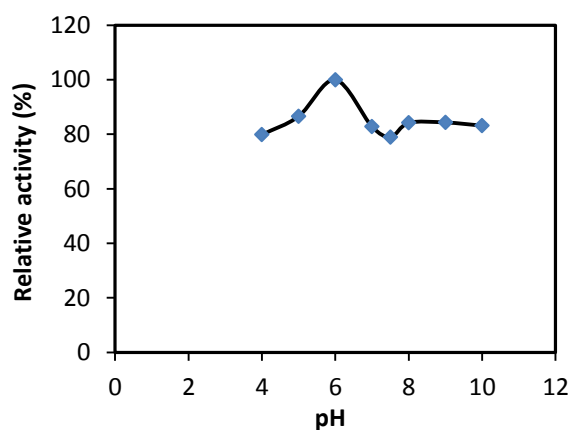


Figure 4. The pH stability of combi-CLEAs [(GA + PUL) + GI] at different pH values.

The effect of temperature on the change of combi-CLEAs [(GA + PUL) + GI] relative activity was studied at five different temperatures of 40, 50, 60, 70, and 80°C, and the temperature showing the maximum relative activity was determined as 60°C. The results obtained are shown as relative activity (%) in Figure 5.

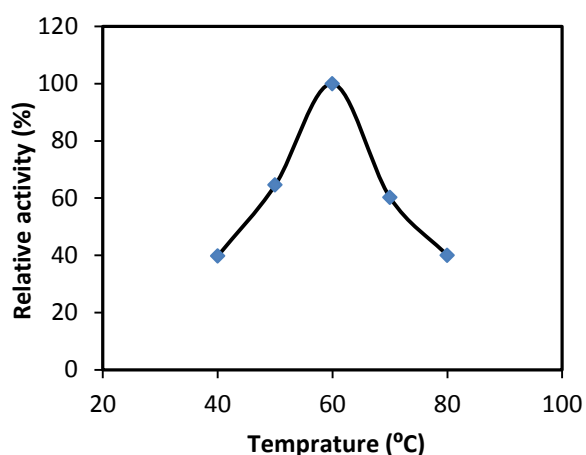


Figure 5. The effect of temperature on combi-CLEAs [(GA + PUL) + GI] relative activity.

The thermal stability of combi-CLEAs [(GA + PUL) + GI] was determined by measuring the remaining activities at two different temperature (i.e. at 60 and 80°C) as a function of time. The results obtained are shown as relative activity (%) in Figure 6. From Figure 6, it is observed that thermal stability is decreased as the temperature is increased. At the end of 24-hours incubation at 60°C, while the remaining relative activity of combi-CLEAs [(GA + PUL) + GI] was approximately 44% of the initial relative activity, its remaining relative activity at 80°C was found to be approximately 30% of the initial relative activity. These values showed that the thermal stability of combi-CLEAs [(GA + PUL) + GI] was very high.

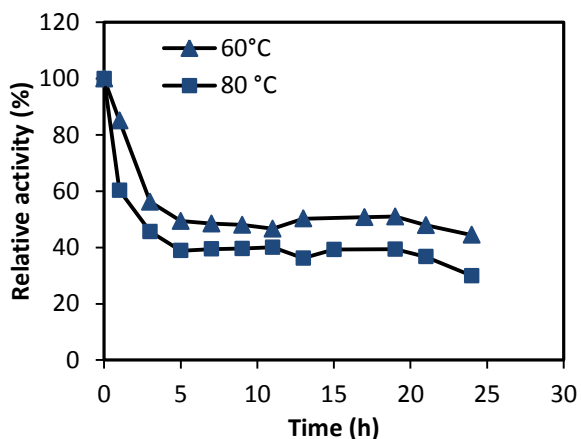


Figure 6. Change of combi-CLEAs [(GA + PUL) + GI] relative activities depending on thermal stability.

In order to determine storage stability of combi-CLEAs [(GA + PUL) + GI], the samples were held at 4 and 25°C, their activities were measured at certain days for 30 days, and their relative activities were calculated. The results obtained are shown in Figure 7. The remaining activities of combi-CLEAs [(GA + PUL) + GI]

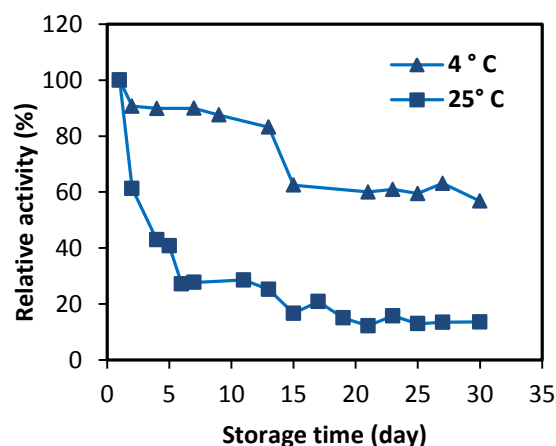


Figure 7. Relationship between combi-CLEAs [(GA + PUL) + GI] relative activity and storage time at different temperatures.

held at 4 and 25°C for one month were found as 56% and 13%, respectively. The high storage capability of combi-CLEAs [(GA + PUL) + GI] provides great economic advantages for the industrialists.

The number of reuse of combi-CLEAs [(GA + PUL) + GI] was determined by using the buffer of pH 6 at 60°C. Depending on number of reuse, the change in relative activity of combi-CLEAs [(GA + PUL) + GI] is shown in Figure 8. After 50 usage, it was seen that combi-CLEAs [(GA + PUL) + GI] was able to maintain the 46% of the initial relative activity. This result is a very big advantage for the industry.

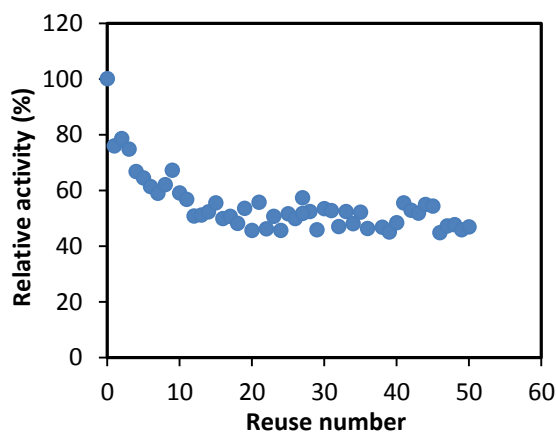


Figure 8. Relationship between the relative activity of combi-CLEAs [(GA + PUL) + GI] and reuse number.

3.2. Kinetic parameters

From the kinetic parameters of combi-CLEAs [(GA + PUL) + GI], V_{max} and K_m were calculated by means of Eq. (1). This equation is known as Michaelis-Menten equation¹⁴ as shown in the following.

$$V = V_{\max} [S] / K_m + [S] \quad (1)$$

where, $[S]$ is the concentration of substrate S, V_{\max} is the maximum velocity achieved by the system, at maximum (saturating) substrate concentrations. K_M is the Michaelis constant indicating the substrate concentration at which the reaction velocity is 50% of the V_{\max} .

Herein W_{\max} and K_m were found as 12 U g^{-1} and $0.1157 \text{ mg ml}^{-1}$, respectively. This parameter changes are shown in Figure 9. If an enzyme has a low K_m , it has high affinity for the substrate. The K_m of the enzyme indicates that the enzyme and substrate relationship is very good.

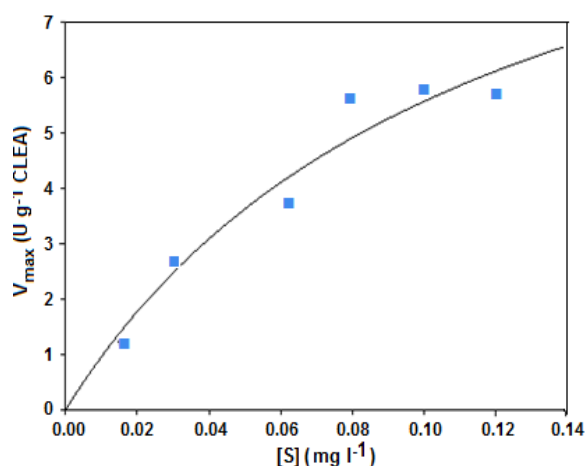


Figure 9. Kinetic graph of combi-CLEAs [(GA + PUL) + GI].

4. CONCLUSION

In this study, in order to obtain fructose syrup from starch, glucoamylase, pullulanase and glucose isomerase were immobilized in the form of combi-CLEAs [(GA + PUL) + GI]. In this immobilization study, the optimum conditions of ammonium sulfate, glutaraldehyde, pH, temperature and immunization time were found as 40%, 6, 60 °C and 5 hours, respectively. The remaining relative activity of combi-CLEAs [(GA + PUL) + GI] after 50 uses was identified as 46%. The remaining activities of combi-CLEAs [(GA + PUL) + GI] after 24-hour incubation at 60 and 80 °C were found as 44% and 30%, respectively. In terms of the storage stability of combi-CLEAs [(GA + PUL) + GI], at the end of 30 days at the temperature level of 4 and 25 °C, the remaining activities were calculated as 56% and 13%, respectively. V_{\max} and K_m values of combi-CLEAs [(GA + PUL) + GI] were calculated as 12 U g^{-1} and $0.1157 \text{ mg ml}^{-1}$, respectively.

Conflict of interest

Authors declare that there is no a conflict of interest with any person, institute, company, etc.

REFERENCES

- Schindler, I.; Renz, A.; Schmid, F.X.; Beck, E. *Biochim. Biophys. Acta* **2001**, 1548, 175-186.
- Cha, X.; Zhou, H.; Li, W.; Shen, J. *J. Chem. Technol. Biot.* **1990**, 47, 161-169.
- Schafhauser, D.Y.; Storey, K.B. *Appl. Biochem. Biotechnol.* **1992**, 36, 63-74.
- Yubin, Ge.; Yingming, W.; Hui, Zhou, S. W.; Yi, T.; Wei, L. *J. Biotechnol.* **1999**, 67, 33-34.
- Sohel, D.; Manali, K.; Munishwar, N. G. *J. Mol. Catal. B-Enzym.* **2007**, 44, 128-132.
- Sachin, T.; Amol, P.; Mayur, L.; Shamraja, N.; Mosin, M.; Kshitija, J.; Kishori, P.; Devika, A. *Bioresour. Technol.* **2013**, 147, 269-275.
- Jolanta, B. *Biochem. Eng. J.* **2003**, 16, 347-355.
- Qiaolin, L.; Long, Y.; Jianguo, S.; Liang, L.; Lin, X.; Aihua, Li. *Biosens. Bioelectron.* **2014**, 51, 158-163.
- Gupta, M.N.; Dalal, S.; Kapoor, M. *J. Mol. Catal. Enzyme B.* **2017**, 44, 128-132.
- Tolsma, A. D. The effects of fire and grazing on the energy reserves of resprouting plants in Victoria's alpine grasslands. PhD Thesis, School of Resource Management, Forestry and Amenity Horticulture, The University of Melbourne, 2002.
- Roushdi, M.; Ghali, Y.; Attia, R. M.; Alaa El-din, M. *Starch/Stärke.* **1979**, 31 (12), 414-417.
- Katwa, L.C.; Raghavendra, M.R. *Technol. Lett.* **1983**, 5, 191-196.
- Mishra, A.; Debnath, M. *App. Biochem. Biotechnol.* **2002**, 102-103.
- Michaelis, L.; Menten, M. *Biochem. Zeitung*, **1913**, 49, 333-369.

ORCID

ID 0000-0002-2622-1341 (Y. Akkoç)

ID 0000-0003-2503-2781 (S. S. Tükel)



Synthesis of complexes Co, Cu, Ni and Pd supported by “ONNO” type Schiff base ligand and their DNA cleavage, antioxidant effects and antimicrobial studies

Ahu ÇELİK¹, Hatice Gamze SOGUKOMEROGULLARI², Sadin OZDEMİR³, M. Serkan YALCIN⁴, Mehmet SÖNMEZ^{1,*}

¹Department of Chemistry, Faculty of Science and Arts, Gaziantep University, 27310, Gaziantep, Turkey.

²Medical Services and Techniques Department, Health Services Vocational School, Gaziantep University, 27310 Gaziantep, Turkey

³Food Processing Programme, Technical Science Vocational School, Mersin University, TR-33343 Yenişehir, Mersin, Turkey

⁴Department of Chemical and Chemical Processing Technologies, Technical Science Vocational School, Mersin University, TR-33343 Yenişehir, Mersin, Turkey

Received: 14 May 2018, Revised: 22 June 2018; Accepted: 25 June 2018

* Corresponding author's e-mail address: msonmez@gantep.edu.tr

ABSTRACT

A new Schiff base ligand was synthesized from a reaction of 5-benzoyl-4-hydroxy-2-methyl-6-phenyl-2H-pyridazine-3-one and 1,3-diaminopropane. Schiff base metal complexes were synthesized from a reaction of Ni(AcO)₂·4H₂O, Cu(AcO)₂·H₂O, Co(AcO)₂·4H₂O, Pd(AcO)₂ metal salts and ligand, respectively. All compounds were characterized using magnetic susceptibility, elemental analysis, NMR (for ligand), UV-Vis and FT-IR spectroscopic analysis. While octahedral structure has been proposed for Ni(II), Pd(II) and Co(II) complexes, square-planar geometry is suggested for Cu(II) complex. Synthesized compounds were evaluated for their antioxidant effect, DNA cleavage and antimicrobial studies. The DPPH free radical scavenging activity of compounds 1, 2, 3, 4 and 5 on DPPH were found as 38.5%, 32.5%, 36.9%, 35.7% and 45.7% at 200 mg l⁻¹, respectively. The compounds 4 and 5 revealed maximum ferrous chelating activity of 64.5% and 78.1% at 200 mg ml⁻¹, respectively. For all the compounds, DNA cleavage studies showed complete DNA digestion at 100 mg ml⁻¹. Antimicrobial activities of 3 and 4 complexes against *Staphylococcus aureus* (ATTC 6538) were determined to be in 12 mm diameter.

Keywords: Pyridazinone complexes, DNA cleavage, antioxidant effect, antimicrobial studies.

“ONNO” tip Schiff baz ligand destekli Co, Cu, Ni ve Pd komplekslerinin sentezi ve DNA bölünme, antioksidan etkileri ve antimikrobiyal çalışmaları

Öz

5-benzoyl-4-hidroksi-2-metil-6-fenil-2H-piridazin-3-on ile 1,3-diaminopropan'ın reaksiyonundan yeni bir Schiff baz ligand sentezlendi. Sırasıyla ligand ile Co(AcO)₂·4H₂O, Cu(AcO)₂·H₂O, Ni(AcO)₂·4H₂O, Pd(AcO)₂ metal tuzlarının reaksiyonundan Schiff baz metal kompleksleri sentezlendi. Tüm bileşikler elementel analiz, manyetik duyarlılık ile NMR (ligand için), FT-IR ve UV-Vis gibi spektroskopik analiz yöntemleriyle karakterize edildi. Ni(II), Pd(II) ve Co(II) kompleksi için oktahedral geometri önerilirken, bakır kompleksi için kare düzlem geometri önerilmiştir. Sentezlenen bileşiklerin antioksidan etkileri, DNA bölünmesi ve antimikrobiyal özellikleri incelendi. 1, 2, 3, 4 ve 5 bileşiklerinin DPPH üzerinde 200 mg l⁻¹'de DPPH serbest radikallerini çıkarma aktiviteleri sırasıyla % 38.5, % 32.5, % 36.9, % 35.7 ve % 45.7 olarak bulundu. Bileşik 4 ve 5'in 200 mg l⁻¹'de % 64.5 ve % 78.1'lik maksimum demir şelatlama aktivitesi gösterdi. Bütün bileşikler için DNA bölünme çalışmaları 100 mg l⁻¹'de tam DNA parçalanması gösterdi. *Staphylococcus aureus* (ATTC 6538)'e karşı kompleks 3 ve 4'ün antimikrobiyal aktivitelerinin 12 mm çapında olduğu belirlendi.

Anahtar Kelimeler: Piridazinon kompleksleri, DNA bölünmesi, antioksidan etki, antimikrobiyal çalışmalar.

1. INTRODUCTION

Pyridazinone compounds have been the focus of researchers in recent years due to many factors such as analgesic, anti-inflammatory, antipyretic, antihypertensive, antiulcer, antibacterial, antifungal, antituberculous and antitumor effects.¹⁻¹⁰ Synthesis of pharmacologically active pyridazinone derivatives has been rapidly increased, as it has been found that compounds of the pyridazinone ring have positive activity-related contributions to the compounds.^{11,12} In our previous study, it was observed that pyridazinone-derived ligands and their complexes were synthesized and that these compounds possess antibacterial and antifungal activity.¹³

Antioxidants play a crucial role in the living system in terms of protecting from oxidative stress and other chronic diseases.¹⁴ Recently, many scientists have been working on compounds newly synthesized or acquired from natural origins in order to prevent or decline the effect of oxidative stress on cells. These compounds can be used as free radicals or active oxygen scavengers or metal chelators which reduce agents and also prevent cancer.¹⁵ DNA is the main target molecule for most of antiviral and anticancer therapies. Therefore, DNA cleavage is helpful in molecular biotechnology, genetic engineering and anticancer drug designing.¹⁶ Besides, these compounds can exhibit satisfactory antimicrobial activity.

In this work, a novel pyridazinone derivative ligand and its Co, Cu, Ni and Pd complexes have been synthesized. The structures of these compounds were characterized by elemental analysis, magnetic susceptibility and NMR, FT-IR, UV-Vis by various spectroscopic methods. DNA cleavage, antioxidant effects and antimicrobial activities of these compounds were investigated. The synthesis, characterization and biological activity results of these compounds are presented here for the first time.

2. EXPERIMENTAL

2.1. Materials and methods

All of the reactants and solvents were purchased from Aldrich or Merck and used without further purification (95-99% purity). 5-benzoyl-4-hydroxy-2-methyl-6-phenyl-2H-pyridazine-3-one was prepared according to the procedure in the literature.¹⁷ NMR spectra were measured on Premium Compact NMR (Agilent-600 MHz). Elemental analyses were measured on a Thermo Scientific Flash EA 2000 CHNS analyzer. Infrared spectra were measured on a Perkin-Elmer Spectrum 100 FTIR spectrophotometer with an ATR sampling accessory. Electronic absorption spectra were recorded on a PG Instruments T80 + UV / Vis spectrometer.

2.2. Synthesis of 5,5'-(((propane-1,3-diylbis(azanylylidene))bis(phenylmethanylylidene))bis(4-hydroxy-2-methyl-6-phenylpyridazin-3(2H)-one) ligand (H₂L) (1)

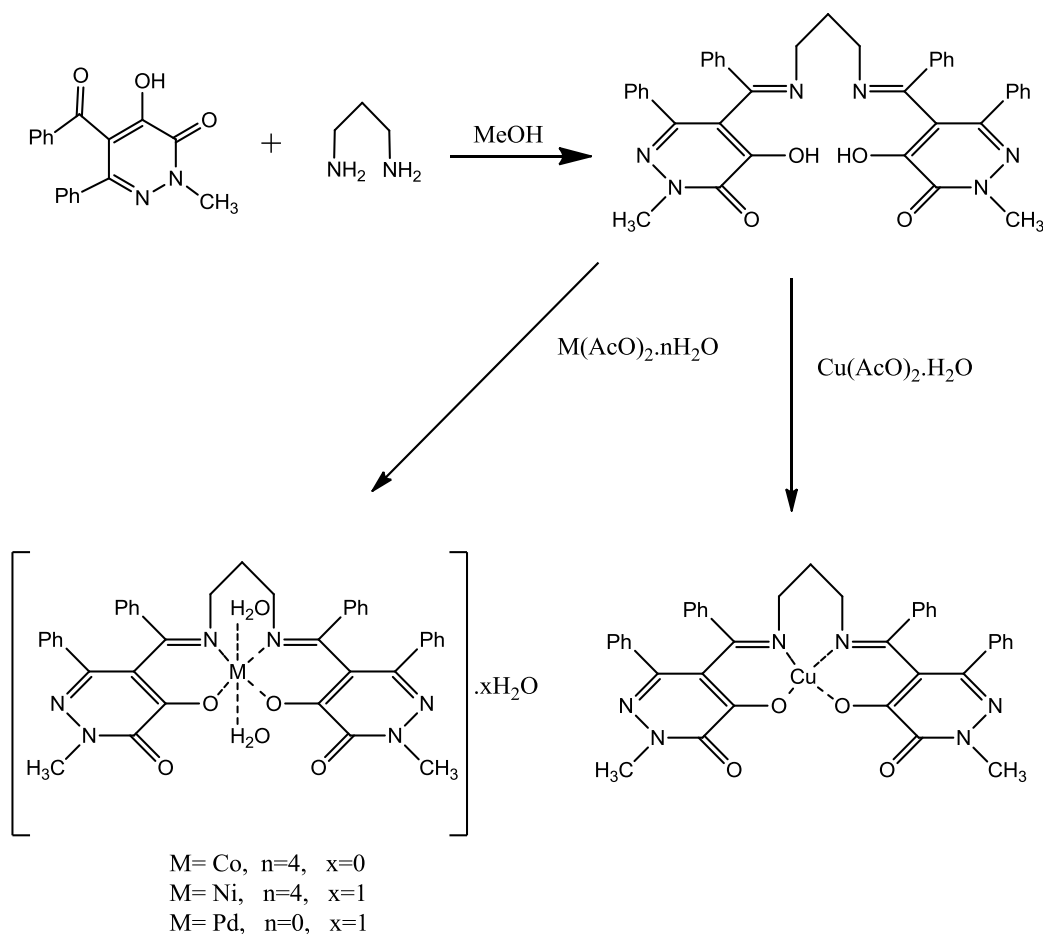
The ligand (H₂L) was prepared by heating a solution of 5-benzoyl-4-hydroxy-2-methyl-6-phenyl-2H-pyridazine-3-one (0.153 g, 0.5 mmol) and *o*-aminophenol (0.055 g, 0.5 mmol) in 20 ml methanol to 65°C for 1 h. (Scheme 1) After cooling to room temperature, the solid in the reaction medium was filtered. The product was washed in diethylether and was purified slowly with vapor diffusion of Et₂O with an ethanol/chloroform (1:1) solution of ligand and then dried in vacuo. Yield 0.150 g (46 %); 239-240°C. IR, (ATR) ν , cm⁻¹: 3524 (O-H); 3089 (C-H)_{arom.}; 1638 (C=O); 1597, 1579 (C=N); 1340 (C-O); 1525 (C=C). UV-Vis (DMF, λ_{max} nm, (Abs.)): 390 (0.155), 294 (0.760), 270 (0.880) nm. ¹H NMR (600 MHz, d₆-DMSO) δ (ppm); s, singlet; m, multiplet; p, pentet: 8.22 (s, 2H, O-H protons), 7.75-7.16 (m, 20H, Harm), 3.59 (s, 6H, CH₃ protons), 2.77 (t, 4H, CH₂ protons), 1.74 (p, 2H, CH₂ protons). ¹³C NMR (600 MHz, d₆-DMSO) δ (ppm); δ 197.18 (C-O)_{pyridazine}, 164.25, 162.85 (C=N), 148.25, 139.24, 138.94, 132.58, 129.46, 128.69, 128.05, 128.37, 127.76, 116.20 (Aromatic carbons), 36.62 (CH₃), 25.87 (CH₂). Anal. Calc. C₃₉H₃₄N₆O₄ (650.73): C, 71.98, H, 5.27, N, 12.91 Found: C, 71.83, H, 5.51, N, 12.60%.

2.3. General synthesis method of the complexes (2-5)

A methanolic solution (10 ml) of metal acetate (Co(AcO)₂·4H₂O (0.062 g), Cu(AcO)₂·H₂O (0.050 g), Ni(AcO)₂·4H₂O (0.062 g), Pd(AcO)₂ (0.056 g), 0.25 mmol) was mixed with a solution of ligand (H₂L) (0.163 g, 0.25 mmol) in 20 ml of ethanol/chloroform (1:1). The reaction mixture was stirred for 30 minutes at 65-70°C, the precipitate was filtered off, it was washed with cold MeOH-H₂O (1:1) and Et₂O, the complex was purified slowly with vapor diffusion of Et₂O with a THF solution of complex and then dried in vacuo.

[CoL(H₂O)₂] complex (2): Brown. Yield 0.043 g (23 %); 220°C decompose. IR, (ATR) ν , cm⁻¹: 3300 (O-H); 3060 (C-H)_{arom.}; 1661 (C=O); 1592 (C=N); 1356 (C-O); 1542 (C=C); 508 (M-O); 540 (M-N). μ_{eff} : 4.99. UV-Vis (DMF, λ_{max} nm, (Abs.)): 405 (0.057), 345 (0.341), 284 (1.143) nm. Anal. Calc. C₃₉H₃₆CoN₆O₆ (743.20): C, 62.99, H, 4.88, N, 11.30 Found: C, 62.82, H, 4.96, N, 10.85%.

[CuL] complex (3): Green. Yield 0.077 g (43 %); 245°C decompose. IR, (ATR) ν , cm⁻¹: 3058 (C-H)_{arom.}; 1655 (C=O); 1594 (C=N); 1364 (C-O); 1538 (C=C); 507 (M-O); 536 (M-N). μ_{eff} : 1.56. UV-Vis (DMF, λ_{max} nm, (Abs.)): 405 (0.033), 327 (0.510), 284 (1.452), 270 (1.985) nm. Anal. Calc. C₃₉H₃₂CuN₆O₄ (712.26): C, 65.77, H, 4.53, N, 11.80 Found: C, 65.56, H, 4.20, N, 10.78%.



Scheme 1. Synthesis of Schiff base ligand and its metal complexes.

[NiL(H₂O)₂] \cdot H₂O complex (**4**): Green. Yield 0.084 g (44 %); 250 °C decompose. IR, (ATR) ν , cm⁻¹: 3350 (O-H); 3058 (C-H)_{arom.}; 1659 (C=O); 1589 (C=N); 1355 (C-O); 1538 (C=C); 508 (M-O); 542 (M-N). μ_{eff} : 3.08. UV-Vis (DMF, λ_{max} nm, (Abs.)): 400 (0.110), 350 (0.437), 286 (1.426), 270 (1.638) nm. Anal. Calc. C₃₉H₃₈N₆NiO₇ (761.45): C, 61.52, H, 5.03, N, 11.04 Found: C, 60.66, H, 4.88, N, 10.41%.

[PdL(H₂O)₂] \cdot H₂O complex (**5**): Brown. Yield 0.047 g (23 %); 135 °C decompose. IR, (ATR) ν , cm⁻¹: 3400 (O-H); 3060 (C-H)_{arom.}; 1642 (C=O); 1578 (C=N); 1338 (C-O); 1538 (C=C); 503 (M-O); 527 (M-N). μ_{eff} : diamagnetic. UV-Vis (DMF, λ_{max} nm, (Abs.)): 420 (0.158), 381 (0.313), 286 (1.508), 270 (1.786) nm. Anal. Calc. C₃₉H₃₈N₆O₇Pd (809.18): C, 57.89, H, 4.73, N, 10.39 Found: C, 57.18, H, 4.84, N, 10.73%.

2.4. DPPH radical scavenging assay

Different solutions (10, 25, 50, 100 and 200 mg l⁻¹) (0.5 ml) in dimethyl formamide (DMF) of compounds and 2 ml of 2,2-diphenyl-1-picrylhydrazyl radical (DPPH) (0.004%) solution were incubated at 25 °C in the dark for half an hour.¹⁸ The absorbance was measured at

517 nm. DMF solution was used as the blank control. The DPPH scavenging activity was calculated as follows: DPPH scavenging activity (%) = [1 - (A_{517 nm, sample} / A_{517 nm, control})] x 100 Trolox and Ascorbic Acid were used as standards in order to compare with the results.

2.5. Ferrous ion chelating activity

Metal chelating ability on ferrous ions examined by the compounds were applied as recorded by Hsu et al.¹⁹ Metal chelating effect was calculated as follows: Metal chelating ability (%) = [(A_{562 nm, control} - A_{562 nm, sample}) / A_{562 nm, control}] x 100 Ethylenediaminetetraacetic acid (EDTA) was used as the positive control.

2.6. DNA cleavage activity

The DNA cleavage studies were carried out by using agarose gel electrophoresis. pBR 322 plasmid DNA (0.1 mg ml⁻¹), Tris-HCl and NaCl (pH 7.4) and ligands and metal complexes (100 mg l⁻¹) were mixed and incubated in an incubator at 37 °C for 90 min. Then, the loading

buffer was added and the reaction mixture was electrophoresed for 1.5 hour at 80 V by. Tris-boric acid-EDTA was used as an electrophoresis buffer. The electrophoresis bands were visualized by UV-A light.

2.7. Antimicrobial activity

Enterococcus hirae (ATCC 10541), *Bacillus cereus*, *Staphylococcus aureus* (ATCC 6538), *Escherichia coli* (ATCC 10536), *Legionella pneumophila* subsp. *pneumophila* (ATCC 33152), *Pseudomonas aeruginosa* (ATCC 9027) and *Candida albicans* were used as test microorganisms. Antimicrobial activity of compounds was evaluated by using disk-diffusion method.²⁰

3. RESULTS AND DISCUSSION

The Schiff base ligand (H₂L) was synthesized from a reaction of 5-benzoyl-4-hydroxy-2-methyl-6-phenyl-2H-pyridazine-3-one and *o*-aminophenol in methanol. The complexes were synthesized from the reaction of (1:1) ligand with cobalt(II), copper(II), nickel(II) and palladium(II) acetate salts, respectively. The structures of compounds were characterized by NMR (for ligand), UV-Vis, FT-IR, magnetic susceptibility and elemental analysis. All of the complexes are air-stable at room temperature in the solid state, soluble in DMF, THF and insoluble in water. The structure of the copper complex appears to be [CuL], while the structure of the other complexes appears to be [ML(H₂O)₂].nH₂O. According to the magnetic susceptibility measurements, the copper complex is square plane geometry while the other complexes are octahedral geometry.

3.1. FT-IR spectra

When the FT-IR spectra of Schiff base ligand (1) and its metal complexes (2-5) are examined, it is found that (C=N) imine group is between 1594 cm⁻¹ and 1589 cm⁻¹. These values are quite compatible with the literature.²¹⁻²³ While the C=N stretching band of the Schiff base ligand is 1597 cm⁻¹, this value is shifted 3-8 cm⁻¹ down in the complexes. This suggests that the complexes are linked to the metal via the imine group. It has been observed that the carbonyl (C=O) stretching bands in all the synthesized compounds are in the range of 1661-1638 cm⁻¹.²⁴ Metal-N and metal-O bands in the metal complexes are 542-527 cm⁻¹ and 508-503 cm⁻¹, respectively.²¹⁻²³

3.2. Electronic spectra and magnetic measurements

The UV-Vis spectra of the synthesized compounds were recorded in the range of 190-1100 nm, at a concentration of 2 x 10⁻⁵ M and in DMF. The n-π* transitions of the azomethine group were observed at 390 nm in the ligand, while the values of the complexes were observed at 345, 327, 350, 381 nm, respectively. Transitions observed 270 nm and between 294-284 nm in the complexes are the n-π* and π-π* transitions of the phenyl and pyridazine rings. It is believed that the transition observed in the complexes between 400-420 nm is due to the weak charge-transfer transition. In the complexes, d-d transition was not observed clearly. For this reason, it is considered that the other transitions mask the d-d transition. In addition, the magnetic susceptibility value of the Cu (II) complex is 1.56 BM. This indicates that the copper complexes have square plane geometry and partial anti-ferromagnetic.²⁵ The magnetic susceptibility value of the cobalt (II) complex is 4.99 BM. This value is above the octahedral geometry values (4.2-4.6 BM) in the literature. This result shows that Co (II) complex has octahedral geometry and partial ferromagnetic properties.²⁶ The magnetic susceptibility value of the Ni (II) complex is 3.08 BM. This value is consistent with octahedral geometry values (2.8-3.1 BM) in the literature. The complex of Pd (II) is diamagnetic. The complex is thought to have octahedral geometry.

3.3. Proton and carbon nuclear magnetic resonance spectra

¹H-NMR and ¹³C-NMR spectrums of the Schiff base ligand (1) were recorded in d₆-DMSO as a deuterated solvent. The ¹H-NMR spectra of the Schiff base ligand (1) exhibits signals due to OH protons as singlet at δ 8.22 ppm (2H), protons of pyridazine and phenyl rings as multiplet at δ 7.75-7.16 ppm (20 H), CH₃ protons as singlet at δ 3.59 ppm (6H), CH₂ protons as triplet at δ 2.77 ppm (4H), CH₂ protons as pentet at δ 1.74 ppm (2H) (Figure 1). Since there are many aromatic rings in the structure of Ligand (1), the aromatic region is complicated in the ¹H-NMR spectrum. The ¹³C-NMR spectra of the Schiff base ligand (1) exhibits signals due to of pyridazine ring (C=O) carbon at 197.18 ppm, azomethine carbons at 162.85 and 164.25 ppm, aromatic carbons at 148.25-116.20 ppm, CH₃ carbon at 36.62 ppm and CH₂ carbon at 25.87 ppm (Figure 2). Since the Pd complex does not have good solubility in solvents such as DMSO and chloroform, the NMR can't be obtained.

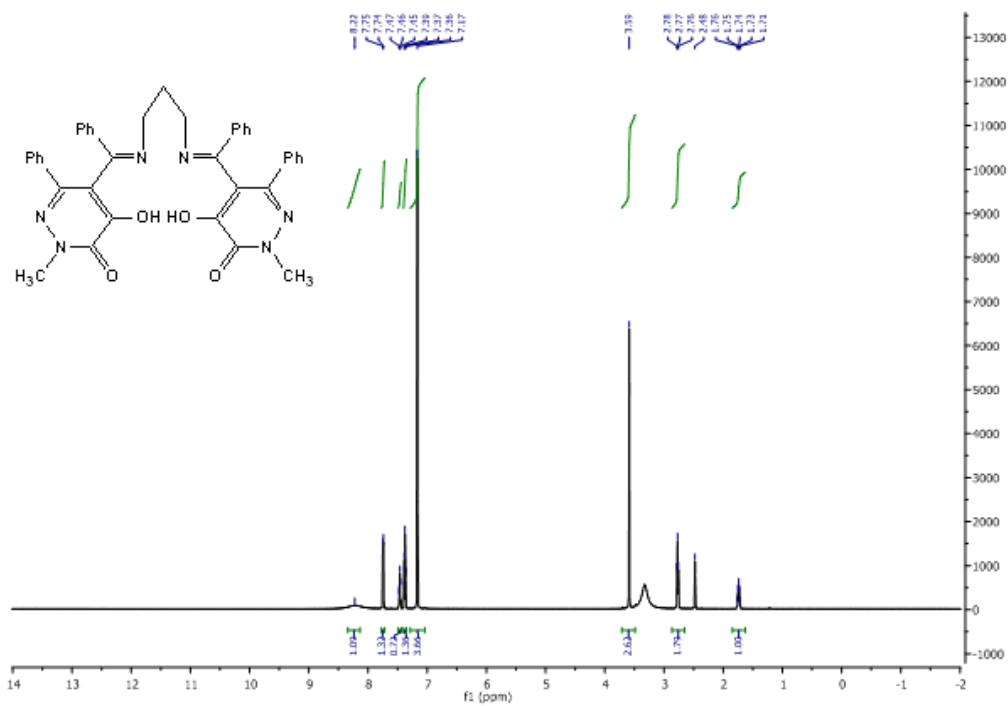


Figure 1. $^1\text{H-NMR}$ spectrum of ligand.

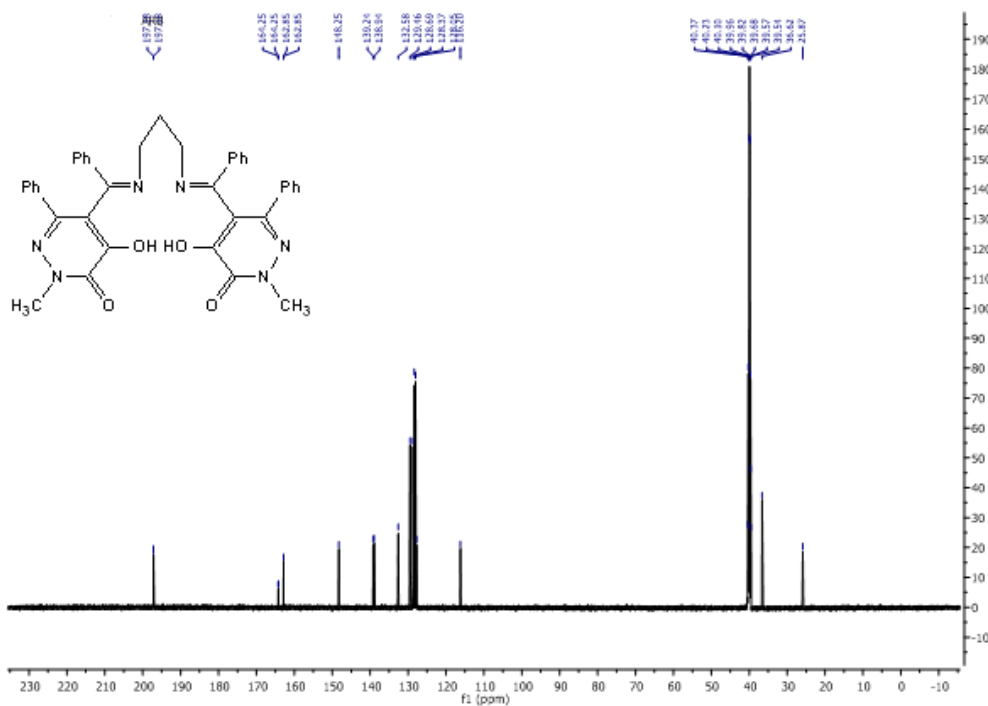


Figure 2. $^{13}\text{C-NMR}$ spectrum of ligand.

3.4. Antioxidant studies

3.4.1. DPPH scavenging activity

The scavenging ability on DPPH radicals test was widely carried out as a screening process for testing the antiradical ability of compounds.^{27,28} Various concentrations of compounds were investigated in order to determine DPPH scavenging activity by comparing with standard Ascorbic acid and Trolox. The obtained results are given in Figure 3. The DPPH scavenging activity of five compounds increased with concentration. The lowest and highest free radical scavenging activity was observed as 8.5% for compound 2 at the concentration of 10 mg/L and 45.7% for compound 5 at the concentration of 200 mg l⁻¹, respectively. Similar results were reported for compound 8 by Ağirtas et al. (2013).²⁹

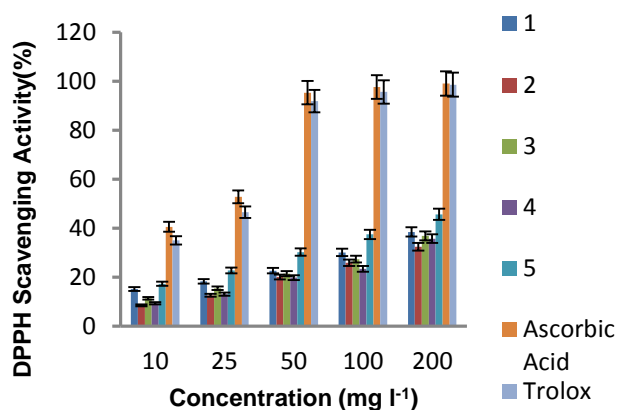


Figure 3. Free radical scavenging activities of the compounds on DPPH radicals.

3.4.2. Metal chelating activity

The metal chelating activity of tested compounds is presented in Figure 4. The chelating activity increased with concentration. The chelating activity of compounds at 200 mg/L concentration was 78.1% for compound 5, 64.5% for compound 4, 54.7% for compound 1, 51.8% for compound 3 and 44.9% for compound 2. EDTA exhibited great activity (90.18–100%) for all concentrations studied. Our results showed greater metal chelating activity than Baykara et al. (2013).³⁰

3.5. DNA cleavage studies

In order to detect the DNA cleavage, the activities of the newly synthesized compounds were studied by supercoiled plasmid DNA as a substrate in a medium of 50 mM Tris-HCl and NaCl buffer (pH 7.4). It is known

that one pair of DNA strands was broken by the metal compounds.³¹

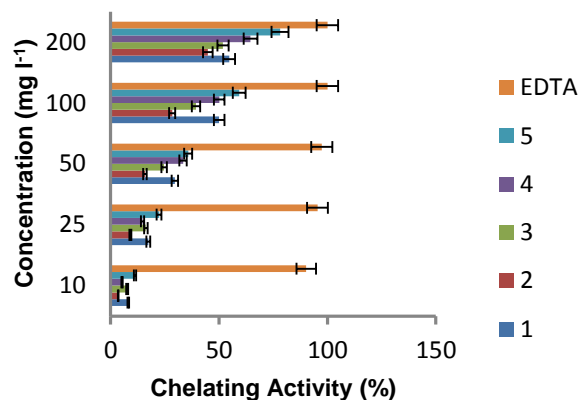


Figure 4. Metal chelating activities of compounds.

The experiment showed that the supercoiled form I cleaved by to varying extent all tested compounds. Form I (supercoiled DNA) was converted to form II (nicked circular DNA) and form III (linear DNA) at 100 µg ml⁻¹ concentrations of all complexes. Figure 5 presents the results of the agarose gel electrophoresis separations of plasmid DNA from form I to form II and III by the compounds. Control experiments clearly revealed that plasmid DNA and DNA in %3 DMF did not show any cleavage. These experimental studies revealed that ligands and metal compounds were cleavage active. These DNA cleavage findings are better than the study of Keypour et al. (2015).³²

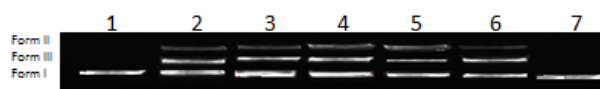


Figure 5. DNA Cleavage of ligand and its metal complexes. Lane 1, pBR 322 DNA; Lane 2, pBR 322 DNA + 100 µg ml⁻¹ of 1; Lane 3, pBR 322 DNA + 100 µg ml⁻¹ of 2; Lane 4, pBR 322 DNA + 100 µg ml⁻¹ of 3; Lane 5, pBR 322 DNA + 100 µg ml⁻¹ of 4; Lane 6, pBR 322 DNA + 100 µg ml⁻¹ of 5; Lane 7, pBR 322 DNA + 3% DMF.

3.6. Antimicrobial activity

The antimicrobial activities of the five newly synthesized compounds were investigated for *E. hirae* (ATCC 10541), *B. cereus*, *S. aureus* (ATCC 6538), *L. pneumophila* subsp. *pneumophila* (ATCC 33152), *P. aeruginosa* (ATCC 9027), *E. coli* (ATCC 10536), and *C. albicans*. In this study, only *S. aureus* was inhibited by all compounds and antimicrobial activity was in order of 3 = 4 > 2 > 1 > 5. Compound 2 inhibited all

microorganisms and showed the highest antimicrobial activity against *E. coli* with inhibition zone value equal to 12 mm (Figure 6).

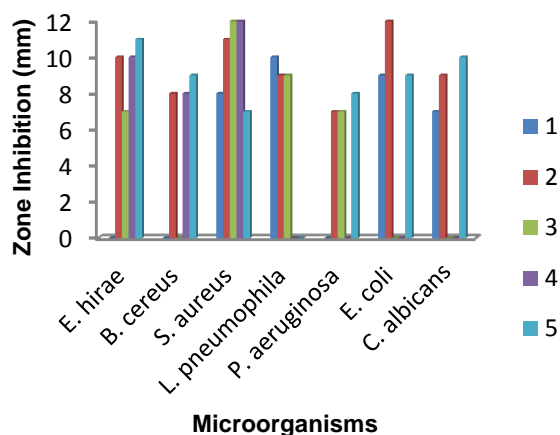


Figure 6. Antimicrobial activities of compounds.

4. CONCLUSION

In this work, new Schiff base ligand and its complexes of Co (II), Cu (II), Ni (II) and Pd (II) were synthesized. The synthesized compounds were characterized by elemental analysis, magnetic susceptibility, NMR, FT-IR and UV-Vis spectroscopy. The synthesized copper (II) complex has square plane geometry, while others have octahedral geometry. The antioxidant activities of the newly synthesized compounds on scavenging of DPPH and metal chelating activity varied depending on the concentration. These compounds showed modest scavenging of DPPH activity when compared with the standards. Also Ni (4) and Pd (5) demonstrated significant metal chelating activity. According to the DNA cleavage studies all compounds were active in cleavage. The obtained results of the antimicrobial studies for compound Co (2) inhibited all tested microorganisms and showed the highest antimicrobial activity against *E. coli*.

Conflict of interest






Authors declare that there is no a conflict of interest with any person, institute, company, etc.

REFERENCES

- Rubat, C.; Coudert, P.; Bastide, P.; Tronche, P. *Chem. Pharm. Bull.* **1988**, 36 (12), 5000-5003.
- Chintakunta, V. K.; Akella, V.; Vedula, M. S.; Mamnoor, P. K.; Mishra, P.; Casturi, S. R.; Vangoori, A.; Rajagopalan, R. *Eur. J. Med. Chem.* **2002**, 37, 339-347.
- Pitarch, L.; Coronas, R.; Mallol, J. *Eur. J. Med. Chem.* **1974**, 9(6), 644-50.
- Rubat, C.; Coudert, P.; Tronche, P.; Bastide, J.; Bastide, P.; Privat, A. M. *Chem. Pharm. Bull.* **1989**, 37(10), 2832-2835.
- Santagati, N. A.; Duro, F.; Caruso, A.; Trombadore, S.; Amico-Roxas, M. *Il Farmaco* **1985**, 40(12), 921-929.
- Rubat, C.; Coudert, P.; Albuissou, E.; Bastide, J.; Couquelet, J.; Tronche, P. *J. Pharm. Sci.*, **1992**, 81(11), 1084-1087.
- Buchman, R.; Scozzie, J. A.; Ariyan, Z. S.; Heilman, R. D.; Rippin, D. J.; Pyne, W. J.; Powers, L. J. *J. Med. Chem.* **1980**, 23(12), 1398-1405.
- Yamada, T.; Shinamura, H.; Tsukamoto, Y.; Yamaguchi, A.; Ohki, M. *J. Med. Chem.* **1983**, 26, 1144-1149.
- Purohit, D. M.; Shah, V. H. *Heterocycl. Commun.* **1997**, 3(3), 367-371.
- Kandile, N. G.; Mohamed, M. I.; Zaky, H.; Mohamed, H. M. *Eur. J. Med. Chem.* **2009**, 44(5), 1989-1996.
- Rohet, F.; Rubat, C.; Coudert, P.; Albuissou, E.; Couquelet, J. *Chem. Pharm. Bull.* **1996**, 44(5), 980-986.
- Corsano, S.; Vezza, R.; Scapicchi, R.; Foresti, S.; Strappaghetta, G.; Nenci, G.G.; Gresele, P. *Eur. J. Med. Chem.* **1995**, 30 (7-8), 627-631.
- Sönmez, M.; Berber, İ.; Akbaş, E. *Eur. J. Med. Chem.* **2005**, 41, 101-105.
- Lopez, V.; Akerreta, S.; Casanova, E.; Garcia-Mina, J.M.; Caverio, R.Y.; Calvo, M.I. *Plant Food. Hum. Nutr.* **2007**, 62, 151-155.
- Alam, M. S.; Lee, D. U. *J. Chem. Crystallogr.* **2012**, 42, 93-102.
- Jing-lin, W.; Ya-qin, Z.; Bin-sheng, Y. *Inorg. Chim. Acta* **2014**, 409, 484-496.
- Akbas, E.; Berber, I.; Sener, A.; Hasanov, B. *Il Farmaco* **2005**, 60, 23-26.
- Blois, M. S. *Nature* **1958**, 181, 1199.
- Hsu, C.; Chen, W.; Weng, Y.; Tseng, C. *Food Chem.* **2003**, 83, 85-92.
- Kalembe, D.; Kunicka, A. *Curr. Med. Chem.* **2003**, 10, 813-829.

21. Sönmez, M.; Gülcan, M; Berber, İ. *Turk. J. Chem.* **2011**, 36, 189 – 200.
22. Uçan, S.; Uçan, M., Mercimek, B. *Synth. React. Inorg. Met.-Org. Nano-Met. Chem.* **2005**, 35, 417-421.
23. Temel, H.; Çakır, Ü.; Uğraş, H.İ.; Şekerci, M. *J. Coord. Chem.*, **2003**, 56, 943-951.
24. Brooker, S.; Iremonger, S. S.; Plieger, P. G. *Polyhedron* **2003**, 22, 665-671.
25. Emine, O.; Mirzaoglu, R. *Synth. React. Inorg. Met.-Org. Chem.*, **1983**, 13, 781.
26. Mishra, V.; Lloret, F; Mukherjee, R. *Inorg. Chim. Acta* **2006**, 359, 4053-4062.
27. Sharma, O.P.; Bhat, T.K. *Food Chem.* **2009**, 113, 1202–1205.
28. Duan, X. J.; Zhang, W. W.; Li, M.; Wang, B. G. *Food Chem.* **2006**, 95, 37–43.
29. Ağırtas M.S.; Çelebi, M.; Gümüş, S.; Özdemir, S.; Okumus, V. *Dyes Pigm.* **2013**, 99, 423-431.
30. Baykara, H.; İlhan, S.; Oztomsuk, A.; Seyitoglu, S.; Levent, A.; Okumus, V.; Dündar, A. *Synth. React. Inorg. Met.-Org. Nano-Met. Chem.* **2015**, 45, 1795–1807.
31. Jin, Q. M.; Lu, Y.; Jin, J. L.; Guo, H.; Lin, G. W.; Wang, Y.; Lu, T. *Inorg. Chim. Acta* **2014**, 421, 91–99.
32. Keypour, H.; Shoostari, A.; Rezaeivala, M.; Ozturk, F.; Kup, H.; Rudbari, A. *Polyhedron* **2015**, 97, 75–82.

ORCID

-  ID 0000-0001-8462-8580 (A. Çelik)
-  ID 0000-0002-0575-8131 (H. G. Soğukomeroğulları)
-  ID 0000-0001-7384-7358 (S. Özdemir)
-  ID 0000-0002-1134-5544 (M. S. Yalçın)
-  ID 0000-0003-3127-666X (M. Sönmez)